LATTICE VIBRATIONS IN MAGNESIUM ALUMINATE

by

Patrick Joseph O'Connor

A thesis submitted to the University of Aston in Birmingham for the degree of

Doctor of Philosophy

Department of Physics

April 1980

SUMMARY

Measurements of low energy phonons in the lattice vibrational spectrum of Spinel, $MgAl_2O_4$ obtained by inelastic neutron scattering spectrometry are reported. Acoustic mode frequencies supplemented by infrared and Raman data have been used to refine rigid ion and shell models with polarizable oxygen ions, both with and without central forces. The elastic, high and low frequency dielectric constants and apparent charge tensors have been calculated. Best fit to normal modes is achieved by a ten parameter shell model with axially symmetric forces.

The heat capacities of these models together with those based on the parameters of Thompson (1977) and Striefler and Barsch (1972) have been found over a range of temperatures. In this respect Thompson's model is shown to be inaccurate.

Landau's theory of second order phase transitions has been used to predict possible structural deformations from Fd3m to other cubic and tetragonal symmetries. The soft modes and resultant space groups are found to be A_{2u}-$F\bar{4}3m$, T_{2u}-$I\bar{4}2d$ and T_{1g}-$I4_1/a$.

Key Words

Spinel/Lattice Dynamics/Neutron Spectrometry/Soft Modes

TO MY FATHER AND MOTHER

CONTENTS

CONTENTS (contd)

CONTENTS (contd)

TABLES

TABLES (contd)

ILLUSTRATIONS

ILLUSTRATIONS (contd)

CHAPTER 1

STRUCTURE AND MODELS OF THE CRYSTAL DYNAMICAL BEHAVIOUR OF SPINELS

1.1 Introduction.

The construction of a theoretical model is necessary for the description of the physical behaviour of a crystalline solid. The extent to which the model describes the observed physical behaviour is limited by the various simplifications and assumptions which have to be made in order to perform calculations. This necessity is actually advantageous as it allows the important features of the physical processes to be elucidated. For example the inclusion of electronic polarization solely due to the presence of an electric field in models for alkali halides (Lyddane and Herzfeld, 1938) was found to give inferiour results compared to a similar model which neglected polarization completely (Kellermann, 1940). These attempts led in turn to the very successful shell models based on the work of Dick and Overhauser (1958) that include field polarization terms and also the overlap interaction of the electron wave functions of neighbouring ions.

The most successful mathematical fiction for the description of crystal dynamical behaviour is the assumption that the inter-particle forces are linearly related to small displacements of the constituent particles from their equilibrium positions. This together with consideration of crystal periodicity enables the solid to be regarded as a system of independent waves called normal modes . When quantisation is included the energy of a normal mode may be specified by the number of quanta, phonons, of energy $\hbar\omega$ for that particlar crystal state. Models based on these criteria are capable, in principle, of describing properties such as normal mode dispersion, one phonon infrared and Raman spectra, elasticity and heat capacity. However some crystal properties such as thermal expansion and multi-phonon spectra elude this formalism.

To perform calculations further assumptions must be made concerning the form of the potential for particlarinteractions which

depends not only on the type of crystal, eg ionic or covalent, but also on phenomema such as polarizability. For covalent crystals the interaction potential at present evades analytical description and in practice is often only described by a set of parameters fixed by fitting the model predicted quantities to existing experimental data. However in ionic crystals at least the form of the overall attractive Coulomb potential is well known and only the short range, essentially repulsive interactions need be parameterised. Models for simple crystals have been very successful and provide surprisingly accurate descriptions of the vibrational behaviour, see fig.1.1 which shows the fit of models to measured dispersion curves of NaI. The physics of the processes which the models describe then is well understood. Therefore crystals of a more complex nature may now be modelled with a fair degree of confidence. In practice extrapolation to more complex crystals requires the use of auxilliary techniques which were not essential for simple cases. The most important is the application of group theory to exploit crystal symmetry properties, not only for the purpose of normal mode classification but also to reduce the quantity of computation needed. Despite the availability of these techniques and the relative simplicity of the systems which have been studied, modelling of structures of greater complexity than the perovskites (five ions per unit cell, Cowley 1964) is uncommon. The most complex crystals considered appear to be gadolinium molybdate, $Gd_2(MoO_4)_3$, with thirty four ions per unit cell and fluorapatite, $Ca_{10}(PO_4)_6F_2$, with forty two ions per cell (Boyer and Hardy, 1973b and Boyer and Fleury, 1974 respectively).

Normal model analysis has been extended to include anharmonic terms in the equations of motion (Cowley, 1963a) although calculations even for simple compounds are formidable. Possibly the most important development is the concept of a soft mode of vibration proposed by Cochran (1960) to account for the ferroelectric transition of barium titanate. A soft mode is generally considerd as a normal mode whose

Dynamical Models for NaI
(after Woods et al, 1963)

Fig 1.1

frequency decreases substantially as the transition temperature is approached and which is responsible for the structural phase transition. For example strontium titanate has two modes that show anomalous temperature dependence. The mode at the zone centre is that normally associated with the perovskite ferroelectric transition. However the phase transition to a tetragonal structure which actually occurs is due to a soft mode at the zone boundary (Cochran and Zia, 1968). Subsequently the phase transitions of several structures have been interpreted in this fashion - see Scott (1974) for a review of theory and experimental results. Previously it had been realised that if the transition was second order, the possible changes of space group and the symmetry species of the normal mode responsible could be predicted (Landau and Lifshitz, 1960a). The technique is not completely reliable as most structural phase transitions are first order. A notable example is the phase transition in A15 compounds from a cubic to a tetragonal structure, found by Shirane and Axe (1971) to go to a space group discounted on symmetry grounds (Perel et al, 1968).

1.2 Spinel Compounds.

Most crystals of compounds with the formula AB_2X_4 have structures related to that of the mineral $MgAl_2O_4$ (Muller and Roy, 1974) known as spinel. The highest symmetry form of the structure can be described as formed by a nearly close packed cubic array of anions X^{2-} with the cations A^{2+}, B^{3+} distributed among certain interstices. In the normal structure the divalent cations lie in sites around which the anions are arranged as a perfect tetrahedron (A sites) while the trivalent are situated in interstices having anions arranged with near octahedral symmetry (B sites). The important features of this unit cell containing eight formula units were first elucidated by W.H.Bragg (1915). The overall and ion site symmetries then conform to the space group $Fd3m(O_h^7)$. The close packing is slightly distorted to accommodate the metal ions by small anion movements in <111> directions from the tetrahedral ion. Table 1.1 lists the coordinates and site symmetries of this structure. The oxygen position parameter is given as u equal to $^3/_8 + \delta$.

In an ideal spinel with perfect close packing δ has the value zero. In practice δ is usually greater than zero although rarely negative values are found (Muller and Roy 1974). The twelve oxygen-oxygen neighbours are separated into groups corresponding to three distinct distances. The three nearest neighbours are equivalent by face centred translations to the group of three neighbours at the furthest distance. The remaining six anions which lie at an intermediate distance in sites almost corresponding to the close packed positions are not so related. The site symmetry of the A site ($\bar{4}3m$) is maintained irrespective of the value of δ while the octahedral site distorts from cubic ($m3m$) to a trigonal ($\bar{3}m$) symmetry in such a way that the anions are equidistant from the trivalent cation. Figure 1.2 illustrates the ideal spinel structure, the whole unit cell being generated by placing identical contents

Centre at $\bar{4}3m$

Point Symmetry	Position Coordinates
$\bar{3}m$	$\frac{5}{8},\frac{5}{8},\frac{5}{8}$; $\frac{5}{8},\frac{7}{8},\frac{7}{8}$; $\frac{7}{8},\frac{5}{8},\frac{7}{8}$; $\frac{7}{8},\frac{7}{8},\frac{5}{8}$;
$\bar{4}3m$	$0,0,0$; $\frac{1}{4},\frac{1}{4},\frac{1}{4}$;
$3m$	u,u,u; $\frac{1}{4}-u,\frac{1}{4}-u,\frac{1}{4}-u$; $u,\bar{u},\bar{u}$; $\frac{1}{4}-u,\frac{1}{4}+u,\frac{1}{4}+u$; $\bar{u},u,\bar{u}$; $\frac{1}{4}+u,\frac{1}{4}-u,\frac{1}{4}+u$; $\bar{u},\bar{u},u$; $\frac{1}{4}+u,\frac{1}{4}+u,\frac{1}{4}-u$;

Centre at $\bar{3}m$

Point Symmetry	Position Coordinates
$\bar{3}m$	$0,0,0$; $0,\frac{1}{4},\frac{1}{4}$; $\frac{1}{4},0,\frac{1}{4}$; $\frac{1}{4},\frac{1}{4},0$;
$\bar{4}3m$	$\frac{3}{8},\frac{3}{8},\frac{3}{8}$; $\frac{\bar{3}}{8},\frac{\bar{3}}{8},\frac{\bar{3}}{8}$;
$3m$	x,x,x ; $x,\frac{1}{4}-x,\frac{1}{4}-x$; $\bar{x},\bar{x},\bar{x}$; $\bar{x},x-\frac{1}{4},x-\frac{1}{4}$; $\frac{1}{4}-x,x,\frac{1}{4}-x$; $\frac{1}{4}-x,\frac{1}{4}-x,x$; $x-\frac{1}{4},\bar{x},x-\frac{1}{4}$; $x-\frac{1}{4},x-\frac{1}{4},\bar{x}$;

$u = \frac{3}{8} + \delta = x + \frac{5}{8}$

Atom Positions of the Basis for Spinels in Space Group Fd3m

TABLE 1.1

Fig 1.2 Spinel Structure (after Gorter,1954)

in octants connected by an edge (Gorter 1954).

Apart from the normal distribution of cations described, other arrangements are possible. Positioning of half the trivalent cations on the A sites with the remaining cations sharing B sites gives rise to the inverse or equipoint (Wyckoff, 1965) structure. Intermediate situations also arise and are known as partially inverse structures. The space group remains unchanged when the cations are randomly distributed on various A and B sites. For example in the normal distribution the structure is centro symmetrical about the B sites. The symmetry is reduced in the inverse structure when the cations order so as to remove the centre of inversion. The highest symmetry is then described by the $F\bar{4}3m(T_d^2)$ space group. Haas (1965) has considered this and other possible orderings on group theoretical grounds with the intention of predicting the order of the phase change from $Fd\bar{3}m$.

The large number of compounds with structures related to $MgAl_2O_4$ is in large part due to the range of different cations which may be substituted into the structure. Spinels are often grouped into series classified by the anions eg. oxides, sulphides, selenides, tellurides (the last may also act as a cation in this structure eg. $Zn_2Co_2TeO_8$). Different trivalent cations may be substituted for B^{3+} and a variety of divalent cations for A^{2+}. However cations of other valencies may be introduced into the structure provided the condition of charge neutrality is maintained eg. $Na_2^{+}W^{6+}O_4^{2-}$.

The ability to predict the distribution of the cations over the A and B sites is important in the study of properties of series of compounds where say the series is to be restricted to normal spinels only (eg Grimes and Collett, 1971a) and the development of magnetic materials (Grimes,1975). Dunitz and Orgel (1957b) and McClure (1957) calculated site energies for transition metal ions on crystal field theory alone. Miller (1959) extended the calculations to non transition metals by including the effects of the Madelung energy as well as a

short range repulsive interaction term due to electron orbital overlap between neighbouring ions. The results (shown in table 1.2) are in broad agreement with the previous estimates for transition metals (though notably not zinc) and with the later thermodynamic calculations of Navrotsky and Kleppa (1967). Particularly notable are the site preference energies of Zn^{2+} and In^{2+} for the tetrahedral site and that of chromium for the octahedral site. The correlation between the anion u parameter and inversion (u = 0.387, normal and u = 0.380, inverse) noted by Gorter (1954) has been shown by Thompson and Grimes (1977a) to be related to changes in the Madelung energy with cation distribution. The balance of energy terms may be small allowing the distribution of cations to be determined by the method of preparation. For example when slowly annealed $CuFe_2O_4$ is fully inverse but when quenched from the synthesis temperature is only partially inverse (Smit and Wijn, 1959).

Site Preference Energies (after Miller (1959))

TABLE 1.2

1.3 Lattice Dynamical Studies of Spinels.

1.3.1 General.

Initial attempts to provide a descriptive basis for spinel dynamics were concerned almost completely with the interpretation of the infra red spectra. All mathematical models were essentially extensions of the Wilson,Decius and Cross (1955) formulation of molecular vibrations until Sammis (1971) introduced a rigid ion, central force model for the calculation of elastic constants. Striefler and Barsch (1972) then used a similar model to calculate all the Brillouin zone centre frequencies and pressure derivatives of elastic constants together with the first model calculation for dielectric behaviour. Thompson (1977) later extended this type of model to account for dispersion throughout the Brillouin zone.

For the interpretation of light scattering spectra it is only necessary to consider Brillouin zone centre frequencies as electromagnetic radiation with energies in the phonon range has much greater wavelengths. For one phonon spectra the simultaneous requirements of conservation of energy and crystal momentum demand that only phonons with almost zero wave vector are involved. The spinel structure may be regarded as a face centred cubic lattice with a basis of fourteen ions situated about each lattice point. Of the corresponding forty two normal modes (three degrees of freedom for each of the fourteen ions) only those of the appropriate symmetry interact with light radiation. For infrared absorption the mode must have a non zero dipole moment whereas for Raman scattering the mode must transform as a second rank tensor to enable light interaction with the polarizability of the atoms. It is only in the long wavelength limit ($q = \frac{2\pi}{\lambda} \rightarrow 0$) that non cancelling values for these quantities are produced in all unit cells.

1.3.2 Waldron Model.

Waldon (1955) measured the infrared spectra of several ferrites

ferrites (MFe_2O_4, M = Co,Fe,Mg,Mn,Ni,Zn) which were essentially composed of two strong broad peaks that did not display any narrowing at liquid nitrogen temperatures. To interpret these spectra Waldron, although realising that isolated molecular groupings did not occur in the spinel structure, proposed the simplification that the two formula units in the basis could be regarded as two MO_4 and one Fe_4 tetrahedra. The normal modes were then classified according to the point group $\bar{4}3m(T_d)$ which predicted eight infrared modes, one of which must always be discarded as it represents a translation of the whole crystal against which there is no restoring force and therefore the mode has zero frequency. Three further frequencies were removed as "internally inactive" by imposing equivalence of the two MO_4 tetrahedra and sites of inversion at the Fe^{2+} ion positions. Thus the symmetry of the problem was effectively raised to $m3m(O_h)$ known to be appropriate for Fd3m spinels. Each oxygen is considered as bonded to the three nearest neighbour trivalent cations in directions parallel to the edges of the crystallographic cubic cell and to the nearest neighbour divalent cation in a direction at forty five degrees to the orthogonal axes (see fig.1.3). Vibrations of the oxygen ion along the tetrahedral ion-oxygen bond were considered to have a higher frequency (ν_1) than those at right angles to it (ν_2). The lower frequency modes ν_3 and ν_4 involve motions of the cations in isotropic fields of force. As only two infrared bands were detected any model, if it was not to be overdetermined, could have at most two disposable parameters. These were chosen to be force constants f_1, f_3 representing tetrahedral ion-oxygen and octahedral ion-oxygen bond stretching respectively (the notation is that of Bruesch and D'Ambrogio,1972). The potential energy is then given by

$$2V = f_1 \Sigma r_t^2 + f_3 \Sigma r_o^2 \qquad (1.1)$$

r_t, r_o are components of displacement along the direction of the appropriate bond. Symmetry coordinates and simple expressions for

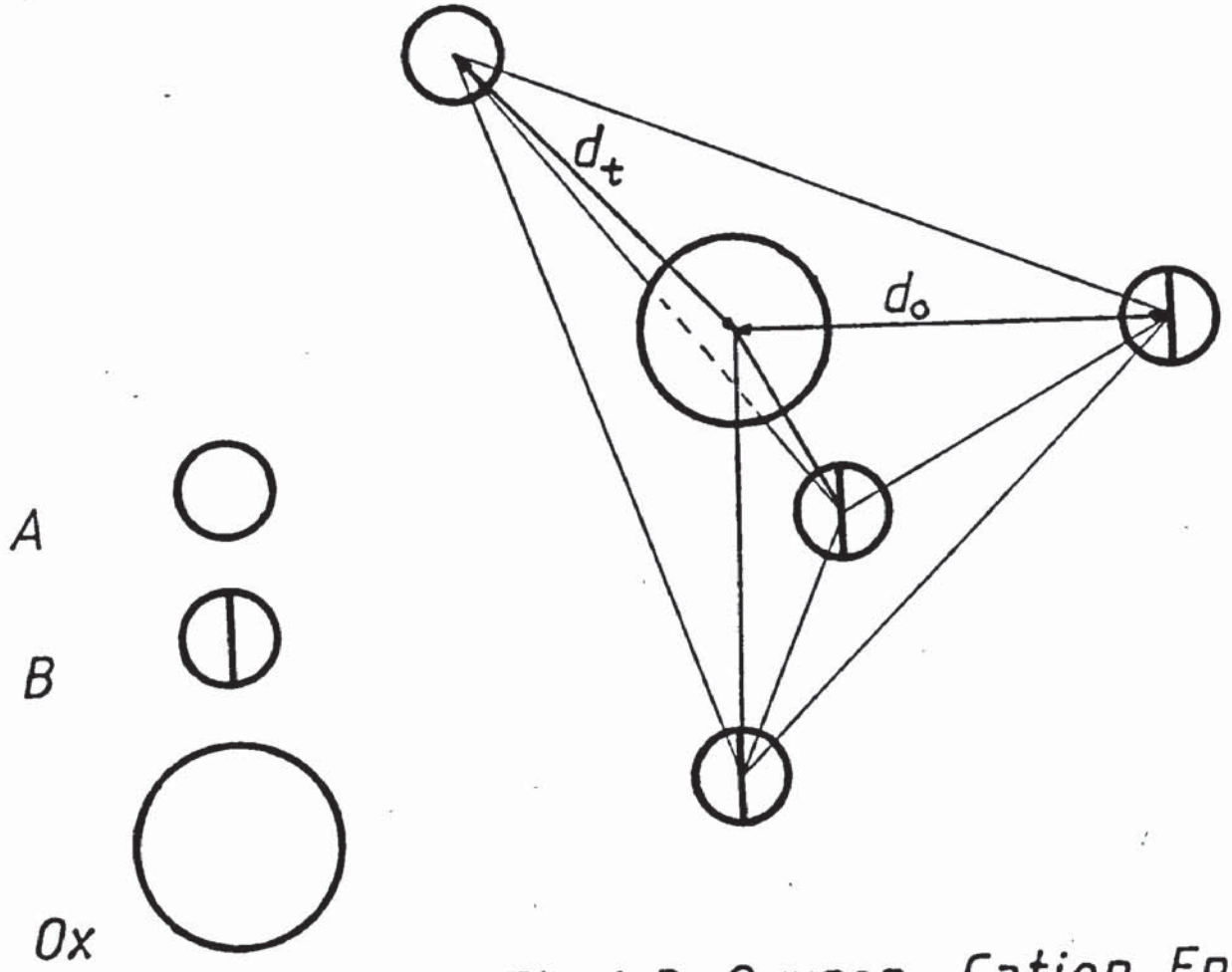

Fig 1.3 Oxygen-Cation Environment

the frequencies of the infrared modes were obtained. The frequency ν_4 of one of the modes was found to be identically zero because no bond bending force constants were assumed. Therefore MO_4 groups were effectively isolated without any restoring force for the bond bending vibration present. The two major peaks were assigned to ν_1 and ν_2 in descending frequency and the possibility that they were of multiphonon origin was discarded as $\nu_1/\nu_2 \simeq \sqrt{2}$ in approximate agreement with the force constant expressions with $f_1 = f_3$. The ratio f_1/f_3 was found to vary from almost two ($CoFe_2O_4$, $f_3 = 0.85$, $f_1 = 1.66$ in units of 10^5 dynes/cm) to seventy five per cent of this value ($MnFe_2O_4$, $f_3 = 0.92$, $f_1 = 1.4$). Various of the quantities such as compressibility, specific heat capacity and infrarad band intensitites were calculated for various of the compounds considered and found to be in reasonable agreement with experiment where data was available. Waldron's calculations were the most extensive in the range of properties obtained from one model until the publication of the rigid ion model (Striefler and Barsch, 1972). Grimes and Collett (1971b) re-examined the spectra of $NiFe_2O_4$ and Fe_3O_4 and found them to consist of four promiment absorptions in agreement with Waldron's prediction. This model was extensively used (Hafner 1961, Grimes and Collett 1971a) until Bruesch and D'Ambrogio (1972) developed a model which incorporated bond bending. Grimes and Collett (1971a) studied the infrared spectra of the series $MgCr_xAl_{2-x}O_4$ and used Waldron's model to obtain values of the force constants at the end points. However their claim that the difference between the values they obtain for the force constants and those obtained by Hafner (1961) was due to a modification of Waldron's theory to allow for $\nu_4 \neq 0$ was erroneous. Hafner, following Waldron, obtained f_3 from the equation for ν_2 and used the equations for ν_1 and ν_3 to determine the constant f_1 whereas Grimes and Collett used only the equations for ν_1 and ν_3. More importantly this method of calculation gave an almost constant value of f_3 together with consideration of

Waldron's compressibility relations and cohesion theory led Grimes and Collett to emphasize the linear relationship of ν_1 and ν_3 to the reciprocal of the square root of the effective octahedral mass and also to the unit cell volume. These relationships hold almost perfectly for the full range of the series.

Hafner (1961) studied a large number of infrared spectra of which the normal to inverse series are particularly important. Included in these are the series $MgAl_2O_4$- $MgGa_2O_4$ and $MgAl_2O_4$-$MgFe_2O_4$ although Hafner and Laves (1961) show that synthetic $MgAl_2O_4$ is partially inverse (now supported by evidence from others, Navrotsky and Kleppa (1967), Schmocker and Waldner (1976). He noted that the major effect of going from a normal to an inverse structure was to broaden the two intense high frequency bands. Waldron's model was used throughout although it was indicated that it was likely to be a better approximation for inverse spinels because in normal structures, especially where the tetrahedral ion is large in comparison to the octahedral ion, anion packing produces considerable oxygen-oxygen compression. This effect was considered to require the use of oxygen-oxygen force constants, which are absent in Waldron's model, for an accurate description. It was generally found that the force constants decreased with decreasing cation radius and were sensitive to cation distribution. The ratio f_1/f_3 varies from two to one reaffirming that $A^{2+}X_4^{2-}$ tetrahedra do not exist as molecular groups.

1.3.3 Group Theoretical Analyses of Zone Centre Optic Modes.

White and DeAngelis (1967) produced the first full group theoretical analysis of the q = 0 phonons for a spinel structure. The forty two vibrations were classified among the irreducible representations of the point group m3m (O_h) with which the factor group of the space group $Fd3m(O_h^7)$ is isomorphic.

$$\Gamma = T_{1g} + 2A_{2u} + 2E_u + 2T_{2u} + A_{1g} + E_g + 3T_{2g} + 5T_{1u} \qquad (1.2)$$

Representatives A,E,T are non,two-and three-fold degenerate respectively.

Representations A_{1g},E_g and T_{2g} are Raman active and may be distinguished by a polarization analysis of the incident and scattered light. Of the five T_{1u} modes one, of necessity has zero frequency, the remaining four are infrared active. This reduction was also performed for other spinel space groups which arise as a result of cation ordering on particular sites. However to assign specific atomic motions to the modes White and DeAngelis introduced the assumption that the basis may be regarded as consisting of four B ions and two AO_4 molecules. The modes were then classified as translatory or rotating, with modes that did not fit into this scheme designated as internal. This categorization was then used to interpret the Raman spectra of Na_2WO_4 and Na_2MoO_4, spinels in which the concept of molecular groups is most likely to hold. However when considering infrared data these authors appear to have reverted to Waldron's system.

Verble (1973) performed a similar analysis using the Waldron basis of three tetrahedra (one B_4 and two AO_4) to obtain a different assignment of the terms translational, rotational and internal. The White and DeAngelis work was criticised for excluding rotational properties of the B_4 tetrahedron. However the White and DeAngelis basis is not identical to Waldron's as the B ions appear to have been considered as independent entities - not as a tetrahedral group. From their remarks on that paper it is not clear if Preudhomme and Tarte (1970a) also appreciated this point. Verble points out that two of the triply degenerate T_{2g} Raman modes and two of the infrared T_{1u} modes derive from the same irreducible representation of the molecular group. Therefore if the molecular model was to have any validity a close frequency correlation is expected between these modes.

Lutz (1969) presented the first complete set of symmetry coordinates for the q = 0 spinel phonons, appropriate linear combinations of which form the eigenvectors of the normal modes. In contrast to White and DeAngelis examination of the symmetry coordinates

led to the conclusion that there did not appear to be any obvious tetrahedral group vibrations although it might be possible to consider some as octahedral group vibrations.

1.3.4 Qualitative Infrared Analysis.

Preudhomme and Tarte have produced a very important series of papers (1970a, 1970b, 1970c, 1971) on the infrared spectra of spinels, both on measurement and interpretation, although quantitative models were not proposed. Reviewing previous work they point out that Waldron's assignation of the highest frequency band to vibrations in which the oxygen ion oscillates along the direction of the oxygen-tetrahedral ion bond is only appropriate if this bond is stronger than the octahedral cation-oxygen bond. Considering data from previous compounds containing "isolated" AO_4 tetrahedra (eg. $KMnO_4$) they conclude that for cations of similar valency and electronic structure "the valency state is generally the most important factor in determining the cation oxygen bonding force and corresponding vibrational frequency." Thus Waldron's approximation is expected to hold for I-VI and normal II-IV spinels (the roman numerals refer to the valency of the A and B cations in AB_2X_4). For II-III and inverse II-IV compounds the situation is less clear. By comparison with absorption data for various "condensed" (i.e. linked by edges with other octahedra) octahedra eg. AlO_6 it was suggested that the highest frequency mode could be assigned to stretching vibrations of octahedral groups for these latter compounds. These claims were supported by data from an isotopic substitution study of lithium in $LiCrGeO_4$ spinels where a low frequency mode is assigned to the LiO_4 vibration. The authors criticise the group theoretical analysis method of interpreting infrared data for the spectra of a continuous series of solid solutions eg. $ZnAl_{2-x}Cr_xO_4$, $x = 0 \rightarrow 2$. In the course of substitution the bands change from their initial forms and positions at one end point to those at the other essentially by one of two major processes:

(i) The band remains almost constant in intensity and continuously changes frequency between the end points.

(ii) Two bands appear in the spectra between the end points with frequencies close to each end member and the strength of each mode varies in proportion to the concentration of each component.

Wakamura et al.(1973) have used the terminology from studies of binary alloys: one mode type and two mode type to describe these processes in spinels. It must be remembered that these figures have no relation whatsoever with the degeneracy associated with the normal mode involved. Preudhomme and Tarte describe the onset of the second process at low concentrations as associated with vibrations of localised groups. Intermediate behaviour between the two extremes of these processes has also been observed. The group theory criticism arises because throughout the series the space group as revealed by X-rays does not change, thus usually only four bands are expected. The extra bands produced from the type (ii) process are therefore not explained. Experimentally Preudhomme and Tarte argued that to attempt a reasonable interpretation of the infrared spectra of spinels knowledge of correlations between the nature of the cations and the observed frequencies is required. Throughout this series of papers however the authors do not consider the effects of anion substitution and the information it would reveal of anion-anion interactions. Using the methods of homogeneous substitution in families of pure spinels, study of the continuous series produced by isomorphic replacement and also the method of isotopic substitution the authors investigated in great detail a wide range of oxide spinels. Analysis of normal II-III spinels showed that the spectra were typified by having two broad intense bands at high frequencies with two much weaker but sharp bands at lower frequencies (fig.1.4). The broadness and shape of the higher frequency bands to some extent depended on the preparation of the compound. Even at maximum sharpness the bands are asymmetric. The lower frequency bands

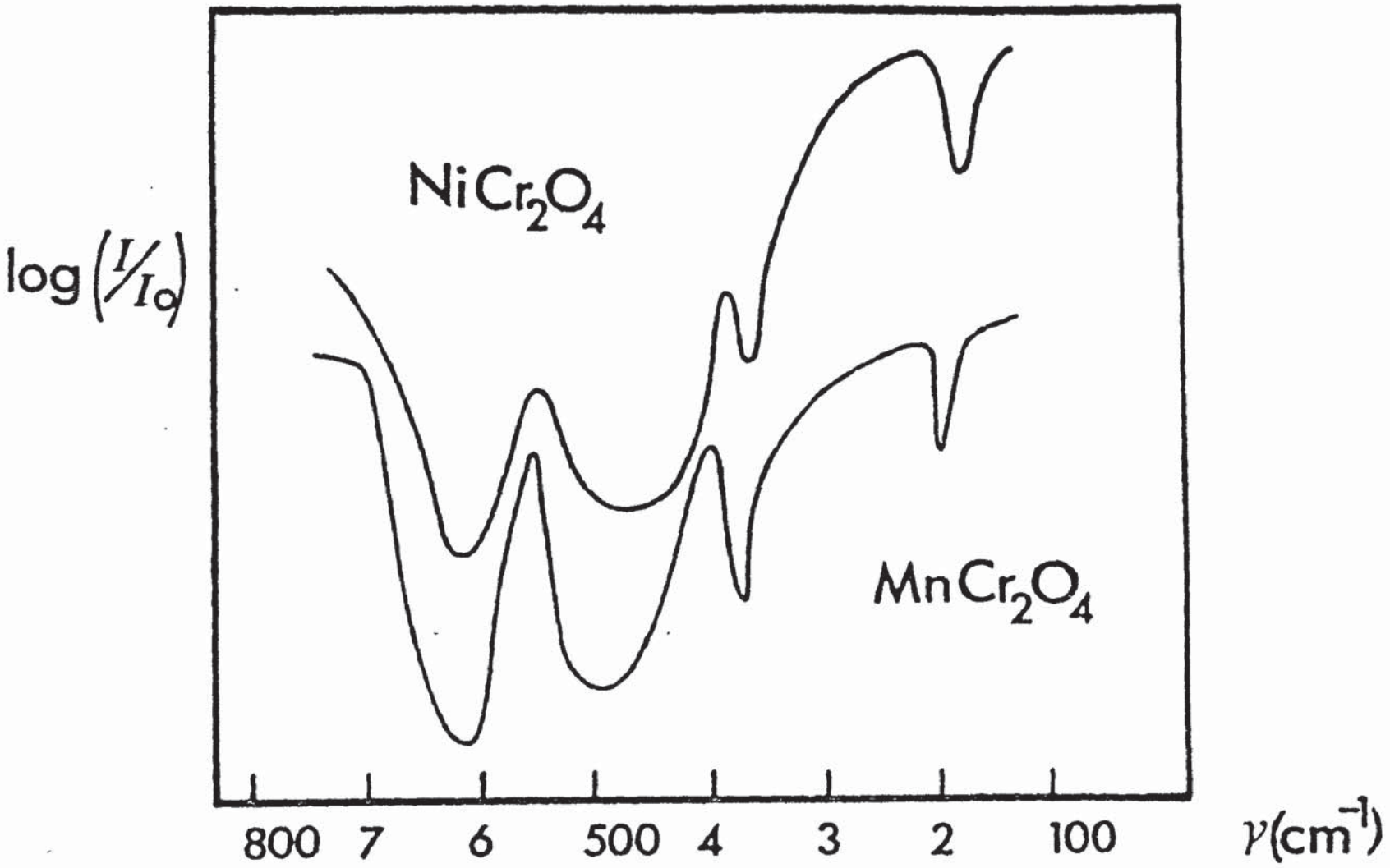

Fig 1.4 Infraced Absorption Spectra

appear to have been unaffected. For these compounds it was concluded that the high frequency bands ν_1 and ν_2 were the vibrations of octahedral groups. The two lower bands were assigned to complex vibrations of both cations. An important exception, in magnesium aluminate, is the assignation of the ν_3 type vibration to a shoulder lying between ν_1 and ν_2. $ZnAl_2O_4$ is another anomalous aluminate as it consists of three strong, broad peaks and one weak, sharp band. This behaviour was thought to be related to the moderate mass of the trivalent cation. Preudhomme and Tarte later (1971) made the suggestion that the highest frequency band in normal structures could be assigned to the vibration between the highest valency cation and the oxide ion regardless of the ion's site symmetry. In all these studies polycrystalline powder samples were used, however later comparison of single crystal data (O'Horo et al. 1972 on $MgAl_2O_4$ and Boldish and White, 1978a on $CdIn_2S_4$) with the frequencies obtained from powder data showed no significant differences. Therefore powder sample spectra can be considered a reliable source of the absorption frequencies associated with the irreducible representation T_{1u}.

1.3.5 Four Force Constant Model.

Bruesch and D'Ambrogio (1972) proposed a dynamical model for the q = 0 spinel phonons which has become the most popular model to date. Very similar to work by Shimanouchi et al. (1961) it is an extension of the Wilson,Decius and Cross (1955) formalism for molecular vibrations appropriate to crystals especially where co-valent bonding is involved. Their dynamical matrix which has to be diagonalised to give the optic mode frequencies may be expressed as a product of matrices GxF. The G matrix contains only information on the atomic masses and internal coordinate information, the F matrix is dependent on the force field only. Wilson,Decius and Cross derived G as the inverse of the kinetic energy matrix and F as the potential energy matrix of the system. Bruesch and D'Ambrogio did not explicitly write their equations in this

manner but in an equivalent form. Only nearest neighbour force constants were assumed with no interaction between stretching and bending type included. Four force constants were used with the oxygen param. set at $u \simeq {}^{3}/_{8}$

f_1 A-X stretch

f_2 X-A-X bend

f_3 B-X stretch

f_4 X-B-X bend

If the oxygen parameter had been set at $u = {}^{3}/_{8} + \delta$ two f_4 type constants would have been required for the two different sets of X-B-X angles ($\cos\phi \simeq -8\delta$ and $\cos\phi \simeq 8\delta$). When block diagonalised by the symmetry coordinates the elements of the dynamical matrix are given by particularly simple equations suitable for rapid calculation. The model then may be easily applied to other spinel structures without modification as the constituent equations are independent of the oxygen parameter. Bruesch and D'Ambrogio used the model for the analysis of the known Raman and infrared data of the normal spinels $CdCr_2Se_4$ and $CdCr_2S_4$. With the parameters

	f_1	f_2	f_3	f_4 in 10^5 dynes/cm
$CdCr_2Se_4$	1.4	0.05	0.7	0.03
$CdCr_2S_4$	1.5	0.07	0.84	0.02

agreement with observed data was about 10% or better. It is interesting to note that the ratio of f_1/f_3 is again about two and the magnitudes of the bending force constants are about fifty to one hundred times smaller than the stretching constants. This indicates how good an approximation Waldron's very simple model had been. The very low frequency (75 cm^{-1}) infrared band of $CdCr_2Se_4$ was shown by the model to be an almost pure bending mode of the Cr-Se-Cr angles. Presumably this is the mode which in Waldron's theory would have had zero frequency because of the lack of bending force constants. The authors attempted to distinguish between internal and external modes by

increasing the f_1 and f_2 force constants to establish rigid units and found that only the A_{1g},E_g and the two T_{2g} high frequency modes may be regarded as internal, and that the optically inactive modes T_{1g} and T_{2u} are translational. However the other modes including all the T_{1u} modes are impossible to classify in this fashion. The authors application of the normal coordinates to the observed influence of magnetic ordering on the optically active modes was less successful. Boldish and White (1978a) used the same model for seven sulphide spinels for which they had measured the infrared and Raman spectra (AB_2S_4,A=Cd,Mg,Zn;B=Sc,Yb,Tm). Of the five Raman modes expected only four were detected except in the cases of Zn,$MgSc_2S_4$ where the fifth band could not be unambiguously assigned as the missing fundamental frequency. The A_{1g} mode frequency has a fairly linear relationship to cell volume whilst the lowest infrared mode varies linearly with the square root of the mass of the A ion. The assignment of the two highest frequency bands is associated with the octahedral ion while the second lowest band has a complex nature agrees with the usual Preudhomme and Tarte classifications. The computed relative intensities for the infrared modes agreed well with experiment although better for cadmium than magnesium compounds.

Wakamura et al.(1973) used a slightly modified form of the four force constant model to account for the infrared spectra of continuous series of spinels ($Hg_xZn_{1-x}Cr_2Se_4$,$Cd_xZn_{1-x}Cr_2Se_4$) although Preudhomme and Tarte analyses indicate that anharmonic forces are significant. Firstly the force constants for the two end points were calculated, then for the mixed crystal the force constants for the tetrahedral ion are given as functions of composition

$$f_1(x) = xf_1(HgCr_2Se_4) + (1-x)f_1(ZnCr_2Se_4) \qquad (1.3)$$

$$f_2(x) = xf_2(HgCr_2Se_4) + (1-x)f_2(ZnCr_2Se_4) \qquad (1.4)$$

with the mass of the ion at the tetrahedral site taken as

$$m(x) = x\, m(Hg) + (1-x)\, m(Zn) \qquad (1.5)$$

where the series $(Hg,Zn)Cr_2Se_4$ has been used as an example. The T_{1u} frequencies were calculated as functions of composition for the force constants f_3 and f_4 fixed at each end point values. Considering the simplicity of the model the fit to the experimental data is good. For modes which change frequency by type (i) process the values predicted using each end point value for f_3 and f_4 are close to each other. For the type (ii) process which occurs for the lowest band in $(Hg,Zn)Cr_2Se_4$ the predicted frequencies for each end point value of f_1 and f_2 are closer to the experimental data than to each other. Overall the fit is better for the two high frequency modes but much worse for the lower pair, in particular the second lowest which is often associated with a complicated vibrational form.

Although model calculations have rarely been used to actually predict properties of spinels Shimuzu et al. (1975) used the four force constant model to provide evidence that the $CdInS_4$ spinel could not be considered as having a normal structure above the phase transition temperature below which the cations are ordered on A sites. Comparing with a similar model for $CdCr_2S_4$ the authors attributed the worse fit for $CdInS_4$ to its greater ionicity.

1.3.6 Ionicity Among Spinels.

Despite the great success of the four force constant model the above remark, if true, would indicate that the parameter values for more ionic spinels could not be interpreted clearly. In any fitting procedure for these compounds the force constant values obtained must have incorporated effects of the long range Coulomb forces. Thus any appreciation of the values of the variables in terms of a change in a particular bond stretch or bend is obscured. Especially important for ionic compounds is explicit inclusion of their dielectric behaviour, in particular the longitudinal-transverse splitting of the infrared modes. This effect is due to the addition of an extra restoring force Z.E for these modes, where Z is an effective charge tensor and E the macroscopic electric field. This field is produced by the slowly varying

polarization associated with this type of optic vibration and may be shown from Maxwell's equations (Born and Huang, 1954) to act in the direction of mode propagation. Thus the extra restoring force has maximum value for infrared modes with dipole moments parallel to the direction of wave propagation (longitudinal) and is zero for modes with dipole moments at right angles to the wave vector (transverse modes). Cochran and Cowley (1962) have shown that the dipole moments in cubic crystals must lie along the cube edges. The effects of the infrared splitting are then made apparent for spinels through the Lyddane-Sachs-Teller relation (equations (2.68)) which relates the ratio of the longitudinal and transverse modes to that of the high and low frequency dielectric constants. Alternatively the longitudinal and transverse modes may be obtained from zeros and poles, respectively, of the frequency response of the dielectric constant (Kurosawa, 1961). In practice these frequencies are obtained by analysis of the reflectance spectra of single crystals either by a Kramers-Kronig method (Landau and Lifshitz 1960b) or using an oscillator model (Barker 1964). The former method is somewhat more objective as it only depends on causality and linearity of the dielectric susceptibility to the electric field, the latter model may always be improved by introducing further parameters.

Although true absorption spectra are the result of an incident electromagnetic wave coupling with the transverse infrared modes the longitudinal-transverse mode splitting also affects powder infrared data. Preudhomme and Tarte (1970c) note that the absorption spectra are the effect of both reflection and true absorption phenomena with the possibilities of either the longitudinal and transverse modes appearing separately or as a single average band depending on particle size and temperature. Boldish and White (1978a) comparing single crystal and powder data for $CdIn_2S_4$ show that the fitted absorption

band frequency from reflectance data is at greatest variance with that of the absorption spectra for the mode with the greatest longitudinal-transverse splitting.

Kramers-Kronig analyses have been performed for three spinels, $CdIn_2S_4$ (Shimuzu et al. 1975), Fe_3O_4 (Schlegel et al. 1979), $MgAl_2O_4$ (O'Horo et al. 1973) of which longitudinal frequencies have only been published for $MgAl_2O_4$ (Grimes et al. 1978). Several calculations based on the classical oscillator model have been performed, the results summarized in table 1.3.

The elements of the apparent charge matrix Z in the product Z.E are functions not only of the ionic charge but also polarizility and charge exchange between bonds. For instance Szigeti (1949,1950) by showing that values of effective charge less than unity were required to account for the infrared spectra of alkali halides demonstrated the need for dynamical models to include polarizability effects. On the other hand Zallen (1968) has shown that although a crystal may have constituents with zero ionic charge it may still exhibit one phonon infrared spectra from polarization effects alone provided there are at least three atoms in the basis. The values of the apparent charge amongst IV-VI compounds appear to be related to charge exchange amongst the bonds (eg. Littlewood and Heine, 1979).

However Mitra and Marshall (1964) have shown that there is a proportionality between the effective Szigeti charge and the fractional increase in the infrared frequencies due to mode splitting for a range of II-VI and III-V compounds. Although the Szigeti charge and the apparent charge tensor are not the same quantity (see section 6.1 and Cochran 1960) these may be related to each other for alkali halide structures. Boldish and White (1978b) have used this approach to classify the ionicity of spinels by defining a mode ionicity

$$I(j) = \frac{\nu_L(j) - \nu_T(j)}{\nu_T(j)} \qquad (1.6)$$

						$\epsilon(0$	$\epsilon(\infty)$
$CdCr_2S_4$(a)	ν_L	389.9	374.2	-	-	9.79	7.8(b)
	ν_T	376.9	321.6	-	-		
	I	0.03	0.08	-	-		
$CdCr_2Se_4$(a)	ν_L	291.4	281.3	-	-	10.3	9.0(a)
	ν_T	281.1	266.2	-	-		
	I	0.04	0.06	-	-		
$CdCr_2Se_4$(b)*	ν_L	292.0	281.0	189.0	76.0	12.8	10.2
	ν_T	287.0	264.0	187.0	74.0		
	I	0.02	0.06	0.01	0.03		
$ZnCr_2Se_4$(c)	ν_L	300.5	289.0	201.0	87.5	11.0	9.0
	ν_T	296.0	272.5	199.0	87.5		
	I	0.02	0.06	0.01	0		
$HgCr_2Se_4$(c)	ν_L	290.0	281.0	172.0	60.0	13.2	10.8
	ν_T	287.0	270.0	170.0	57.5		
	I	0.01	0.04	0.01	0.04		
$CdIn_2S_4$(d)	ν_L	339	270	172	69	-	-
	ν_T	307	215	171	68		
	I	0.10	0.26	0.01	0.01		
$MgAl_2O_4$(e)	ν_L	855	630	-	305	8.42(f)	2.96(g)
	ν_T	670	485	-	305		
	I	0.28	0.30	-	0		

*Using the Lyddane-Sachs-Teller relation for the top two bands and the measured value $\epsilon(\infty)$ = 9(a) the value of 10.6 is obtained for $\epsilon(0)$.

a) Lee (1971), (b) Bongers and Zanmarchi (1968), (c) Wakamura et al. (1976), (d) Yamamoto et al. (1973), (e) Grimes et al. (1978), (f) Wang and Zanzucchi (1971), (g) Vedam et al. (1975)

TABLE 1.3 - Ionicity of Spinels.

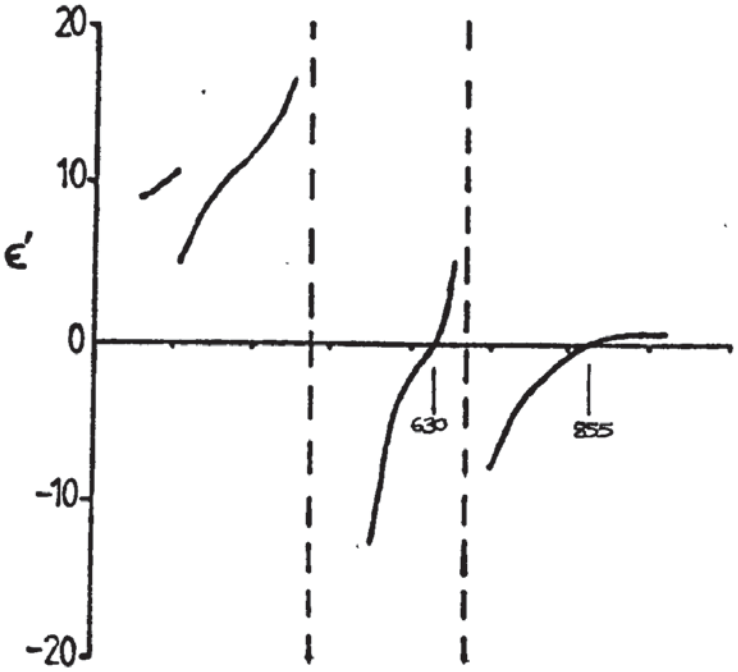

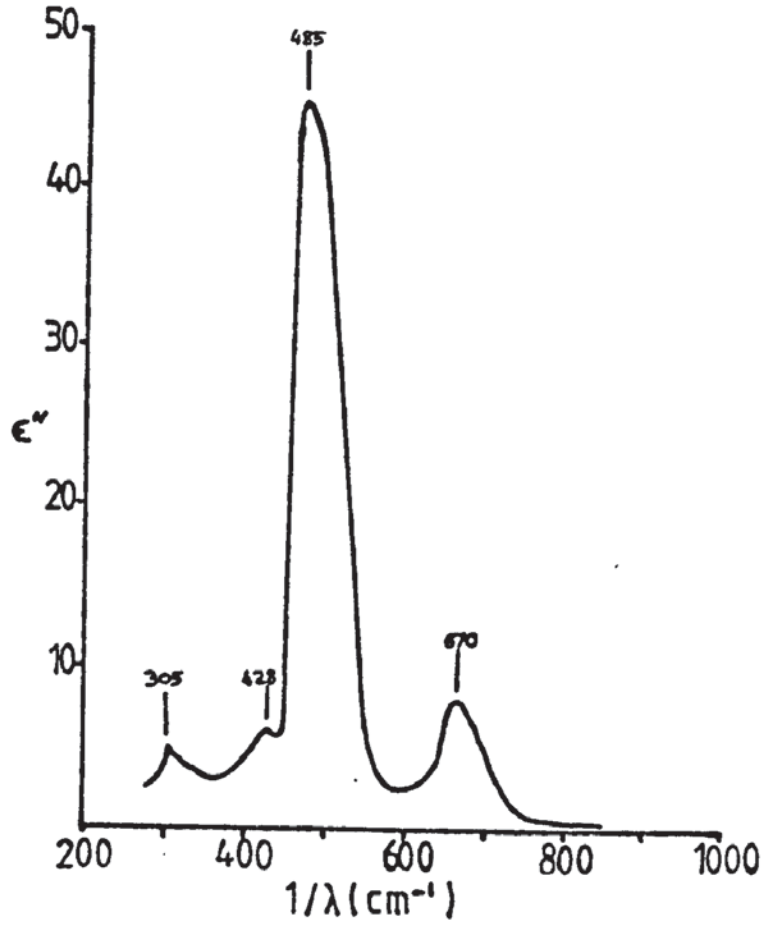

Components of the Dielectric Function $\epsilon = \epsilon' + i\epsilon''$ of $MgAl_2O_4$

Fig 1.5

where j labels the infrared modes. The concept of relating ionicity to mode splittings in spinels is less apparent than in alkali halides where only one mode occurs. From table 1.3 it can be seen that $MgAl_2O_4$ is the most ionic of the spinels listed although much less so than MgO (I = 0.79, Jasperse et al. 1966) or the alkali halides NaCl I = 0.6 and KBr I = 0.46 (Jones et al. 1961). In all spinels listed the longitudinal-transverse splitting is only significant for the two high frequency modes. The sulphides and selenides have frequency band splittings about one sixth the size of those in $MgAl_2O_4$, the only exception being $CdIn_2S_4$. Also noteworthy is the much greater electronic polarizability for the covalent compounds as indicated by the high values of $\epsilon(\infty)$, (where these are unreferenced in Table 1.3 they are obtained from the oscillation models). It could then be supposed that model calculations which account for the Coulomb field but excluded polarizability would be a good approximation for $MgAl_2O_4$ but of dubious value for covalent spinels.

1.3.7 Rigid Ion Models.

Sammis (1971) used a rigid ion model to calculate elastic constants of various compounds including $MgAl_2O_4$. Central forces were included together with a scale factor for the ionic charges to account for polarizability. As the calculations were not very successful for spinel Sammis concluded that explicit account must be taken of non-central forces and polarizability.

In 1972, Striefler and Barsch reported calculations for $MgAl_2O_4$ of the Brillouin zone centre optic frequencies, elastic constants and their pressure derivatives and microscopic Gruneisen parameters. Central forces together with nominal charges were used. The short range, repulsive forces were taken to be effective between nearest neighbours for cation-oxygen interactions and out as far as the first group of neighbouring oxygens for the anion interactions. The corresponding parameters were determined from the central force equilibrium conditions, the Eg mode frequency and the two lowest infra-red frequencies. Overall agreement with experiment is fairly good although notable exceptions are the A_{1g} and highest T_{2g} modes.

Striefler and Barsch also presented the results of an extended model which included three body forces based on that of Basu and Sengupta (1968) for alkali halides. The optimization of this model was somewhat inconsistent as the central force conditions were waived and the short range parameters of the original model held constant. However the additional parameter improved the fit to the elastic constants.

Thompson (1977) extended the rigid ion model to include parametric charges and interactions between all the anion groups formed when δ is greater than zero (section 1.2) with non-central forces. Calculations were performed for Fe_3O_4 and $MgAl_2O_4$ throughout the Brillouin zone with emphasis on fitting the acoustic modes to the

inelastic neutron scattering data. Samuelson and Steinsvoll (1974) measured the lower energy dispersion curves for Fe_3O_4 using triple axis and time of flight spectrometers. Thompson (1977) measured portions of the $MgAl_2O_4$ acoustic curves with a rotating crystal time of flight spectrometer.

More detailed discussion of the $MgAl_2O_4$ models will be made in Chapter 6, by comparison with the models obtained in this work. Errors were made in the calculation of the elastic constants in both rigid ion models. Thompson classified the modes by inspection of the eigenvectors rather than by group theory which led to some inaccuracies at the zone centre.

The model fit to Fe_3O_4 dispersion curves was superior to that of $MgAl_2O_4$, a surprising result considering the more complex nature of the material, it is inverse and has electron hopping conduction. Some of the adjustable parameters however appear unlikely eg. charge on the oxygen ion of -0.9e.

It is pertinent to note that all these authors recommend the introduction of parameters to describe the polarizability of the ions.

1.4 Lower Symmetry Space Group for Spinels.

Many spinels undergo phase changes to lower symmetry structures, the olivine-spinel and ordering space group alterations have already been mentioned (see section 1.2). Magnetite (Fe_3O_4) undergoes a phase transition to a trigonal structure (Iizumi and Shirane, 1975) due to coupling between charge density and phonons. The resultant cubic lattice instability is associated with a soft mode.

Extremely common are transitions from cubic to tetragonal structures as a consequence of the pressure of transition ions with orbitally degenerate ground states eg Cu^{2+},Mn^{3+} (Dunitz and Orgel, 1957a). The Jahn-Teller effect produces local distortions to remove the degeneracy which order with reduction of temperature to produce a long range symmetry reduction (Finch,Sinha and Sinha, 1957). Although it is claimed that a Raman mode softening is associated (Siratori et al. 1965) no theoretical justification has been put forward, nor have the Raman spectra been measured through the phase transition. However, Siratori (1967) has observed softening of the lowest infra-red mode for $NiCr_2O_4$ and Fe V_2O_4, the latter accompanied by some broadening attributed to phonon relaxation. Kino et al. (1972) have observed a marked decrease in the ultrasonic velocity of the transverse mode in the [110] direction with velocity proportional to $c_{11}-c_{12}$. This was interpreted as a soft mode due coupling between electronic ordering and macroscopic strains. Similar effects have been seen in Fe_3O_4 (Moran and Luthi, 1969).

Any theoretical interpretation of crystal phase transitions requires as a minimum knowledge of the space group of one of the phases if not both. Therefore Grimes' proposal (1971,1972a) that some spinel compounds may be more accurately assigned to the space group $F\bar{4}3m$, then requires examination.

The $F\bar{4}3m$ structure may be obtained from Fd3m by allowing the

anions forming the two tetrahedra in the basis to move outwards in <111> directions by different extents in the two groups. Alternatively or accompanying the above the same space group may be obtained by small displacements of the octahedral ions in <111> directions, alternative tetrahedra of B site ions having displacements in opposite directions.

The coordinates for the basis positions are given in table 1.4. The centre of symmetry of the Fd3m structure is eliminated removing the equivalence of the two tetrahedra of anions about the A site and that of the A ions themselves. The anion positions are controlled by the x_2 and x_3 parameters which may be expressed as $^3/_8 + \delta_2$, $^7/_8 + \delta_3$, the octahedral ions by $x_1 = {}^5/_8 + \delta_1$. The Fd3m structure may be recovered by setting $\delta_2 = \delta_3$, $\delta_1 = 0$. The octahedral site symmetry has now been reduced from $\bar{3}m$ to 3m, together with the elimination of glide planes.

The change of reference space group was originally forwarded to explain the various physical behaviour of the series $Mg(Cr_xAl_{2-x})O_4$ and $Zn_{1-x}Mg_xCr_2O_4$. Both Grimes and Collett (1971a) and Tarte and Preudhomme (1963) observed increasing complexiity of infrared spectra with x until nine bands appear in $MgCr_2O_4$. Grimes and Hilleard (1969) discovered an accompanying increase in Debye Waller factor for the $Mg(Cr,Al)O_4$ series in a similar fashion to that of a Jahn Teller series. Lou and Ballentyne (1968) studying the optical fluorescence spectra of $Mg(Cr_xAl_{2-x})O_4$ single crystals found, above 2wt% of Chromium, a selection rule identifying the B site symmetry as 3m, which is incompatible with Fd3m. Electron spin measurements of Stahl-Brada and Low, (1959) also indicate trigonal distortions orientated in <111> directions about the octahedral sites. The evidence supports the view that structural distortions exist in $MgCr_2O_4$ and that the space group which is compatable with these various phenomena is $F\bar{4}3m$. This space group both contains C_{3v} symmetry for the octahedral ions and

Point Symmetry	Position Coordinates
3m	$x_1, x_1, x_1; x_1, \bar{x}_1, \bar{x}_1; \bar{x}_1, x_1, \bar{x}_1; \bar{x}_1, \bar{x}_1, x_1;$
$\bar{4}3m$	$0,0,0;$
$\bar{4}3m$	$\frac{1}{4},\frac{1}{4},\frac{1}{4};$
3m	$x_2, x_2, x_2; x_2, \bar{x}_2, \bar{x}_2; \bar{x}_2, x_2, \bar{x}_2; \bar{x}_2, \bar{x}_2, x_2;$
3m	$x_3, x_3, x_3; x_3, \bar{x}_3, \bar{x}_3; \bar{x}_3, x_3, \bar{x}_3; \bar{x}_3, \bar{x}_3, x_3;$

Atom Positions of the Basis for Spinels in Space Group F$\bar{4}$3m

TABLE 1.4

gives rise to seven infrared modes (White and DeAngelis, 1967).

Further plausibility arguments were employed to extend the range of spinels more appropriately assigned to the $F\bar{4}3m$ space group (Grimes 1972a,1973). Theoretical explanation of the increase of low frequency dielectric constants of some spinel ferrites with decreasing temperature by two to four orders of magnitude (Polder, 1950) was hampered by the impossibility of introducing the concept of permanent dipoles for an Fd3m structure. Peters and Standley (1958) found that the temperature and frequency dependence of the dielectric constant for magnesium manganese ferrite displayed behaviour very similar to that of true dielectric relaxation. An order of magnitude calculation indicated that dipole moments produced by a charge separation of the order of 0.1Å were required to explain the high frequency dielectric constant at 200°C. Grimes (1971) considered displacements of the octahedral ions in $MgCr_2O_4$ to be responsible for the change of space group. Moreover Grimes (1973) realised that these displacements in $F\bar{4}3m$ produced permanent dipole moments that were arranged in an antiferroelectric manner.

Kino and Luthi (1971) discovered a broad softening of the shear mode elastic constant around 40K for $ZnCr_2O_4$. Similar effects have been observed in other materials eg. Fe_3O_4 (Moran and Luthi 1969) and $NiFe_2O_4$ (Gibbons 1957) but these contain Jahn Teller ions. If this softening is interpreted according to the selection rules of Nowick and Heller (1965), Nowick (1968) the presence of a defect with trigonal distortion may be inferred.

Direct evidence has been sought using electron, neutron and X-ray diffraction. In principle the groups may be distinguished by the observation of reflexions of the type {hko} with $h+k = 4n\pm2, h, k$ even which are forbidden in an Fd3m structure. Such reflections have been observed in electron diffraction patterns from single crystals $MgAl_2O_4$ and $MgFe_2O_4$. Hwang et al. 1973, $MnFe_2O_4$ Berg et al, 1976.

Hwang eliminated the possibility of double diffraction by choosing a specimen with a [001] orientation. Reflections of the type h,k = 2n are the only ones occurring in the zero layer of reciprocal space and providing suitably thick crystals are selected it is impossible to obtain reflexions of type h+k = 2n±2 by double diffraction. Mishra and Thomas (1977) have reported that the forbidden reflections disappear at 450°C in $MgAl_2O_4$ and reappear on cooling. As no microstructural changes were found that could result in the transition involving two coexisting phases it was concluded that the phase transition was of the second order.

Smith (1978) has criticised these experiments because the possibility of rediffraction of strong reflections in the first order layers had been discounted. Electron diffraction experiments were performed on the mineral $Mg_{0.85}Fe_{0.15}Al_2O_4$ to demonstrate that the intensity of the (200) reflections is almost wholly due to double diffraction.

Neutron measurements have been similarly impeded by multiple diffraction effects (Thompson and Grimes, 1977b). However careful experiments by Samuelson (1974) and Samuelson and Steinsvoll (1975) showed negligible intensity for the (002) reflection in Fe_3O_4.

X-ray diffraction however is less susceptible to these effects as the spread of wavelength is much smaller. Also X-ray measurements in comparison to electron diffraction data readily lend themselves to structural analysis. Thompson (1977) pointed out that the structural analysis by Marumo et al. (1974) of Ni_2SiO_4 could be reinterpreted in terms of $F\bar{4}3m$. Eight peaks had been found in a Fourier difference synthesis map about the Ni ion lying in <111> directions. These were attributed to the charge density asphericity around the cation.

Similar X-ray data has been analysed by Thompson (1977) from a spherical single crystal mounted on a four circle diffractometer. In this case 3,968 non Friedel related reflections were collected which

could be reduced to 242 non equivalent reflections including 20 Fd3m-forbidden reflections. The overall residual factors were found to be $R = 2.6\%$ for Fd3m and $R = 2.4\%$ for $F\bar{4}3m$. Hamiltons R factor test showed that the space group $F\bar{4}3m$ could be taken as correct with 99.50% certainty.

1.5 Dynamical Calculations for $F\bar{4}3m$ Spinel.

Model calculations of the same nature as those for the Fd3m structure have not been attempted with the exception of Grimes and Collett work discussed in section 1.3.1. Grimes (1972) has made calculations of the infrared absorption frequencies assuming them to be due to a two phonon process.

The conservation of crystal momentum requires that the phonon wave vectors are related by $q_1 = \pm q_2$ with the energy conservation law simultaneously satisfied $h\nu_1 + h\nu_2 = h\nu(\text{photon})$. Absorption peaks then correspond to discontinuities in the combined density of the states produced when the sum of the slopes of the two dispersion curves involved are zero. When the wave vectors are at the Brillouin zone boundary the discontinuities may be analysed in terms of phonons at critical points on the Brillouin zone surface.

Grimes noted that if the phonons involved were acoustic then the energies of these modes at the zone boundaries calculated from elastic constants with the assumption of linear dispersion had half the energies of the infrared bands (see table 1.5).

Taking these to be the two phonon processes responsible Grimes made the tacit assumption that the structure was given by a space group such as $F\bar{4}3m$. Lax (1965) proved that any structure containing the inversion symmetry operation cannot give rise to overtone states i.e. two phonon processes involving phonons from the same branch. This has been confirmed for the Fd3m spinel structure by the group theoretical analysis of the multiphonon modes by Gashimzade and Rustamov (1975). It is possible however to form combination absorption bands not only from interactions of phonons belonging to different irreducible representations but also between phonons belonging to distinct repetitions of the same phonon branch.

Noting the general relationship between discontinuities of the density of states curve and the intersection of phonon dispersion curves

Correlation of Infrared and Phonon Energies in $MgAl_2O_4$ (after Grimes (1972b)).

TABLE 1.5

with the zone boundary Grimes found an empirical relationship for the specific heat capacity as a function of the infrared frequencies and corresponding density of states (fig.1.6)

$$C_v = 2E\left(\frac{\nu_1}{T}\right) + 2D\left(\frac{\nu_2}{T}\right) + 2E\left(\frac{\nu_3}{T}\right) + D\left(\frac{\nu_4}{T}\right)$$

where ν_1-ν_4 are the infrared frequencies in wave numbers in order of descending magnitude, E and D are Einstein and Debye functions respectively.

This formula fits experimental data within experimental uncertainty and also was adequate for the sensible estimation of the lattice contribution of various ferrites (Grimes 1974).

Fig 1.6 Density of States (after Grimes,1972b)

1.6 Outline of Present Work.

Despite the extensive range of infrared spectra, increasing quantity of Raman data and large number of elastic constant measurements available for spinels very little attempt has been made to consider these measurements as aspects of a single vibrational spectrum of a particular material. Dynamical models for covalent spinels have been restricted to the calculation of Brillouin zone centre frequencies without extension to calculation of other quantities such as macroscopic tensors. Partly this is due to lack of experimental data, measurements of selenium and sulphide spinels generally post dating those on the more ionic oxide spinels.

The situation is somewhat better for $MgAl_2O_4$ and Fe_3O_4 where the infrared and Raman spectra, elastic constants and specific heat capacity have been measured, including the longitudinal mode frequencies of the infrared band for $MgAl_2O_4$. These compounds are the only spinels for which dispersion curves have been extensively measured (Watanabe and Brockhouse 1962, Samuelson and Steinsvoll 1974 on Fe_3O_4 and Thompson and Grimes 1977c on $MgAl_2O_4$).

These ionic materials require models which take explicit account of the long range Coulomb force. Rigid ion models have been proposed by Striefler and Barsch (1972) and Thompson (1977) but it is the opinion of all these authors that improvements are expected by the inclusion of polarizability terms.

In Chapter 2 the background theory to the various models is presented for which this author takes no credit. Chapter 3 is concerned with the group theoretical analysis of the vibrational modes necessary for the identification of the various branches of the dispersion curves for a complex material. Also derived are soft modes for second order phase transitions to near cubic tetragonal structures together with the identification of the irreducible representation associated with the $Fd3m$-$F\bar{4}3m$ phase transition. Chapter 4 presents

some new measurements of the low energy dispersion curves for $MgAl_2O_4$ obtained from inelastic neutron scattering. Finally two rigid ion and shell models for $MgAl_2O_4$ are described in Chapter 5. Chapter 6 contains discussion and conclusions drawn from the work presented.

CHAPTER 2

LATTICE DYNAMICS THEORY.

2.1 Born-von Karman Theory.

The Born-von Karman formalism (Born & Huang, 1954) is based on the assumptions of the existence of a crystal potential function which describes the binding of the atoms and the adiabatic approximation. The latter requires that the electrons instantaneously follow the nuclear motions. These continuous adjustments occur if the frequencies of the nuclear motions are much smaller than those of the electronic transition frequencies. The approximation is therefore valid for materials with a large band gap. The crystal is considered as perfect, infinite in extent and stress free. Also it is supposed the crystal is at OK and zero point effects may be ignored. The temperature conditions ensure that the equilibrium configuration of the crystal corresponds to a minimisation of the potential energy when the previous assumptions are imposed.

The equilibrium position of the κ^{th} nucleus in the ℓ^{th} cell is given by

$$r(\ell,\kappa) = r(\ell) + r(\kappa) \qquad (2.1)$$

where

$$r(\ell) = \ell_1 a_1 + \ell_2 a_2 + \ell_3 a_3 \qquad (2.2)$$

$\kappa = 1,2 \ldots n$, n being the number of atoms in the primitive unit cell, ℓ_1,ℓ_2,ℓ_3 are integers and a_1,a_2,a_3 are the basis vectors of the crystal lattice.

For small displacements $u(\ell,\kappa)$ of the ions from their equilibrium positions the crystal potential may be expressed in a Taylor expansion

$$\Phi = \Phi_0 + \Phi_1 + \Phi_2 + \ldots \tag{2.3}$$

where

$$\Phi_1 = \sum_{\ell\kappa\alpha} \left(\frac{\partial\Phi}{\partial u_\alpha(\ell,\kappa)}\right)_0 u_\alpha(\ell,\kappa) \tag{2.4}$$

$$\Phi_2 = \sum_{\ell\kappa\alpha}\sum_{\ell'\kappa'\beta} \left(\frac{\partial^2\Phi}{\partial u_\alpha(\ell,\kappa)\,\partial u_\beta(\ell'\kappa')}\right)_0 u_\alpha(\ell,\kappa)u_\beta(\ell',\kappa') \tag{2.5}$$

The derivatives are evaluated at the equilibrium positions of the atoms. This expansion is valid for most solids with the exception of helium where the root mean square displacement is 30% of the lattice constant.

The Φ_0 term is a potential reference level and may be scaled to zero. The first order term $\Phi_1 = 0$ since the crystal is considered to be in equilibrium with the atoms at their rest positions $r(\ell\kappa)$. If the potential had been expanded with respect to displacements from rest positions which were not the equilibrium positions the Φ_2 term would not necessarily be zero. This is important in the study of the temperature dependence of the structure of crystals in which the atom positions are not determined by symmetry alone (Leibfried and Ludwig 1961) and the effects of externally imposed stresses and strains on crystal properties (Ganesan et al. 1970),

In the harmonic approximation the series is cut off after the Φ_2 term as higher order terms are considered small in comparison to Φ_2 and neglected. The crystal potential is now completely described by the second order differential term of the series expansion. Truncation after the second order term means that in this formalism crystals would have elastic constants which are temperature and pressure independent, zero thermal expansion and zero thermal conductivity (Peierls 1955).

The α component of the force on atom $(\ell\kappa)$ is

$$F_\alpha(\ell\kappa) = - \frac{\partial \Phi}{\partial u_\alpha(\ell,\kappa)} \tag{2.6}$$

and so the equation of motion for this atom of mass m_κ for a displacement in the α direction is given by

$$m_\kappa \ddot{u}_\alpha(\ell,\kappa) = - \sum_{\ell'\kappa'\beta} \phi_{\alpha\beta}(\ell k, \ell' k') u_\beta(\ell'\kappa') \tag{2.7}$$

where

$$\phi_{\alpha\beta}(\ell\kappa,\ell'\kappa') = \left(\frac{\partial \Phi}{\partial u_\alpha(\ell\kappa)\partial u_\beta(\ell'\kappa')}\right)_o \tag{2.8}$$

The equation of motion is similar in form to Hooke's Law governing the small amplitude extension of a spring.

The quantities $\phi_{\alpha\beta}$ act as force constants giving the negative of the force in the direction α on atom $(\ell\kappa)$ due to a small unit displacement of atom $(\ell'\kappa')$ in the β direction.

Symmetry properties of the crystal lattice and invariance conditions impose restrictions on the indices in $\phi_{\alpha\beta}$'s which limit the number of actually independent force constants. Newton's third law requires

$$\phi_{\alpha\beta}(\ell\kappa,\ell'\kappa') = \phi_{\beta\alpha}(\ell'\kappa',\ell\kappa) \tag{2.9}$$

Translational periodicity of the lattice requires physical quantities such as potential to be invariant after a lattice translation. Thus $\phi_{\alpha\beta}(\ell\kappa,\ell'\kappa')$ depends only on the relative cell indices $\ell-\ell'$ and not on ℓ and ℓ' independently.

As the net force on an atom is zero after a uniform translation of the entire crystal the potential function must also be invariant against any arbitrary translation. Consider the expansion

$$\frac{\partial \Phi}{\partial u_\alpha(\ell\kappa)} = \phi_\alpha(\kappa) + \sum_{\ell'\kappa'\beta} \phi_{\alpha\beta}(\ell\kappa,\ell'\kappa') u_\beta(\ell'\kappa') \tag{2.10}$$

If all the nuclei are displaced by the same arbitrary vector

$u_\beta(\ell'\kappa') = \epsilon_\beta$ and since $\frac{\partial \Phi}{\partial u_\alpha(\ell\kappa)}$ remains unchanged we have

$$\sum_{\ell'\kappa'} \phi_{\alpha\beta}(\ell\kappa,\ell'\kappa') = 0 \tag{2.11}$$

Therefore the terms $\phi_{\alpha\beta}(\ell\kappa,\ell\kappa)$ is not considered as a second order differential term but is defined by the summation

$$\phi_{\alpha\beta}(\ell\kappa,\ell\kappa) = - \sum_{\ell'\kappa'}{}' \phi_{\alpha\beta}(\ell\kappa,\ell'\kappa') \tag{2.12}$$

where the prime on the summation indicates that terms $\ell'\kappa' = \ell\kappa$ are excluded. The self force constant is the negative sum of force constants describing the forces acting on a particular atom due to all other atoms.

Because of the periodicity of the lattice plane wave solutions for $u_\alpha(\ell\kappa)$ in equation (2.7) may be assumed

$$u_\alpha(\ell\kappa) = m_\kappa^{-\frac{1}{2}} U_\alpha(\kappa q)\exp(iq.r(\ell\kappa)-i\omega(q)t) \tag{2.13}$$

where q is the wave vector of the travelling wave of circular frequency $\omega(q)$. Substitution in equation (2.7) leads to

$$\omega^2(q)U_\alpha(\kappa q) = \sum_{\kappa'\beta'} D_{\alpha\beta}(\kappa\kappa',q)U_\beta(\kappa' q) \tag{2.14}$$

or in matrix notation

$$\omega^2 U = [D]U \tag{2.15}$$

where the elements of the dynamical matrix are given by

$$D_{\alpha\beta}(\kappa\kappa',q)=(m_\kappa m_{\kappa'})^{-\frac{1}{2}} \sum_{\ell'} \phi_{\alpha\beta}(\ell\kappa,\ell'\kappa')\exp(iqr(\ell'\kappa',\ell\kappa)) \tag{2.16}$$

with

$$r(\ell'\kappa',\ell\kappa) = r(\ell'\kappa') - r(\ell\kappa) \tag{2.17}$$

The infinite number of simultaneous equations in (2.7) have now been reduced to a set of 3n equations where n is the number of atoms in the primitive unit cell. The condition for solubility is

$$|[D] - \omega^2 \delta_{\alpha\beta}\delta_{\kappa\kappa'}| = 0 \tag{2.18}$$

The $3n$ solutions are the eigenvalues $\omega^2(qj)$, for each value of which there are a set of values for the displacements $U_\alpha(\kappa q,j)$. The eigenvectors of [D], $e(\kappa q,j)$ describe the displacement pattern in the mode of wavevector q, branch j ($j = 1,2 \ldots 3n$).

As a direct consequence of Newton's third law (2.9)

$$D^*_{\alpha\beta}(\kappa\kappa' q) = D_{\beta\alpha}(\kappa'\kappa\, q) \qquad (2.19)$$

where the asterisk denotes complex conjugation. Thus the dynamical matrix is Hermitian and therefore has real eigenvalues ω^2. In order that the crystal is stable the $\omega(qj)$ must also be real since from (2.13) it is seen that the vibration amplitudes will otherwise increase exponentially along the positive or negative direction of the time axis. The condition for this is that the principal minors of the dynamical matrix should be positive.

The appearance of three of the modes which tend to zero frequency linearly as q tends to zero is due to the translational invariance condition. These modes are the acoustic modes. The remaining $3n-3$ modes which tend to a finite limit at infinite wavelengths ($q = 2\pi/\lambda$) are called the optic modes.

2.2 Quantum Treatment.

A quantum mechanical approach yields essentially the same results as the above classical method but is useful for connecting lattice dynamics with neutron scattering results. This outline follows Ziman, 1960 and Venkateraman et al. 1974.

The Hamiltonian is expressed in terms of displacements $u(\ell\kappa)$ and momentum $p(\ell\kappa)$

$$H = \sum_{\ell\kappa\alpha} \frac{p_\alpha^2(\ell\kappa)}{2m} + \sum_{\ell\kappa\ell'\kappa'\alpha\beta} u(\ell\kappa)\phi_{\alpha\beta}(\ell\kappa\ell'\kappa')u(\ell'\kappa') \qquad (2.20)$$

This is transformed to a more convenient form using

$$Q_\alpha(\kappa q) = (m_\kappa/N)^{-\frac{1}{2}} \sum_{\ell} u(\ell\kappa)\exp(iqr(\ell\kappa)) \tag{2.21}$$

$$P_\alpha(\kappa q) = (Nm_\kappa)^{-\frac{1}{2}} \sum_{\ell} \dot{p}_\alpha(\ell\kappa)\exp(-iqr(\ell,\kappa)) \tag{2.22}$$

$$\omega^2(qj)e_\alpha(\kappa qj) = \sum_{\kappa'\beta} D_{\alpha\beta}(\kappa\kappa' q) \; e_\beta(\kappa' qj) \tag{2.23}$$

which, when substituted, leads to

$$H = \tfrac{1}{2}\sum_{q\kappa\alpha} P_\alpha^*(\kappa q)P_\alpha(\kappa q) + \tfrac{1}{2}\sum_{q\kappa\kappa'\alpha\beta} Q_\alpha^*(\kappa q)D_{\alpha\beta}(\kappa\kappa', q)Q(\kappa' q) \tag{2.24}$$

Now defining

$$Q(qj) = \sum_{\kappa\alpha} Q_\alpha(\kappa q)e_\alpha^*(\kappa qj) \tag{2.25}$$

$$P(qj) = \sum_{\kappa\alpha} P_\alpha(\kappa q)\; e_\alpha(\kappa q \tag{2.26}$$

we may obtain

$$H = \tfrac{1}{2}\sum_{qj} \left\{ P^*(qj)P(qj) + \omega^2(qj)Q^*(qj)Q(qj) \right\} \tag{2.27}$$

Thus we have used (2.23) regardless of the problem being quantum mechanical. The quantity $Q(qj)$ is the normal coordinate and $\omega(qj)$ the normal mode frequencies. In the quantum approach u,p,Q and P are all regarded as operators.

The form of the Hamiltonian (2.27) is that of the sum of the Hamiltonians of $3nN$ harmonic oscillators.

Introducing new operators $a(qj)$ and $a^+(-qj)$ by (Maradudin et al. 1971)

$$Q(qj) = \left(\frac{\hbar}{2\omega(qj)}\right)^{\frac{1}{2}} (a(qj)+a^+(-qj)) \tag{2.28}$$

$$P(qj) = i\left(\frac{\hbar\omega(qj)}{2}\right)^{\frac{1}{2}} (a(qj)-a^+(-qj)) \tag{2.29}$$

Then

$$H = \sum_{qj} \frac{\hbar\omega(qj)}{2} \left(a(qj)a^{+}(qj)+a^{+}(qj)a(qj)\right) \tag{2.30}$$

and $$E = \sum_{qj} \hbar\omega(qj)\left(n(qj)+\tfrac{1}{2}\right) \tag{2.31}$$

and in terms of the normal mode coordinate the displacement in mode (qj) is written

$$u_{\alpha}(\ell\kappa) = (Nm_{\kappa})^{-\frac{1}{2}} \sum_{qj} e_{\alpha}(\kappa qj)Q(qj)\exp(iq.r(\ell\kappa)) \tag{2.32}$$

The annihilation a(qj) and creation $a^{+}(qj)$ operators follow the standard relationships

$$a^{+}(qj)|n(qj)\rangle = (n(qj)+1)^{\frac{1}{2}}|n(qj)+1\rangle \tag{2.33}$$

$$a(qj)|n(qj)\rangle = (n(qj))^{\frac{1}{2}}|n(qj)-1\rangle \tag{2.34}$$

$$\langle a^{+}(qj)a(qj)\rangle_{T} = \langle n(qj)\rangle_{T} = \left(\exp\left(\frac{\hbar\omega(qj)}{k_{B}T}\right) - 1\right)^{-1} \tag{2.35}$$

where $\langle O\rangle_{T}$ is the thermodynamic average of operator O. This formalism is useful in describing the deexcitation and excitation of oscillators by external sources such as thermal neutrons.

The quantum treatment permits two equivalent interpretations. Either the crystal is a set of 3nN distinguishable oscillators each being in various states labelled by n(qj) = 0,1, ... and $E(qj) = [n(qj)+\tfrac{1}{2}]\hbar\omega_{j}(q)$. Alternatively the crystal may be described as a set of indistinguishable particles (phonons) labelled by quantum numbers (q,j), the number in any state being given by n(qj).

2.3 Rigid Ion Model.

In the previous sections the explicit form of the potential has not been considered. Some numerical calculations have been undertaken in which the force constants $\phi_{\alpha\beta}$ are treated as disposable parameters varied to fit the available experimental data. This approach

is most commonly found in calculations for covalent crystals such as Germanium (Herman, 1959). The situation for metals is more satisfactory where pseudopotentials are employed (Harrison 1966). Cowley (1962b) has shown that the form of the equations of motion from a first order perturbation quantum mechanical theory (based on work by Mashkevich, 1961) is equivalent to those obtained by a phenomenological approach for ionic and covalent crystals. However it is generally impossible to obtain the matrix elements required from first principles. Any form of potential assumed for ionic crystals is therefore likely to be an oversimplification.

In ionic crystals the potential energy may be considered as arising from two sources (i) the long range Coulomb potential, the form of which is well known, tending to collapse the crystal and (ii) a short range overlap potential of nearby ions tending to explode the crystal.

The Rigid Ion model of Kellermann (1940) is the most simple model to use this kind of potential. The ions are considered as rigid and unpolarizable. The Coulomb potential is then considered only to act between point charges and may be calculated to any desired degree of accuracy. The short range interactions may be described by functional forms of the potential such as $b\exp(-r/\rho)$ or $br^{-\rho}$ with b and ρ determined by comparison with experiment or used as disposable parameters.

It is assumed the two contributions to the potential are independent and separable allowing the total potential to be written as

$$\Phi = \Phi^{C} + \Phi^{R} \tag{2.36}$$

where C and R represent the Coulomb and short range contributions respectively. Similarly for the dynamical matrix

$$D_{\alpha\beta}(\kappa\kappa',q) = D^{C}_{\alpha\beta}(\kappa\kappa',q) + D^{R}_{\alpha\beta}(\kappa\kappa',q) \tag{2.37}$$

The Coulomb contribution can be written in terms of the dimensionless coefficients $C_{\alpha\beta}(\kappa\kappa'q)$ introduced by Kellermann (1940) which only depend on the crystal structure

$$D^{C}_{\alpha\beta}(\kappa\kappa' q)=(m_{\kappa}m_{\kappa'})^{-\frac{1}{2}}\frac{e^2}{v_a}Z_{\kappa}Z_{\kappa'}C_{\alpha\beta}(\kappa\kappa' q)-\delta_{\kappa\kappa'}\frac{e^2}{v_a}\frac{Z_{\kappa}}{m_{\kappa}}\sum_{\kappa''}Z_{\kappa''}C_{\alpha\beta}(\kappa\kappa'',q=0) \tag{2.38}$$

where Z_{κ} is the change on ion κ per electron and v_a is the volume of the primitive unit cell. The final term in (2.38) arises from the translational invariance of the lattice. The Coulomb force constants are given by

$$\phi^{C}_{\alpha\beta}(\ell\kappa,\ell'\kappa') = -Z_{\kappa}Z_{\kappa'}\frac{\partial^2}{\partial u_{\alpha}(\ell\kappa)\partial u_{\beta}(\ell'\kappa')}\frac{1}{|r(\ell'\kappa')-r(\ell\kappa)|} \tag{2.39}$$

with

$$C_{\alpha\beta}(\kappa\kappa' q) = -\sum_{\ell'}{}'\frac{\partial^2}{\partial u_{\alpha}(\ell\kappa)\partial u_{\beta}(\ell'\kappa')}\frac{\exp(iq[r(\ell'\kappa')-r(\ell\kappa)])}{|r(\ell'\kappa')-r(\ell\kappa)|} \tag{2.40}$$

The short range contribution may be reduced to a similar dimensionless matrix $R_{\alpha\beta}(q\kappa\kappa')$ using two parameters A and B where

$$A = \frac{2V_a}{e^2}\left(\frac{\partial}{\partial r^2}\phi(|r|)\right)_{11}, \quad B = \frac{2v_a}{e^2}\left(\frac{\partial^2\phi(|r|)}{\partial r^2}\right)_{\underline{1}} \tag{2.41}$$

where A is evaluated parallel to the line joining the ions and B perpendicular. Thus

$$D^{R}_{\alpha\beta}(\kappa\kappa' q) = (m_{\kappa}m_{\kappa'})^{-\frac{1}{2}}\frac{e^2}{v_a}R_{\alpha\beta}(\kappa\kappa' q) \tag{2.42}$$

where

$$\phi^{R}_{\alpha\beta} = -\tfrac{1}{2}\left[\frac{r_{\alpha}r_{\beta}}{r^2}(A-B) + \delta_{\alpha\beta}B\right] \tag{2.43}$$

with indices $(\ell\kappa\ell'\kappa')$ suppressed

$$R_{\alpha\beta}(\kappa\kappa' q) = \sum_{\ell}\phi^{R}_{\alpha\beta}(\ell\kappa\ell'\kappa')\exp(iq[r(\ell'\kappa')-r(\ell\kappa)]) \tag{2.44}$$

In matrix notation the dynamical matrix may be written as

$$D = \frac{e^2}{v_a}\left[M^{-\frac{1}{2}}\right]\left[ZCZ+R\right]\left[M^{-\frac{1}{2}}\right] \tag{2.45}$$

where D is Hermitian of order $3n$, Z and M are diagonal containing the ionic charges and the square roots of the masses respectively. The results of this section apply for general wave vectors greater than $q = 0$, but not at $q = 0$ itself, because of the problem of the divergence

of the Coulomb series in the limit of infinite wavelengths. The comparison of macroscopic quantities with the theory in this region and the mathematical method used to overcome this difficulty is discussed in section 2.5.

One macroscopic quantity which may be evaluated directly for the Rigid Ion model is the high frequency dielectric constant $\epsilon(\infty)$. The polarization of a crystal may be approximated by the polarizabilities α_i of the ions with the local electric fields E_i

$$P = \sum_i N_i \alpha_i E_i \qquad (2.46)$$

and with the susceptibility given by $\chi = P/E$

$$\epsilon(\infty) = 1+4\pi\chi \qquad (2.47)$$

Therefore if the ions are unpolarizable ($\alpha_i = 0$) the dielectric constant has a value of unity.

2.4 Shell Model.

To overcome the limitations of the Rigid Ion model with respect to the high frequency dielectric constant, various models which take account of polarizability have been developed. The first, by Lyddane and Herzfeld (1938), assigned an electronic polarizability α_κ to each ion and included the induced dipoles in the equations of motion. Using the then available values of α_κ the model was unstable. It was apparent that another polarization mechanism, believed due to the short range overlap potential must also be included. Dick and Overhauser (1958) suggested that each atom could be considered to consist of a non polarizable core linked by a harmonic spring to a spherical shell representing the outer electrons. The overlap interaction was found to have the form $b\exp(-r/\rho)$ where r is the intershell distance rather than the internuclear separation. In general the effect of this interaction is to reduce the electronic polarization induced by the electric field. Dick and Overhauser also suggest a further polarization mechanism.

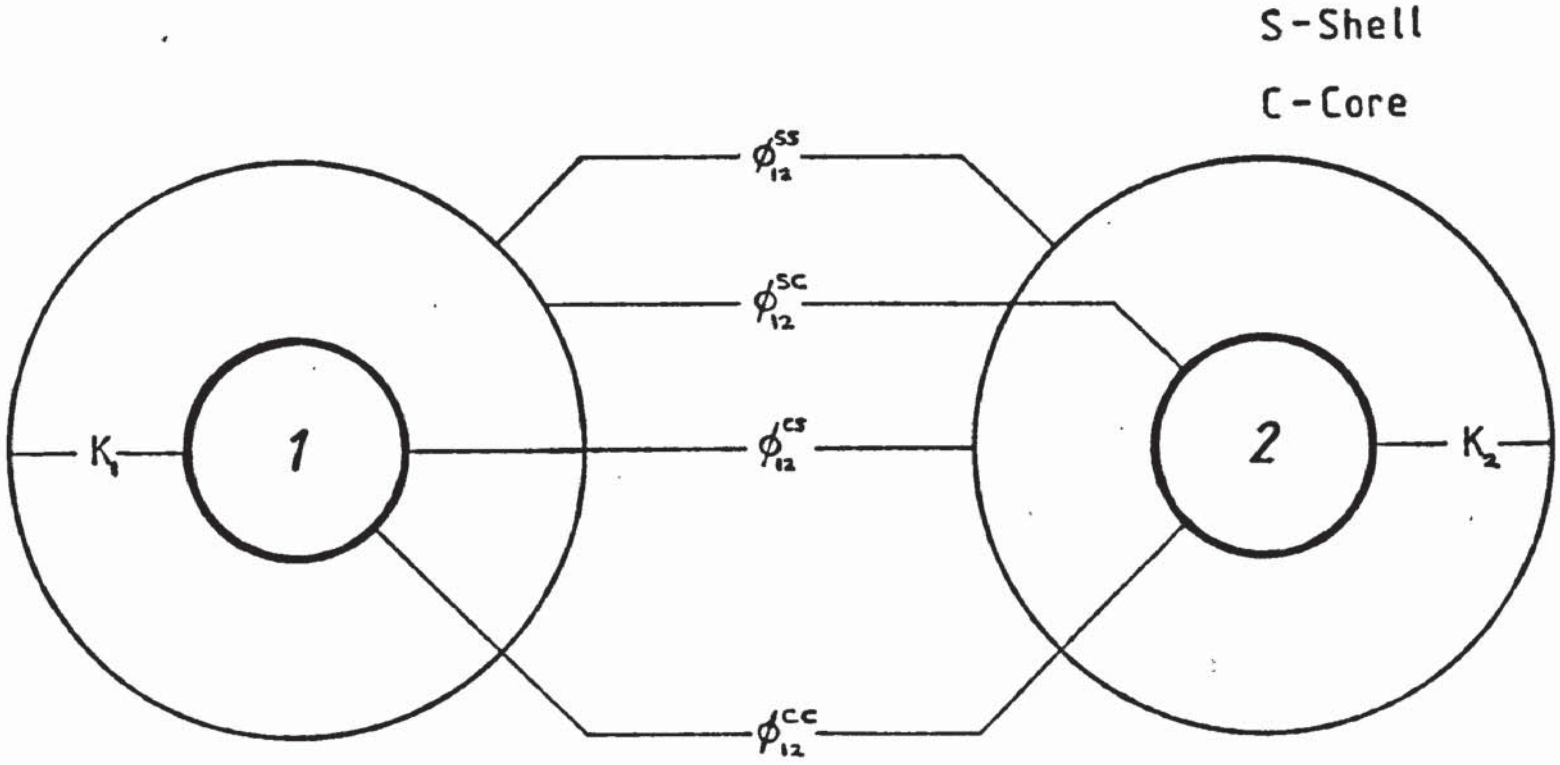

Fig 2.1 Shell Model Interactions

Due to Pauli's exclusion principle the electron density in the overlap region is reduced and may be represented by a point "exchange charge". This is then compensated by an adjustment of the shell charges. This model was developed by Cochran and co-workers (Cochran 1959, Woods et al. 1960) for ionic crystals. The exchange charge mechanism was not explicitly included but in effect was considered as contributing to the dipole distortion. Short range core-core and core-shell interactions were introduced. Subsequently several further modifications have been introduced such as the breathing shell model (Schroder 1966), the incorporation of three body forces (Basu and Sengupta, 1968) and the deformable shell model (Hardy 1962).

The model used in this study is based on that for sodium chloride with only the anions polarizable (Woods et al. 1960).

For an atom κ the ionic charge Z_κ may be expressed as the sum of shell charge Y_κ and core charge X_κ. Each core is linked to its shell by a force constant $K_{\alpha\beta}(\kappa)$ which is not assumed to be isotropic. The other force constants are denoted by

$$\phi^{ij}_{\alpha\beta}(\ell\kappa,\ell'\kappa') = \left(\frac{\partial^2\Phi}{\partial u_\alpha^i(\ell\kappa)\,du_\beta^j(\ell'\kappa')}\right)_o \qquad (2.48)$$

where i,j = c,s where c denotes core and s denotes shell. $\phi^{ij}(\ell\kappa,\ell'\kappa')$ denotes the coupling of i of atom $(\ell\kappa)$ with j of $(\ell'\kappa')$ with

$$\phi^{ij}_{\alpha\beta}(\ell\kappa,\ell'\kappa') = 0 \text{ for } i \neq j \qquad (2.49)$$

as this is already denoted by $K_{\alpha\beta}(\kappa)$. The short range forces are indicated in figure (2.1). The long range Coulomb forces are described by Kellermann's coefficients (equation (2.40)). Newton's third law is taken into account by having the force constants symmetric in the sets of indices $(i\ell\kappa)$, $(j\ell'\kappa')$.

With the definitions for $(\ell\kappa) \neq (\ell'\kappa')$

$$\begin{aligned}\phi^{AA} &= \phi^{CC} + \phi^{CS} + \phi^{SS}\\ \phi^{AD} &= \phi^{CS} + \phi^{SS}\end{aligned} \qquad (2.50)$$

$$\phi^{DA} = \phi^{SC} + \phi^{SS}$$
$$\phi^{DD} = \phi^{SS}$$

the potential in the harmonic approximation is now given by

$$\Phi_2 = \tfrac{1}{2} \sum_{\ell\kappa\alpha} \sum_{\ell'\kappa'\beta} \Big\{ \phi^{AA}_{\alpha\beta}(\ell\kappa,\ell'\kappa') u_\alpha(\ell\kappa) u_\beta(\ell'\kappa') + \phi^{AD}_{\alpha\beta}(\ell\kappa,\ell'\kappa') u_\alpha(\ell\kappa) w(\ell'\kappa')$$
$$+ \phi^{DA}_{\alpha\beta}(\ell\kappa,\ell'\kappa') w_\alpha(\ell\kappa) u_\beta(\ell'\kappa') + \phi^{DD}_{\alpha\beta}(\ell\kappa,\ell'\kappa') w_\alpha(\ell\kappa) w_\beta(\ell'\kappa') \Big\}$$
$$+ \tfrac{1}{2} \sum_{\ell\kappa\alpha\beta} K_{\alpha\beta}(\kappa) w_\alpha(\ell\kappa) w_\beta(\ell\kappa) \qquad (2.51)$$

where A indicates atoms and D induced dipoles.

To maintain the adiabatic approximation the mass of the shells is assumed to be zero. The equations of motion then become

$$m_\kappa \ddot{u}_\alpha(\ell\kappa) = - \frac{\partial\Phi}{\partial u_\alpha(\ell\kappa)}$$
$$0 = \frac{\partial\Phi}{\partial w_\alpha(\ell\kappa)} \qquad (2.52)$$

Using wave solutions

$$u_\alpha(\ell\kappa) = m_\kappa^{-\frac{1}{2}} U_\alpha(\kappa q) \exp(iqr(\ell\kappa) - i\omega(q)t)$$
$$w_\alpha(\ell\kappa) = m_\kappa^{-\frac{1}{2}} W_\alpha(\kappa q) \exp(iqr(\ell,\kappa) - i\omega(q)t) \qquad (2.53)$$

and the following definitions (a) for the short range parts of the potentials

$$D^{ij}_{\alpha\beta}(\kappa\kappa' q) = \sum_{\ell'} \phi^{ij,SR}_{\alpha\beta}(\ell\kappa\ell'\kappa') \exp(iq(r(\ell\kappa) - r(\ell'\kappa'))$$

i,j = A,D

$$R_{\alpha\beta}(\kappa\kappa' q) = D^{AA}_{\alpha\beta}(\kappa\kappa' q)$$
$$T_{\alpha\beta}(\kappa\kappa' q) = D^{AD}_{\alpha\beta}(\kappa\kappa' q) \qquad (2.54)$$
$$\mathcal{S}_{\alpha\beta}(\kappa\kappa' q) = D^{DD}_{\alpha\beta}(\kappa\kappa' q) + \delta_{\kappa\kappa'} K_{\alpha\beta}(\kappa)$$

(b) for the Coulomb part;

$$\begin{aligned} [ZCZ] &= [D^{AA,C}] \\ [ZCY] &= [D^{AD,C}] \\ [YCZ] &= [D^{DA,C}] \\ [YCY] &= [D^{DD,C}] \end{aligned} \tag{2.55}$$

the equations of motion can be rewritten in matrix form as

$$\begin{aligned} \omega^2(q)U &= [M^{-\frac{1}{2}}][R+ZCZ][M^{-\frac{1}{2}}]U + [M^{-\frac{1}{2}}][T+ZCY][M^{-\frac{1}{2}}]W \\ 0 &= [\tilde{T}^* + YCZ]U + [\mathcal{S} + YCY]W \end{aligned} \tag{2.56}$$

This is, eliminating W

$$\omega^2(q)U = [M^{-\frac{1}{2}}]\{[R+ZCZ] - [T+ZCY][\mathcal{S}+YCY]^{-1}[\tilde{T}^*+YCZ]\}[M^{-\frac{1}{2}}]U \tag{2.57}$$

The final term in the braces is the correction to the Rigid Ion model for polarizability. This equation may be further simplified using approximations introduced by Cowley et al. (1963). To represent all the short range forces as interacting through the shells it is assumed that $T \equiv R$ for all q and $\mathcal{S} = R+K$. In particular $T \equiv R$ for $q = 0$ removes the overdetermination involved in specifying the polarizability in terms of the shell charge Y together with the relative core-shell displacement w. This approximation has also been successfully used for the relatively complex material, $SrTiO_3$ (Cowley, 1964).

2.5 Macroscopic Quantities.

In the long wavelength limit the equations and quantities of the dynamical theory must be directly related to those of the marcoscopic treatment. For ionic crystals some mathematical difficulties are incurred due to the long range nature of the Coulomb interaction. The electrical and mechanical effects are impossible to separate because the actual ionic motions set up an electric field. Therefore the stress ($S_{\alpha\beta}$) tensor is not related to the strain ($s'_{\alpha\beta}$) tensor through Hooke's law but instead is given by

$$S_{\alpha\gamma} = \sum_{\beta\gamma} c_{\alpha\gamma,\beta\lambda}\, s_{\beta\lambda} - \sum_{\beta} e_{\beta,\alpha\gamma}\, E_{\beta} \qquad (2.58)$$

and also the dielectric polarization P_α is given by

$$P_{\alpha} = \sum_{\beta\gamma} e_{\alpha,\beta\gamma}\, s_{\beta\gamma} + \sum_{\beta} a_{\alpha\beta}\, E_{\beta} \qquad (2.59)$$

where c,e,a and E are the elastic, piezoelectric, dielectric susceptability tensors and the macroscopic electric field respectively. The macroscopic equation of motion for a plane wave travelling through the medium is then

$$\rho\omega^2 \bar{u}_\alpha = \sum_{\beta} \Big(\sum_{\gamma\lambda} c_{\alpha\gamma,\beta\lambda}\, q_\lambda q_\gamma \Big) \bar{u}_\beta + i \sum_{\beta} \Big(\sum_{\gamma} e_{\beta,\alpha\gamma} q_\gamma \Big) \bar{E}_\beta \qquad (2.60)$$

A further complication is the irregularity of the Coulomb contribution in the long wavelength limit the magnitude of which depends on the direction from which the origin of reciprocal space is approached. This is overcome by recognising that the irregular part is related to the macroscopic electric field of the crystal and may be separated out from the dynamical equations of motion (Huang, 1949). For the shell model the equations may be rewritten as

$$\begin{aligned} A\,\omega^2\,U &= AU + BW - ZE \\ 0 &= CU + DW - YE \end{aligned} \qquad (2.61)$$

where, for example, matrix A corresponds to [R+ZCZ] of (2.56) after separation of the macroscopic electric field E. A perturbation technique, "the method of long waves" (Born and Huang, 1954), can then be used to obtain expressions for the macroscopic tensors in terms of the dynamical theory quantities. The matrices, after separation of the electric field, are expanded in the form

$$G(\epsilon q) = G(q=0) + i\epsilon \sum_{\gamma} G_{\gamma}^{(1)} q_{\gamma} + \frac{\epsilon^2}{2} \sum_{\gamma\lambda} G_{\gamma\lambda}^{(2)} q_{\gamma} q_{\lambda} \qquad (2.62)$$

where ϵ is the expansion parameter and $A_{\gamma}^{(1)}$ is the first derivative of A with respect to q_{γ} etc.

Cowley (1962c) has performed these calculations for the shell model. Only the main results will be given here and the effects of polarization indicated. The expression for the elastic constant is

$$c_{\alpha\beta,\gamma\lambda} = [\alpha\beta,\gamma\lambda] + [\beta\gamma,\alpha\lambda] - [\beta\lambda,\alpha\gamma] + (\alpha\gamma,\beta\lambda) \qquad (2.63)$$

where the square brackets correspond to contributions from external strain and the round brackets from internal strain. The square bracket term is given by

$$[\alpha\beta,\gamma\lambda] = (8\pi^2 v_a)^{-1} \sum_{\kappa\kappa'} A_{\alpha\beta,\gamma\lambda}^{(2)} (\kappa\kappa', q=0) \qquad (2.64)$$

and surprisingly does not contain any contribution from polarization. The round bracket term is given by the much more complex expression

$$(\alpha\gamma,\beta\lambda) = -(4\pi^2 v_a)^{-1} \sum_{\kappa\kappa'} \left[\tilde{F}_{\gamma}^{(1)} L^{(0)-1} F_{\lambda}^{(1)} + \tilde{C}_{\gamma}^{(1)} D^{(0)-1} C_{\lambda}^{(1)} \right]_{\alpha\beta} \qquad (2.65)$$

where the $(\kappa\kappa', q=0)$ indices have been suppressed. $L^{(0)-1}$ is the pseudo-inverse of the dynamical matrix formed by deleting three rows and columns, inverting the resultant $(3n-3) \times (3n-3)$ matrix, and replacing the three rows and columns with all elements set at zero. This device must be employed because the translational invariance condition makes the actual dynamical matrix singular. The matrix F_{γ}^{1} is defined by

$$F_{\gamma}^{(1)} = A_{\gamma}^{(1)} - B^{(0)} D^{(0)-1} C_{\gamma}^{(1)} \qquad (2.66)$$

For the Rigid Ion model equation (2.65) reduces as the second term of the right hand side is zero, the correction terms in the dynamical matrix are also zero and $F_{\gamma}^{(1)} \equiv A_{\gamma}^{(1)}$.

In crystals for which every ion is at a centre of symmetry

equation (2.63) is simplified as all round bracket terms are then zero.

The high frequency dielectric tensor is given by

$$\epsilon_{\alpha\beta}(\infty) + 1+4\pi \sum_{\kappa\kappa'} Y[\mathcal{S}(\kappa\kappa',q=0)+Y\ C(\kappa\kappa',q=0)Y\ ]^{-1}_{\alpha\beta}\ Y \qquad (2.67)$$

where C refers to the matrix of Kellermann coefficients. To reduce to the Rigid Ion model set Y = 0 and K = ∞ in the definition of $\mathcal{S}$ (equation 2.54) and the dielectric constant becomes unity in agreement with previous remarks.

The low frequency dielectric constant may be obtained from the Lyddane-Sachs-Teller (1941) relation as generalised by Cochran and Cowley (1962). For cubic materials this becomes

$$\frac{\epsilon_{\alpha\alpha}(0)}{\epsilon_{\alpha\alpha}(\infty)} = \prod_{s(n-1)} \frac{\omega_L(q=0)}{\omega_T(q=0)} \qquad (2.68)$$

where L and T refer to modes that have dipole moments lying either along the direction of propagation (longitudinal) or perpendicular to it (transverse modes). It is emphasised that, even in a cubic material, these modes may involve ionic motions in neither of these directions provided that these motions do not produce a non zero dipole moment.

Finally it is noted that in general it is impossible to obtain an explicit expression for the electronic polarizability of the ions. Only in the case of diagonally cubic crystals (i.e. crystals in which each ion is in an environment of at least tetrahedral symmetry) can the electronic contribution to the polarization of the crystal be written in terms of a product $\alpha\xi$, α the ion polarizability and ξ the local electric field at the ion site. In all other crystals the local field varies over the ion sites.

CHAPTER 3.

THE APPLICATION OF GROUP THEORETICAL ANALYSIS.

3.1 Availability of Group Theoretical Techniques.

The development of group theoretical techniques has allowed the non specialist to sensibly interpret models and measurements of complex crystals which may be of less interest to lattice dynamics experts. As each atom has three degrees of freedom and because of crytal anisotropy the phonon dispersion system even for a fairly simple structure may be quite complex. In such circumstances the application of group theory allows any simplification which may be involved because of the symmetry of the problem to be fully exploited before calculations are performed. The phonon spectrum may then be clarified by classification of the different branches according to their symmetry, as group theory predicts the essential degeneracies of the normal modes and gives information on the motions involved. Similarly the dynamical matrix may be simplified and the independent elements numbered and identified. Various selection rules may be obtained, for example, two phonon infrared absorption and possible second order structural phase transitions.

It must be emphasized, however, that despite the great advantages to be gained by this application no quantitative information may be obtained. For instance a mode may be predicted to be Raman active but no explicit indication is given of the expected intensity or frequency.

Maradudin and Vosko (1968) produced an influential paper containing a complete theory for the analysis of normal mode vibrations which has been subsequently extended by various authors; Warren (1968), Venkateraman and Sahni (1970) and Warren (1974). This theory was at first applied to simple structures such as diamond. Extension to more complex structures involves the manipulation of large matrices, a tedious process prone to error (see Stirling, 1972b on Cowley's 1964 symmetry coordinates for perovskite). Worlton and Warren (1972) produced a computer program to perform these manipulations based on the Maradudin and Vosko treatment of the theory. This program has undergone several modifications and an updated version produced (Warren and

Worlton 1979, 1976) which includes extensions for time reversal invariance and the treatment of molecular crystals. This program has been used to perform the complete analysis of the symmetry of the lattice vibrations of several crystals (Warren and Worlton, 1973).

3.2 Outline of the Maradudin and Vosko Formalism.

The space group of a crystal is that collection of symmetry operations which leave the spatial configuration of the crystal structure invariant. These operations consist of rotations, roto inversions, translations and their combinations. The effect of a space group operation on an atom position is given by

$$\{S|V(S)+x(\ell')\}x(\ell\kappa) = Sx(\ell\kappa)+ V(s) + x(\ell') \equiv x(L\ K) \qquad (3.1)$$

where $\{S|V(S)+x(\ell')\}$ is the symbol denoting the particular space group operation which consists of a rotation or rotoinversion represented by a 3×3 orthogonal matrix S, a fractional translation V(S) (i.e. one smaller than any primitive translation of the crystal) associated with the operation S and a translation equivalent to the lattice vector $x(\ell')$. If an origin of coordinates can be found for which the fractional translations associated with all the rotationary operations are all zero the crystal has the symmetry of one of the seventy three symmorphic space groups. Otherwise the space group is described as nonsymmorphic. The effect of a space group operation on a displacement vector is given by

$$u_\alpha'(LK) = S_{\alpha\beta}u_\beta(\ell\kappa) \qquad (3.2)$$

Thus the displacement at the $(\ell\kappa)$ site is rotated and transferred to the (LK) site. Similarly the invariance of the crystal potential under space group operations leads to the transformation law for the atomic force contents:

$$\phi_{\alpha\beta}(LK,L'K') = \sum_{\mu\nu} S_{\mu\alpha}\phi_{\mu\nu}(\ell\kappa\ \ell'\kappa')\, S_{\nu\beta} \qquad (3.3)$$

The central problem however is concerned with the Fourier transformed dynamical matrix and its eigenvectors:

$$\omega^2(qj)e(qj) = D(q)e(qj) \tag{3.4}$$

Maradudin and Vosko considered the dynamical matrix in a form different to that in equation (2.16) which was periodic in q and related to (2.16) by

$$D^{mv}_{\alpha\beta}(\kappa\kappa',q) = \exp(-(qr(\ell'\kappa',\ell\kappa))D_{\alpha\beta}(\kappa\kappa',q) \tag{3.5}$$

However in the following discussion the form of the dynamical matrix in (2.16) will be assumed and the equations modified accordingly. This form of the dynamical matrix is not periodic with q, nor are the eigenvectors. Thus

$$D(q- G) = \exp[iG.(x(\kappa) - x(\kappa'))]D(q) \tag{3.6a}$$

$$e(q-G,j)= \exp[iG.x(\kappa)]e(qj) \tag{3.6b}$$

where G is a reciprocal lattice translation vector. The effect of a space group operation on a normal mode (2.13) propagating with wave vector q is to produce a normal mode of wave vector Sq. The frequency of the normal mode is invariant as the relative atom positions are unchanged:

$$\omega^2(qj) = \omega^2(Sq,j) \tag{3.7}$$

Equation (3.7) strictly only applies if the mode is not degenerate. However, if more than one mode does have the same eigenfrequency the labelling j=j' is convenient. A similar argument is used to obtain the effect of a space group operation on the eigenvectors. Thus

$$e(Sq,j) = \Gamma(q,S\{V(S)+x(\ell')\})e(qj) \tag{3.8}$$

where Γ is a $3n \times 3n$ matrix. If attention is restricted to those elements of the space group, the rotational part of which leave the wave vector invariant or send it into a wave vector equivalent by a reciprocal lattice translation

$$Sq = q - G(S) \tag{3.9}$$

the matrices Γ commute with the dynamical matrix. This subgroup of

the space group of the crystal is known as the group of the wave vector. Maradudin and Vosko showed that the matrices Γ then provide a representation of the space group of the wave vector but did not use them for the discussion of the normal mode symmetry properties. The subgroup containing only the rotational elements of the space group which satisfy (3.9), known as the point group of the wave vector, was then considered. The matrices $T(qS)$ given by

$$T(qS) = \exp[iq(V(S)+x(\ell))]\Gamma(q,\{S|V(S)+x(\ell)\}) \tag{3.10}$$

$$T_{\alpha\beta}(\kappa\kappa',q,S) = S_{\alpha\beta}\delta(\kappa,F(\kappa',S))\exp[iG.(x(\kappa)-V(S)] \tag{3.11}$$

are unitary and provide a multiplier representation for the point group of the wave vector

$$T(q,S_i)T(q\ S_j) = \lambda(q,R_i,R_j)T(q,R_iR_j) \tag{3.12}$$

where the multiplier λ is given by

$$\lambda(q,R_i,R_j) = \exp[iG(q,S).V(S_j)] \tag{3.13}$$

The arguments of the exponentials in (3.11) and (3.13) are zero for symmorphic space groups and the interior of the Brillouin zone for nonsymmorphic space groups. The Kronecker delta in (3.11) shows that the matrix T only has nonzero values for atoms κ with which the the atoms κ' are brought into coincidence by the rotation S. As with the matrices Γ for the space group of the wave vector, the matrices T also commute with the dynamical matrix. Using this fact in the eigenvalue equation (3.4) we have

$$D(q)\{T(q,S)e(q,j)\} = \omega^2(q,j)\{T(q,S)e(q,j)\} \tag{3.14}$$

The quantities $\{Te\}$ are eigenvectors of the dynamical matrix with the same eigenvalues as $e(qj)$ and may be expressed by the linear combination

$$T(q,S)e(q,\sigma\rho) = \sum_{\rho'=1}^{n(\rho')} \tau^{\sigma}_{\rho'\rho}(q,S)e(q,\sigma\rho') \tag{3.15}$$

with j replaced by $\sigma\rho$ where ρ labels the eigenvectors with eigenvalues $\omega^2(q,\sigma)$ and σ labels the distinct eigenvalues. The $n(\rho)$ dimensional matrices τ^{σ} constitute an irreducible multiplier representation of the

point group of the wave vector q with the same multipliers as T(qS). This argument assumes that all the degeneracy is due to symmetry properties thus preventing interaction among the eigenvalues $e(q\sigma\rho')$ of different $\sigma\rho'$ which should only occur if, accidentally, $\omega(q,\sigma_i\rho_i) = \omega(q,\sigma_j\rho_j)$. If the eigenvectors were already known the matrices T would be block diagonalised by a similarity transform with e(q). To include the possibility that T(q,S) may contain an irreducible multiplier representation more than once the index σ is replaced by $\dot{s}a$ where $\dot{s}$ labels the irreducible representation and a the repetition. The eigenvectors can then be classified, for a given wave vector according to the irreducible representation $\dot{s}$ by which they transform under the operations of the point group of the wave vector, a and ρ label the repetition and degeneracy of this representation.

In equation (3.15) the eigenvectors may be taken as basis vectors for τ^{σ}. However the choice is not unique and another set may be chosen in terms of which the eigenvectors can be expressed as a linear combination. Such a set may be obtained by the use of a projection operator

$$P_{\rho\rho'}(q,\sigma) = \frac{n(\sigma)}{g} \sum_{S} \tau^{\sigma}_{\rho\rho'}(q,S)^{*}T(q,S) \qquad (3.16)$$

on an arbitrary 3n dimensional vector ψ for fixed ρ'

$$E(q,\sigma\rho) = P_{\rho\rho'}(q,\sigma)\psi \qquad (3.17)$$

where $n(\sigma)$ is the dimensionality of representation σ and g the order of the point group of the wave vector q.

$E(q,\sigma\rho)$ is a linear combination of eigenvectors $e(q,\sigma\rho)$, the coefficients of which are dependent on the dynamics of the problem. However if the irreducible representation s only appears once in the decomposition of T(q,S) the set $E(q,\sigma\rho)$, $\rho = 1, n(s)$ may be taken as the eigenvectors for the representation. The $E(q,\sigma\rho)$, known as symmetry coordinates, give the relative motion of the atoms in the eigenvectors.

After orthonormalisation the 3n × 3n matrix E(q) will block

diagonalise the matrices T(qS) and the dynamical matrix D(q) after suitable rearranging of the columns. In the latter case the sequence is such that the repetition index a varies before the degeneracy index ρ for each irreducible representation s. This produces a block diagonalised matrix consisting of ρ identical n(s)xn(s) blocks for each representation. The eigenfrequencies of the dynamical matrix are obtained by only diagonalising one such block for each irreducible representation.

Apart from labelling the phononspectrum the above simplification is the most important result obtained from group theory, one which has made the modelling of complex crystals possible. As the computer time required for each diagonalisation is proportional to the cube of the order of the matrix, any reduction in the size of the matrices involved results in a great economy, especially when an iterative fitting procedure is used.

Further degeneracies can arise from the time reversal invariance of the equations of motion, however as none are produced for the directions of wavevector q and space group used here these will not be considered further. Accidental degeneracies resulting from the crossing of normal modes in the phonon spectrum are not predicted by group theory and this gives rise to some difficulty in labelling. Modes of different representations do not interact and may be labelled as in fig.3.1a, while modes of the same irreducible representation which "cross" do interact. In the latter circumstance it is in general impossible to say if two branches are touching or in fact crossing. Usually the former point of view is taken and the modes are labelled as in fig.3.1b.

3.3 Previous Analyses for $Fd3m(O_h^7)$ Spinels.

A number of group theoretical analyses of the spinel structure have already been performed for various facets of the dynamical problem. Haas (1965) determined which of the space groups that result

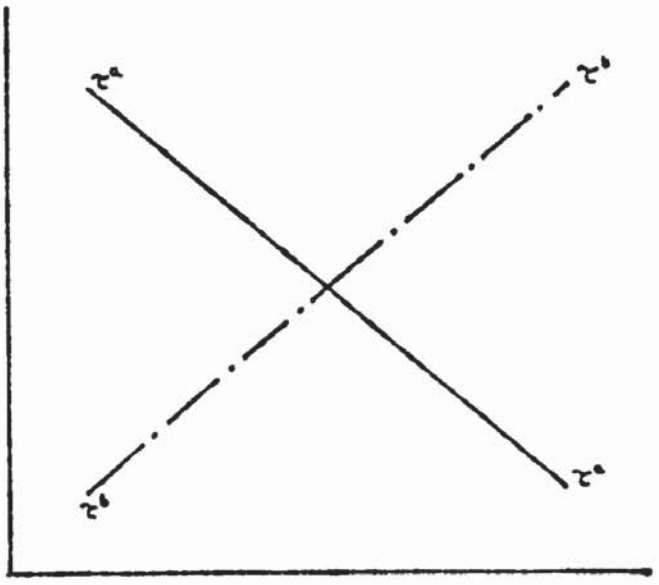

a) Inequivalent Representations

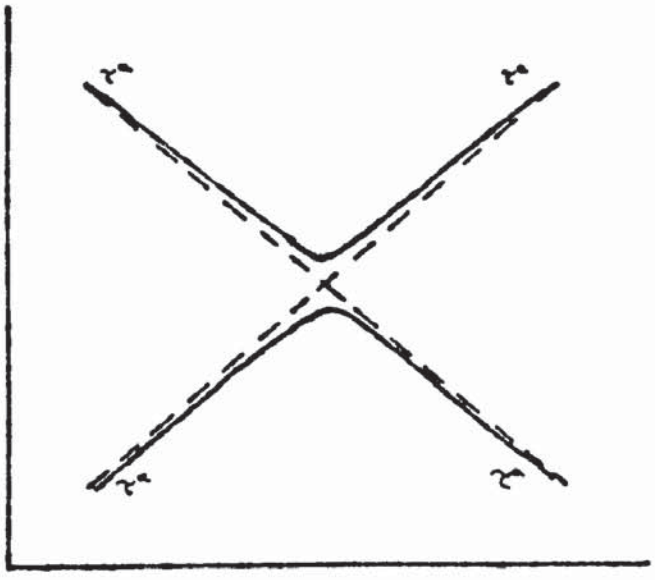

b) Equivalent Representations

Fig 3.1 Mode Crossing

from different orderings of the cations over the octahedral and tetrahedral sites may be obtained from Fd3m by a second order phase transition. Gashimzade and Rustamov (1975) have presented the selection rules for Raman and infrared activity in two and three phonon processes. Several authors, now, have decomposed the set of matrices T(q,S) for the point group at zero wave vector to obtain the numbers and types of irreducible representations present (White and DeAngelis 1967, Lütz 1969, Bruesch and D'Ambrogio 1972, Boldish and White 1978a). The last three authors have also published symmetry coordinates for q = (0,0,0). The decomposition may be obtained from the equation

$$a(\sigma) = \frac{1}{g} \sum_{S} \chi^*(q = 0,\sigma)\ \chi(q=0,S) \qquad (3.18)$$

where g is the order of the point group (for O_h, g = 48), $\chi(q,\sigma)$ the character (sum of the diagonal elements) of the matrices that correspond to the elements of the point group for the irreducible representation σ. $\chi(qS)$ is similarly the character of T(q = 0,S). $a(\sigma)$ is the number of times the irreducible representation σ is contained in T(qS). The resulting equation

$$\chi(q = 0,S) = \sum_{\sigma} a(\sigma)\chi(q = 0,\sigma) \qquad (3.19)$$

is known as a compatability relation.

In Maradudin and Vosko's treatment the point group of the wave vector is obtained by considering only the rotational part of those elements of the space group which leave the wave vector invariant, in this case the point group O_h (m3m) is obtained. In a factor group analysis the subgroup of the space group obtained by removing all lattice translations is considered. This group is not the point group O_h but a group which is isomorphic to it (i.e. the elements have a one to one correspondence to those of O_h). This difference occurs

because an origin cannot be chosen in the spinel structure such that the fractional translations associated with the rotational elements of the space group are all simultaneously zero. The group cannot therefore be a point group as elements other than pure rotations are included. However both approaches immediately yield identical results at the Brillouin zone centre. The characters of the irreducible representations are readily available in tables. The characters of the $T(q=0,S)$ are given by

$$\chi(q = 0,S) = n(S)(\pm 1 + 2\cos[\theta(S)]) \qquad (3.20)$$

where $\theta(S)$ is the angle associated with the rotational part of the element S, the plus and minus signs are used for rotations and roto-inversions respectively, $n(S)$ are the number of ions left unmoved by S. At points on the Brillouin zone boundary equation (3.18) has to be modified to take account of the phase factor in equation (3.11).

The nomenclature for group theoretical data is not standardised (for review see Warren, 1968). In table 3.1 the characters of the irreducible representations are given with common notations for the rotation elements and irreducible representations. In connection with spinels the electron band system (Bouckaert et al. 1936) of labelling the representations is used by Haas,Gashimzade and Rustamov whereas authors studying one phonon optical activity invariably have employed the labelling of molecular dynamics (Wilson et al. 1955). In this thesis I shall use a hybrid notation. The zone centre shall be labelled as the point Γ but the irreducible representations shall be labelled according to the molecular system both to facilitate comparison with other work and to have the advantage of the letter revealing the mode degeneracy immediately (A = 1, E = 2, T = 3). For all other points of the Brillouin zone Bouckaerts notation will be used. The Schoenflies and international notation for point and space groups (International Tables, 1962) will both be used, usually together unless it is repetitious.

		Γ_1	Γ_2	Γ_{12}	Γ_{15}'	Γ_{25}'	Γ_1'	Γ_2'	Γ_{12}'	Γ_{15}	Γ_{15}
		A_{1g}	A_{2g}	E_g	T_{1g}	T_{2g}	A_{1u}	A_{2u}	E_u	T_{1u}	T_{2u}
E	E	1	1	2	3	3	1	1	2	3	3
$8C_3$	$8C_3$	1	1	-1	0	0	1	1	-1	0	0
$3C_2$	$3C_2$	1	1	2	-1	-1	1	1	2	-1	-1
$6C_4$	$6C_4$	1	-1	0	1	-1	1	-1	0	1	-1
$6C_2'$	$6C_2$	1	-1	0	-1	1	1	-1	0	-1	1
i	J	1	1	2	3	3	-1	-1	-2	-3	-3
$8S_6$	$8JC_3$	1	1	-1	0	0	-1	-1	1	0	0
$3\sigma_h$	$3JC_4$	1	1	2	-1	-1	-1	-1	-2	1	1
$6S_4$	$6JC_4$	1	-1	0	1	-1	-1	1	0	-1	1
$6\sigma_d$	$6JC_2$	1	-1	0	-1	1	-1	1	0	1	-1

Character Table for Point Group O_h

TABLE 3.1

The decomposition for the zone centre has already been given in equation (1.2). The Raman and infrared active modes may be obtained by examination of the basis vectors for this irreducible representations (often included with the character tables). Raman activity is associated with the polarizability tensor and therefore it may be shown that Raman active modes must transform as a second rank, symmetric tensor under the group operations (Loudon 1967). Thus the basis vectors of these representations must be linear combinations of ab, with a,b = x,y,z for example $x^2+y^2+z^2$. Inspection reveals that A_{1g},E_g,T_{2g} are Raman active. Similarly infrared activity depends on the dipole moment of a mode. As this is proportional to a vector any mode which transforms as a component of a vector is potentially infrared active. For Fd3m (O_h^7) the T_{1u} irreducible representation carries the whole of the vector representation. It must be reiterated that these selection rules only indicate potentially optically active modes, the degree of activity depends on the dynamics of the problem. Of the five T_{1u} modes that appear in the decomposition one must be discounted from being optically active to allow the three acoustic modes to have zero frequency at zero wave vector. Of the remaining four threefold T_{1u} modes any splitting due to the effect of the macroscopic field is not predicted. This degeneracy removal could be predicted if infrared activity was considered as occurring at small but finite wave vector as no point in the Brillouin zone has higher symmetry than the zone centre.

3.4 Symmetry Coordinates.

For present purposes Warren and Worlton's modified program (Group 2, 1974) was obtained from the Computer Physics Communications program library, Queens University, Belfast. After adaptation for use on the CDC 7600 computer at the University of Manchester Regional Computer Centre, a small error was found in that part of the program which produced symmetry coordinates suitable for the form of the dynamical

matrix used in this thesis. The only numerical data required are the ion position coordinates of the basis and the wave vectors of interest. Generalised versions of T(q,S) and the projection operators are used throughout to include possible consequences of time reversal degeneracy. One effect of this is that the eigenvectors are related to the symmetry coordinates by linear combinations with wholly real coefficients (Warren, 1974). The space group of the crystal and the irreducible multiplier representations are generated internally. The character table for the particular wave vector is printed, followed by the decomposition of the group of the wavevector. The irreducible representations are only only labelled by a number and have to be identified by comparison with a standard set of character tables.

The independent elements of the dynamical matrix are identified and the combinations of these which form the elements of the blocks in the transformed dynamical matrix are listed. The number of independent elements found is often lower than that predicted from theory (Casella, 1975). This occurrence for the spinel structure is probably due to the large number of independent elements expected, over 130 for most wave vectors. The program identifies the elements by inspecting a symmetry reduced random matrix. The differences between the elements may be too small to be distinguished. Fortunately this disparity is not important as it is quicker and more accurate to construct dynamical matrices for complex structures and models from general terms rather than from special equations for particular elements. However at zero wave vector the number of independent elements predicted (thirty three) is in agreement with the number found. It should be emphasized that the number of non-zero elements can be less because of the simplicity of the potential function used. The independent elements of the short range and Coulomb matrices at q = 0 are tabulated in Appendix I in terms of the quantities defined in Chapter 5. Also given in Appendix II are equations for the elements of the block diagonalised dynamical matrix of the optically active

modes for a rigid ion model. The matrix inversion in the shell equation (2.57) would make the corresponding equations too complicated to be worth tabulating. The equations given are accurate for all modes except the two lowest T_{1u} which are sensitive to the approximations made in the expressions for the short range contributions.

Bearing in mind that the number of ion types taking part in any normal mode vibration may not exceed the number of times the mode appears in the decomposition of the vibrational spectrum (Montgomery, 1968) it is instructive to perform the reduction (3.18) for each of the ion types. Inspection of the results (Table 3.2) shows that in the interior of the Brillouin zone most modes involve all ion types, the exceptions being Δ_2, Δ_1' and Λ_2 which do not involve the magnesium ion. The decomposition at the zone centre is more informative. The infrared modes T_{1u} may involve all ion types but the Raman active modes A_{1g}, E_g, T_{2g} do not involve the aluminium ions. In particular the A_{1g} and E_g modes are completely dependent on the oxygen sublattice vibrations. The optically inactive modes $A_{2u}, E_u, T_{2u}, T_{1g}$, on the other hand have no magnesium ion components. These decompositions act as useful checks on the symmetry coordinates and therefore the eigenvectors. The symmetry coordinates for the Brillouin zone centre and the lines Λ, Σ, Δ are tabulated in Appendix III. To reduce the amount of space required that part of the symmetry coordinates which are necessarily zero are not given. As no symmetry operation can exist which interchanges nonequivalent ions the only parts of the symmetry coordinates which need be given are those involving one species of ion.

The Gamma point symmetry coordinates are illustrated in fig.3.2. The axis may be taken towards the top of the page, the x axis to the right, with the y axis entering the plane of the diagram obliquely. The basis is drawn as three tetrahedra for convenience only are not considered as independent units. One partner only is given for the threefold representations, the others may be obtained by rotation of

Irreducible Representation	No.of Modes Containing			Total No. of Modes
	Al	Mg	Ox	
A_{1g}	-	-	1	1
E_g	-	-	1	1
T_{1g}	-	-	1	1
T_{2g}	-	1	2	3
A_{2u}	1	-	1	2
E_u	1	-	1	2
T_{1u}	2	1	2	5
T_{2u}	1	-	1	2
Λ_1	3	2	6	11
Λ_2	1	-	2	3
Λ_3	4	2	8	14
Σ_1	3	2	7	12
Σ_2	2	1	5	8
Σ_3	4	2	7	13
Σ_4	3	1	5	9
Δ_1	2	1	4	7
Δ_1'	1	-	2	3
Δ_2	1	-	2	3
Δ_2'	2	1	4	7
Δ_5	3	2	6	11

Ionic Sublattice Contributions to the Irreducible Representations at the point Γ and along Lines Λ, Σ and Δ of Brillouin Zone.

TABLE 3.2

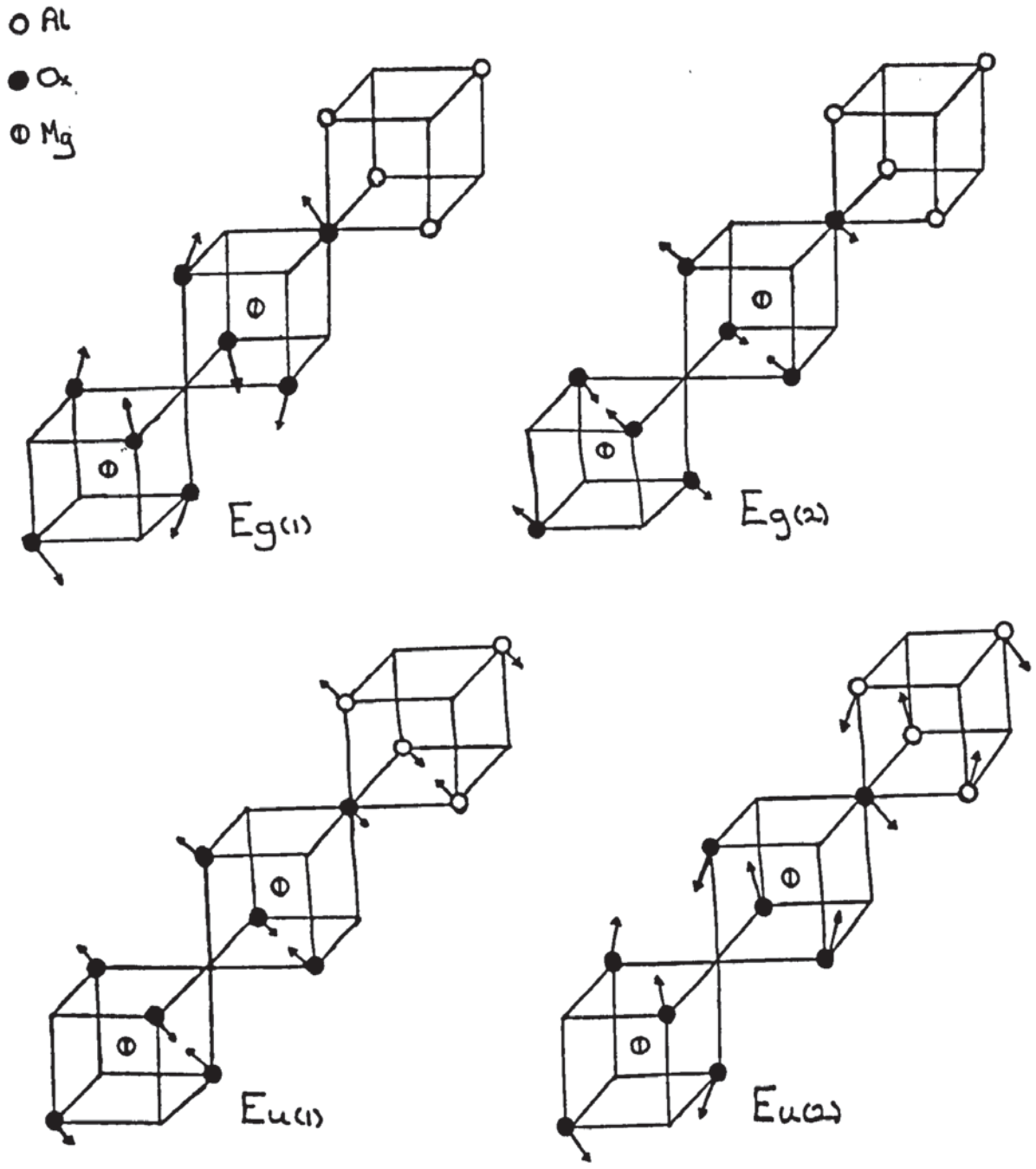

Γ Point Symmetry Coordinates

Fig 3.2a

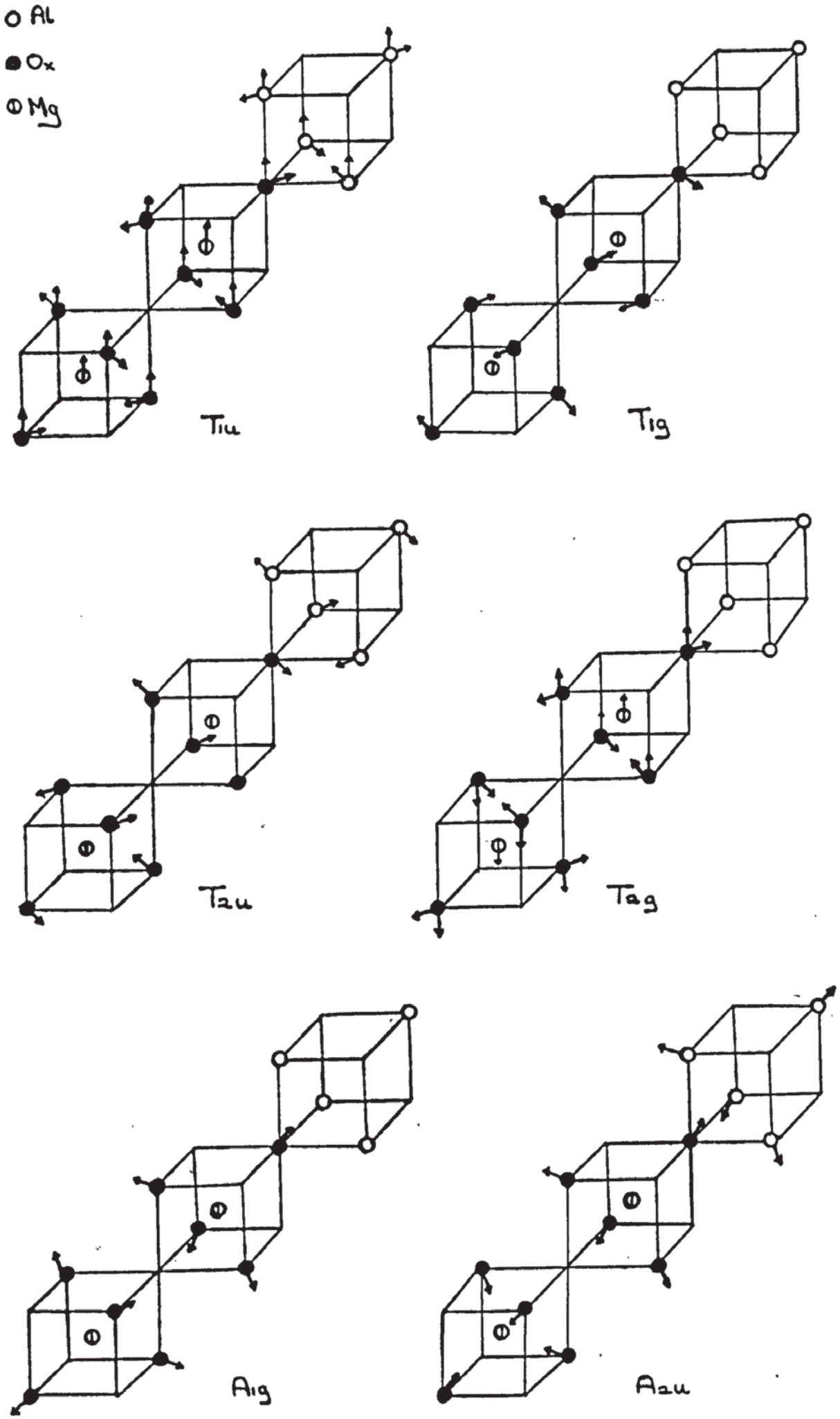

Fig 3.2b

the vectors through ninety degrees about the axes. Repeated representations have more than one ion type involved sometimes with more than one vector associated with the same ion type. In the latter case the atom may vibrate in the plane of the vectors. The even modes (denoted by subscript g) are invariant under the action of the inversion operator, therefore ions interchanged by inversion have oppositely directed vectors. Throughout it must be remembered that the actual amplitudes of vibration are determined by the force constants. The symmetry coordinates only provide information concerning the relative motion of the ions in a given mode. The A_{1g} mode consists of motions of the oxygen ions in <111> directions from the tetrahedral ions. In the A_{2u} modes these motions for the two oxygen tetrahedra are oppositely directed. The T_{1g} and T_{2u} modes may be considered as rotationary motions of the tetrahedra about the z axis. In the former the rotations are in the same direction but in the latter they have opposite senses. The infrared modes T_{1u} have aluminiums and oxygen motions in the zy plane while the magnesium ions vibrate parallel to the z axis. The Raman active T_{2g} modes again have the magnesium ions vibrating parallel to the z axis but in opposite directions. The oxygen ions move in planes parallel to the xy directions to distort their tetrahedra. The symmetry coordinates produced by the program for the doubly degenerate modes E_g and E_u are complex quantities, witn the partners obtained by complex conjugation. As the dynamical matrix at q = 0 is a real quantity and as the irreducible representations of the point group O_h may be taken as real this is an unnecessary complication. The effect arises from the form of the matrices

$$S(\theta) = \begin{pmatrix} \exp(\theta) & 0 \\ 0 & \exp(-(\theta)) \end{pmatrix} \text{(a)} \quad S(\theta) = \begin{pmatrix} \cos\theta & -\sin\theta \\ \sin\theta & \cos\theta \end{pmatrix} \text{(b)} \qquad (3.21)$$

obtained by the program. Matrices of the form (3.21a) are employed rather than the conventional choice (3.21b) the use of the matrices of type (3.21b) is found to be equivalent to taking the real and

imaginary parts of a single partner for choice (3.21a) as separate partners for that representation. This method has been used to obtain the diagrams for the E_g and E_u representations. $E_g(2)$ and $E_u(1)$ have ionic motions in xy directions producing complicated twisting distortions of the tetraheda. $E_u(2)$ and $E_g(1)$ have ionic motions in xy and xz directions tending to flatten the tetrahedra in planes parallel or perpendicular to the z axis. The diagrams given here are drawn in the manner of Verble's (1973) Raman mode illustrations. However Verble appears to have grouped together symmetry coordinates of the T_{2g} representation to form partners from suggested eigenvectors without having explained the basis on which these groupings were chosen. The highest frequency mode was taken to comprise only of distortions of the oxygen tetrahedra in XY directions. The two lower frequency modes had ion motions only in the z directions, the two frequencies being distinguished by having the magnesium ions either opposing the oxygen tetrahedra motions or moving in the same sense. While these arguments are plausible they are not of necessity the only arrangements that may occur. The actual eigenvectors produced would depend on interionic forces which are likely to vary among different spinel materials. The normal coordinates, however, apply for all Fd3m spinels. Lutz (1969) diagrams are more complex as more ions than constitute the basis are included. However the same criticism applies here for the T_{2g} and T_{1u} modes.

The symmetry coordinates for wave vectors greater than zero are in general complex as the ionic motions are then no longer constrained to be vectors in a single direction or plane and differ in phase corresponding to a vibrational ellipsoid which may be non-spherical. In general the phase is also a function of the magnitude and direction of the wave vector. Even along high symmetry directions in the Brillouin zone the symmetry coordinates may not be completely described as transverse or longitudinal where the terms refer to ionic motions

perpendicular or parallel to the wave vector. The compatability relations between the Brillouin zone centre representations and those along the high symmetry lines $\Lambda(qqq)$, $\Sigma(qq0)$ and $\Delta(q00)$ are given in table 3.3. Inspection of the symmetry coordinates confirms that only those representations compatible with T_{1u} may have dipole moments. Invariably the dipoles would be aligned either perpendicularly or parallel to the wave vector. Even these representations may have some symmetry coordinates with ionic motions at variance with the direction of the dipole moment. These coordinates however do not have a net dipole moment. The T_{1u} representations also give the acoustic modes at small wave vectors.

In directions Δ only Δ_1' and Δ_2 have purely transverse components but it is Δ_5 which carries the transverse components of the acoustic wave. Similarly Λ_2 is transverse but Λ_3 carries the transverse component of the acoustic mode. It is notable that none of these optic transverse modes have Mg ions participating. In the Σ direction it does not appear possible to classify any mode as completely transverse. The longitudinal acoustic modes belong to the identity representations in each case, $\Delta_1, \Lambda_1, \Sigma_1$. Along the lines Λ and Σ, ions which were equivalent become distinct. In the former case ions at the corners of the tetrahedra along the [111] direction become inequivalent to the other corners. Similarly in the Σ direction with the axis along the [110] direction. In all cases the Mg ions remain equivalent. The $q = 0$ data from the program has been checked by hand. The symmetry coordinates for the zone interior have been verified by their ability to block diagonalise the relevant dynamical matrix with none of the other elements exceeding 0.003 and eigenvalues in agreement with those from the diagonisation of the full matrix to 0.01 TH_3. The symmetry coordinates for the zone boundary proved to be incorrect as the block diagonalisation was incomplete, large non block elements, both real and imaginary were found. In practice the X point modes have been examined using the compatability

Γ	Λ	Δ	Σ
A_{1g}	Λ_1	Δ_1	Σ_1
E_g	Λ_3	$\Delta_1 + \Delta_2$	$\Sigma_1 + \Sigma_4$
T_{1g}	$\Lambda_2 + \Lambda_3$	$\Delta_1' + \Delta_5$	$\Sigma_2 + \Sigma_3 + \Sigma_4$
T_{2g}	$\Lambda_1 + \Lambda_2$	$\Delta_2' + \Delta_5$	$\Sigma_1 + \Sigma_2 + \Sigma_3$
A_{2u}	Λ_1	Δ_2'	Σ_3
E_u	Λ_3	$\Delta_1' + \Delta_2'$	$\Sigma_2 + \Sigma_3$
T_{1u}	$\Lambda_1 + \Lambda_3$	$\Delta_1 + \Delta_5$	$\Sigma_1 + \Sigma_2 + \Sigma_4$
T_{2u}	$\Lambda_2 + \Lambda_3$	$\Delta_2' + \Delta_5$	$\Sigma_1 + \Sigma_2 + \Sigma_4$

Compatability Relations Between Γ Point Representations and Those for the Lines Λ, Δ and Σ

TABLE 3.3

relations

$$X_1 = \Sigma_1 + \Sigma_3 = \Delta_1' + \Delta_2$$

$$X_2 = \Sigma_2 + \Sigma_4 = \Delta_1 + \Delta_2'$$

$$X_3 = \Sigma_3 + \Sigma_4 = \Delta_5$$

$$X_4 = \Sigma_1 + \Sigma_2 = \Delta_5$$

The L point modes have been classified according to their dimensions as the eigenvectors of the full matrix were too inaccurate to resolve the even and odd representations.

3.5 Structural Phase Transitions from Fd3m Spinels.

In recent years it has become customary to characterise structural phase transitions by reference to the softening of one of the normal modes. This mode, the frequency of which decreases markedly near the transition temperature has ionic displacements of the same symmetry as that occurring in the crystallographic change. The frequency softening results from a decrease in the restoring force owing to a "freezing in" of these displacements. In Cochrans treatment (1960) the structural transition is characterised by a single eigenvector. Landau (1937) had previously considered second order transitions on symmetry grounds with what is now recognised as a soft mode classified by a single irreducible representation. Soft modes have been found experimentally for both first and second order transitions. However only Landau's theory enables these to be predicted from structural information alone. It is also possible to predict the space group to which the crystal may distort.

Several phase transitions are known to exist for spinels. Those resulting from ionic ordering have been reviewed by Haas (1965). The soft mode for electronic ordering in Fe_3O_4 was predicted by Yamada (1974) and confirmed by Shirane et al. (1975). Most structural transitions have been to the tetragonal system via long range ordering of distortions produced by cations exhibiting the Jahn-Teller effect (Dunitz and Orgel 1957a). Marked softening of elastic constant (Kino et al.1972) and band splittings in the infrared spectra (Siratoriet el. 1967) have been observed for such transitions. The latter author claims that the transition is accompanied by the softening of a Raman active mode without providing any justification. One of the difficulties in assigning a soft mode here is that the space group of the lower symmetry phase is rarely given. Mishra and Thomas (1977) have reported a phase change from Fd3m to $F\bar{4}3m$ for magnesium aluminate. Examination of the experimental data suggests that the phase transition

is second order, in agreement with Haas (1965) work. However, the symmetry of a possible soft mode has not yet been suggested.

As it seems improbable that neutron beam time will be allocated for the direct observation of soft modes at the Brillouin zone boundary the remainder of this chapter will be devoted to transitions produced by an irreducible representation of zero wave vector. That is only those transitions in which the volume of the unit cell is left unchanged will be considered. In particular only cubic and tetragonal systems in the low symmetry phase will be investigated as data for other structural transitions among spinels is sparse. To make general predictions it appears that Landau's theory must be used despite criticisms (Dimmock 1963, Kadanoff et al. 1967). Therefore only possible second order transitions will be given.

3.6 Soft Mode Prediction

3.6.1 Landau Theory

A second order transition is taken to be one in which the state of a crystal and its related thermodynamic functions change continuously. However derivatives of these functions, such as specific heat, change discontinuously through the transition. Landau (Landau and Lifshitz, 1960a) considers a probability distribution function $\rho(x,y,z)$ of the atom positions which is invariant under all operations of the space group G of the high symmetry phase. This may be expanded as a linear series of the basis functions ϕ of the irreducible representations

$$\rho = \sum_{n} \sum_{i} c(n,i)\phi(n,i) \qquad (3.21)$$

where n is the irreducible representation and i the number of functions in its basis. The expansion always includes the identity representation, function ρ_o, of the space group which is invariant under all its symmetry operations. Thus ρ may be rewritten as

$$\rho = \rho_o + \sum_n{}' \sum_i c(n,i)\phi(n,i) = \rho_o = \delta\rho \qquad (3.22)$$

The symmetry of the transition point is assumed to be that of the high symmetry phase. Therefore, in general ρ has lower symmetry. Towards the transition point the coefficients c vary continuously to zero from the low symmetry side to give the high symmetry group at the transition point. It is assumed that the state of the body may be described by a single scalar thermodynamic potential as a function of temperature, pressure and a parameter which gives a measure of the difference from the actual atomic configuration to that of the high symmetry phase, in this case c(n,i). The thermodynamic potential may then be expanded as a power series of c(n,i) and various conditions imposed to enable the space groups to which the crystal may distort to be identified. These conditions arise from the minimisation of the thermodynamic potential to give stable conditions at the transition point and its invariance under the operations of the space group. Also it is assumed that there exists a line of phase transition points between the two phase rather than a single point on a temperature against pressure graph.

Instead of Landau's original treatment which becomes rather tedious (e.g. see Liubarskii 1960) a simplified method due to Birman (Birman 1966, Goldrich and Birman, 1968) was applied.

The conditions on the irreducible representation responsible for the phase transition are then given as:

1) It is impossible to construct a third order invariant from functions which transform like the irreducible representation. That is the third order symmetric product does not contain the identity representation of the high symmetry space group.
2) The first order spatial derivatives of c(n,i) for this value of n must be zero. This has the effect (Landau and Lifshitz 1960), that the second order antisymmetric product of the representation must

2) contd.

not contain any representation by which the components of a vector transform (in this work T_{1u}).

3) The irreducible representation is compatable with the identity representation of the lower symmetry space group. In particular if the lower symmetry space group contains only half the number of symmetry elements of the high symmetry space group a second order phase transition is always possible.

4) If the same irreducible representation is compatable with two space groups, one of which is a subgroup of the other and its decomposition with respect to these groups contains the identity representation of each once only, then the transition to the group with the lower symmetry of the two is forbidden. This condition, known as the chain subduction criterion, like condition 1 arises from the assumption that the phase transition does not occur at an isolated point on a pressure temperature graph. Condition 1 is necessary in this respect but not sufficient.

5) The irreducible representation corresponds to a physical field. This condition was introduced by Birman (1966) as implied in most physical arguments. Here the physical field would be the set of normal coordinates at the given wave vector.

3.6.2 Application to Spinels with Fd3m (O_h^7)Symmetry.

Considering cubic and tetragonal distortions which leave the volume of the unit cell unchanged the relevant point groups are $C_4(4)$, $S_4(\bar{4})$, $C_{4h}(4/m)$, $D_4(422)$, $C_{4v}(4mm)$, $D_{2d}(\bar{4}2m)$, $D_{4h}(4/mmm)$, $T(23)$, $T_d(\bar{4}3m)$, $T_h(m3)$, $O(432)$, $O_h(m3m)$

Condition 1 is applied by considering the characters of the irreducible representations of O_h and those of their symmetric triple products given by (Liubarskii, 1960).

$$[\chi]^3(S) = \tfrac{1}{3}\chi(S^3) + \tfrac{1}{2}\chi(S^2)\,\chi(S) + \tfrac{1}{6}\chi^3(S)$$

and decomposing. This condition leaves only the irreducible representations A_{2u}, E_u, T_{1u}, T_{2u}, T_{1g}. Application of condition 2 is similarly performed using

$$\{\chi\}^2(S) = \tfrac{1}{2}\chi(S^2) + \tfrac{1}{2}\chi^2(S)$$

This leads to no further simplification. It is pertinent to note that while the symmetric square product of T_{1g} contains the vector representation the antisymmetric product does not. This has caused some difficulty among other workers performing a similar analysis (see Perel et al. 1968). As T_{1g} is the only even representation remaining it is the only one that may be compatable with the identity representation of point groups containing the inversion. As it is incompatable with D_{4h} and T_h these point groups are eliminated. Candidate structures are obtained by inspection of the space group tables (International Tables 1972). The process is simplified by remembering that if a particular ion type is not involved in the irreducible representation (Table 3.2) compatable with a particular point group that ion type will have positions completely determined by symmetry in the corresponding space group. Table 3.4 summarises the results.

Of the cubic space groups T_d^2 and T^2 the latter is eliminated by the chain subduction criterion (condition 4). Inspection of the soft mode A_{2u} (fig.3.2) to $F\bar{4}3m$ shows that the aluminium motions are in the same directions as predicted by Grimes (1973). However as the oxygen motions are determined by a single symmetry coordinate an important condition is imposed: for the transition to be second order the ionic displacements of the two oxygen tetrahedra must be opposite in direction and equal in extent from the O_h^7 ($Fd3m$) positions. As no X-ray measurements have been made just above and below the transition temperature (450°C) it is not known if this holds. However there is no evidence of contradictory data, Grimes (1979) gives the δ parameters for the oxygen ions when single crystal data of $MgAl_2O_4$ is refined to T_d^2 as

Irreducible Representation	Point Group	Space Group
A_{2u}	T_d	$T_d^2(F\bar{4}\,3m)$
A_{2u}	T	$T^2(F23)$
T_{1g}	C_{4h}	$C_{4h}^6(I4_1/a)$
T_{1u}	C_{4v}	$C_{4v}^{11}(I4_1md)$
E_u, T_{1u}, T_{1g}	C_4	$C_4^6(I4_1)$
E_u	D_4	$D_4^{10}(I4_122)$
A_{2u}, E_u, T_{2u}	S_4	$S_4^2(I\bar{4})$
A_{2u}, E_u, T_{2u}	D_{2d}	$D_{2d}^{12}(I\bar{4}2d)$

Candidate Structures for Phase Transition From Fd3m.

TABLE 3.4

$$\delta_1 = 0.0136(1) \qquad \delta_2 = 0.0116(9)$$

but when refined to O_h^7

$$\delta = 0.0126(0) \pm 0.0003$$

The differences between δ_1, δ_2 and δ are equal in extent with the error. It is of course expected that a least square refinement of a T_d^2 structure to O_h^7 should produce a delta which is an average of δ_1 and δ_2

Madelung constant calculations give nearly equal values for the two structures as M(Fd3m) = 132.650, M($F\bar{4}3m$) = 132.835. This 0.1 percentage difference corresponds to only a 0.33 eV actual difference in the cohesive energy. Thus it can be assumed that if this transition actually occurs non-Coulomb contributions will also be important.

Application of the subduction criterion removes C_4 with respect to C_{4h}, C_{4v} and D_4 and also S_4 with respect to D_{2d}. The T_{1u} transformation to C_{4v}^{11} is also eliminated as this structure may not be achieved by small displacements from the O_h^7 space group.

The atom position coordinates for the remaining structures are given in the International Tables with respect to a body centred tetrahedron. By rotating through forty five degrees about the z axis the resulting coordinates may be compared to the symmetry coordinates.

Thus the E_u-D_4 transition and the possibilities of the A_{2u} and E_u as soft modes for D_{2d}^{12} are removed. Then the only possible second order transitions are:-

T_{1g} $\quad C_{4h}^{6}(I4_1/a)$

T_{2u} $\quad D_{2d}^{12}$ $(I\bar{4}2d)$

The position coordinates of the spinel ions in these space groups are given in table 3.5 (with respect to body centred tetragonal axes). A second order transition is only possible if the y and z oxygen parameters have the values 2u and u is in O_h^7 at the transition point.

Of these two structures only D_{2d}^{12} has been observed and that arises in $CuCr_2O_4$ (Prince 1957) and $CuRh_2O_4$ (Bertaut et al. 1959). Both of these compounds have a c/a ratio less than unity. Whereas it is more common for tetragonal spinels to have the Hausmannite structure (D_{4h}^{19}) with a c/a ratio greater than one. Of the two compounds more is known about $CuCr_2O_4$. The transition occurs in the latter at 600°C (Siratori, 1967) and at room temperature four infrared bands are observed. The decomposition of the space group at the zone centre is now

$$\Gamma = 6A_1 + 3A_2 + 3B_1 + 8B_2 + 11E$$

where A_2 is optically inactive and the remaining modes all Raman active. However the representations B_2 and E also give rise to a total of nineteen possible infrared bands.

In both the compounds given the distortion to the tetragonal structure is believed to be due to the Jahn-Teller copper ions. However according to Gehring and Gehring (1975) the transition will be first order for spinels of this type. However it may be that there are actually two competing mechanisms present, one the softening of the T_{2u} mode and the other the ordering of the Jahn-Teller distortions.

Space Group: $I\bar{4}2d$

Mg: 000; $0\ \frac{1}{2}\ \frac{1}{4}$

Aℓ: $x\ \frac{1}{4}\ \frac{1}{8}$; $\bar{x}\ \frac{3}{4}\ \frac{1}{8}$; $\frac{3}{4}\ x\ \frac{7}{8}$; $\frac{1}{4}\ \bar{x}\ \frac{7}{8}$;

Ox: $x\ y\ z$; $\bar{x}\ \frac{1}{2}+y\ \frac{1}{4}-z$;

$\bar{x}\ \bar{y}\ z$; $x\ \frac{1}{2}-7\ \frac{1}{4}-z$;

$y\ x\ \bar{z}$; $y\ \frac{1}{2}+x\ \frac{1}{4}-z$;

$y\ \bar{x}\ \bar{z}$; $\bar{y}\ \frac{1}{2}-x\ \frac{1}{4}-z$;

Space Group: $I4_1/a$

Mg: 000; $0\ \frac{1}{2}\ \frac{1}{4}$;

Aℓ: $0\ \frac{1}{4}\ \frac{5}{8}$; $0\ \frac{3}{4}\ \frac{5}{8}$; $\frac{1}{4}\ 0\ \frac{3}{8}$; $\frac{3}{4}\ 0\ \frac{3}{8}$;

Ox: $x\ y\ z$; $x\ \frac{1}{2}+y\ \frac{1}{4}-z$

$\bar{x}\ \bar{y}\ z$; $\bar{x}\ \frac{1}{2}-y\ \frac{1}{4}-z$

$\bar{y}\ x\ \bar{z}$; $y\ \frac{1}{2}-x\ \frac{1}{4}+z$

$y\ \bar{x}\ \bar{z}$; $\bar{y}\ \frac{1}{2}+x\ \frac{1}{4}+z$

Atom Positions for Spinels in Space Groups $I\bar{4}2d$ and $I4_1/a$

TABLE 3.5

CHAPTER 4

INELASTIC NETRON SCATTERING FORM $MgAl_2O_4$

4.1 Inelastic Neutron Scattering

4.1.1 Thermal Neutrons

Following de Broglie, the neutron wavelength energy relationship

$$\lambda = \frac{h}{p} = \frac{h}{\sqrt{(2m_n E)}} \approx \frac{9.044}{\sqrt{E}} \text{ Å with Ein meV} \qquad (4.1)$$

is such that thermal neutrons with energies about 6THz have wavelengths around 1.8Å. Thus neutrons with typical phonon energies have wavelengths of the order of interparticle distances in solids. In comparison other common probes such as X-rays have similar wavelengths but much greater energies whereas infrared radiation with similar energies has much greater wavelength . It follows that any inelastic interaction between thermal neutrons and phonons would result in a large fractional change in both the wavevectors and energies of the neutrons. This relationship together with the zero charge on the neutron allows the exploitation of experimental techniques employing thermal neutrons as a probe, for the examination of the vibrational properties of bulk condensed matter. To date, inelastic neutron scattering is the only reliable method for tracing phonon dispersion curves throughout the Brillouin zone. The neutron's magnetic moment also allows magnetic interactions to be studied (see Jacrot and Riste 1969, for review).

The principal sources of high fluxes of thermal neutrons are, at present, nuclear fission reactors. The neutron velocity distributions in the thermal region is almost Maxwellian with a peak wavelength given approximately by

$$\lambda_{peak} = h/(5k_B Tm)^{\frac{1}{2}} \qquad (4.2)$$

where m is the neutron mass and T the moderator temperature. k_B and h are the Boltzmann and Planck constants respectively. To produce peak intensity in other regions the peak position may be displaced by heating or cooling parts of the moderator. Long wavelength neutrons are produced by introducing a liquid deuterium source. High energy neutrons

are obtained using heated graphite.

In scattering experiments a narrow range of wavelengths are selected from the Maxwellian spectrum either by Bragg reflection from crystals or by mechanical monochromators.

4.1.2 Scattering Theory.

As the wavelengths of thermal neutrons are much greater than the dimensions of the nuclei with which they interact the scattered waves from a single nucleus are essentially spherical and can be written as

$$\psi_s = - \frac{b}{r} \exp(i\ k\ r) \qquad (4.3)$$

where b is a constant known as the scattering length. The total cross section for scattering from a single fixed nucleus is given by

$$\sigma = 4\pi b^2 \qquad (4.4)$$

In general b may be dependent on the energy of the incident neutrons and complex, the imaginary part corresponding to absorption. Nuclei exhibiting these characteristics - although useful for shielding are not often employed in scattering experiments. The scattering lengths of most nuclei are almost totally real and energy independent for incident thermal neutrons. The spin state of the nucleus and the particular isotope involved, however have an important effect on the value of b. As the present state of nuclear theory does not allow scattering lengths to be accurately calculated they are experimentally determined quantities.

A theoretical expression for the partial differential cross section for scattering from an assembly of nuclei may be obtained which gives the number of neutrons scattering into a solid angle $d\Omega$ with final energy in the range E' to E' + dE' (Squires, 1978):-

$$\frac{d^2\sigma}{d\Omega\ dE'} = \frac{k'}{k} \frac{1}{h} \sum_{jj'} b(j)b(j') \int_{-\infty}^{\infty} \langle \exp(-iQ.R(j',0) \exp(iQ.R(j,t)) \rangle \times \exp(-i\omega t) dt \qquad (4.5)$$

where k,k' are the wave numbers of the incident and scattered neutrons

respectively. E,E' the corresponding energies

$$Q = k - k' = G + q \tag{4.6}$$

$$\hbar\omega = E - E' = \frac{\hbar^2}{2m}(k^2 - k'^2) \tag{4.7}$$

G is a reciprocal lattice vector

<A> denotes the thermal average of the included operator A.

The R(j,t) are the Heisenberg operators corresponding to the positions of the j^{th} nucleus at time t. To obtain this expression various assumptions have been made

i) The Born Approximation holds

ii) The scattering potential of a nucleus j may be represented by the short range Fermi pseudo potential

$$V_j(r) = \frac{2\pi\hbar^2}{m} b\ \delta(r - R(j,t)) \tag{4.8}$$

iii) The b's are real, energy independent quantities which allows them to be taken outside the thermal average.

In practice the cross section measured for a particular system is due to scattering from a large number of nuclei. Therefore the values of b(j) may be replaced by averages over their isotopic and spin concentration. Further, if various isotopes of a particular nucleus type are distributed randomly over the sites of these nuclei the following hold

$$\overline{b(j')\ b(j)} = (\bar{b})^2 \qquad j' \neq j \tag{4.9}$$

$$\overline{b(j')\ b(j)} = (\overline{b^2}) \qquad j' = j \tag{4.10}$$

where the bar denotes an average. These allow equation (4.5) to be replaced by the sum of two cross sections known as the coherent and incoherent cross sections

$$\left(\frac{d^2\sigma}{d\ell\ dE'}\right)_{COH} = \frac{\sigma_{COH}}{4\pi}\ \frac{k'}{k}\ \frac{1}{2\pi\hbar}\ \sum_{jj'}\int \langle j'j\rangle \exp(-i\omega t)dt \tag{4.11}$$

$$\left(\frac{d^2\sigma}{d\ell\ dE}\right)_{INCOH} = \frac{\sigma_{INC}}{4\pi}\ \frac{\ell'}{k}\ \frac{1}{2\pi\hbar}\ \sum_{j}\int \langle jj\rangle \exp(-i\omega t)dt \tag{4.12}$$

where $\sigma_{COH} = 4\pi(\bar{b})^2$ and $\sigma_{INC} = 4\pi\left[\overline{b^2} - (\bar{b})^2\right]$

Incoherent scattering then is due to a correlation between the positions

of the same nucleus at different times and does not give rise to interference effects. Alternatively coherent scattering does, as it is largely a correlation between different nuclei at different times. Incoherent scattering cross sections are usually smaller than their coherent counterparts with the notable exceptions of hydrogen and vanadium which are almost totally incoherent scatterers.

The partial differential cross section for one phonon coherent scattering from a harmonic crystal may be shown to be given by (Lomer and Low, 1965)

$$\left(\frac{d^2\sigma}{d\Omega\, dE'}\right)_{COH} = \frac{(2\pi)^3}{v_a}\sum_{qj}\frac{k'}{k}\delta(\hbar\omega \mp \hbar\omega(qj))\sum_{G}\delta(\bar{Q}+q-G)\hbar(n+\tfrac{1}{2}\pm\tfrac{1}{2})/2\omega(qj)\times$$

$$\times\left|\sum_{\kappa}\bar{b}(\kappa)\exp(iQ.r(0,\kappa))Q.e(\kappa,qj)m^{-\frac{1}{2}}e^{-W_\kappa}\right|^2 \qquad (4.13)$$

the upper and lower signs indicating processes in which phonons are created and annihilated respectively. The average number of phonons n in any state is given by equation (2.35). Examination of (4.13) shows that the cross section is higher for phonon creation than for annihilation. Taken to the limit $T \to 0$ all phonons are in their ground states and thus may not give up any energy. Bearing in mind the definition of $\hbar\omega$, equation (4.7) the first delta function in (4.13) expresses conservation of energy between the neutrons and phonons. Similarly the second delta function expresses the conservation of neutron momentum and phonon crystal momentum with G as a reciprocal lattice vector. For phonon dispersion curves these two delta functions will be simultaneously satisfied only for discrete values of q and ω thus giving rise to peaks rather than continua. In comparison the corresponding equation for one phonon incoherent scattering does not have a delta function for crystal momentum conservation, The partial differential cross section then is continuous in q. In practice incoherent scattering, if present contributes to the background in

coherent scattering experiments.

The relative amplitudes and phases of the normal modes are accounted for by the polarization vectors e(qj) in the final term called the "dynamic structure factor". Here W_κ is the Debye-Waller factor which is linear in Q. Thus although the structure factor increases with Q because of the factor Q.e, the effect of $\exp(-W_\kappa)$ eventually dominates. Although the dynamical equations which give the frequencies and polarization vectors are periodic with the Brillouin zone the inelastic neutron structure factor repeats in a volume of reciprocal space given by

$$\exp(iG.r(0,\kappa)) = 1 \qquad (4.14)$$

for all atom positions in the unit cell. For structures in which all the atoms have coordinates which are simple fractions of the cell dimensions the repeat volume is readily given. For spinels with δ set to zero the repeat volume is a cube bounded by the reciprocal lattice vectors [8,0,0],[0,8,0],[0,0,8]. However in general δ is not zero and the repeat volume is effectively infinite. Calculation of the structure factor is important in planning and interpretation of scattering experiments, particularly for complex crystals. By suitable choice of crystal orientation the product Q.e may be made to vanish for modes with polarization vectors that must be essentially transverse to the direction of Q. Also the intensity of any particular mode varies characteristically in different parts of reciprocal space within the structure factor repeat zone. Therefore comparison of the intensities of the same mode measured in different regions enables it to be identified. Measurement of dispersion curves is often an iterative process requiring a dynamical model to provide information for structure factor calculations and a knowledge of the dispersion curves to improve the model parameters.

In an experimental measurement the delta functions in equation (4.13) are found to be spread out into peaks because of effects such

as instrumental resolution and anharmonicity not incorporated in the derivation of the partial differential cross section. The total cross section measured is then the integral of (4.13) over the delta functions and is given by (Brockhouse, 1966)

$$\sigma_j(k\to k') = \frac{k'}{k}(n+\tfrac{1}{2}\pm\tfrac{1}{2})\frac{\hbar}{2\omega(q_j)}\,|F(j,Q)|^2\;|J(j)|^{-1} \qquad (4.15)$$

where the dynamical structure factor has been represented by $F(j,\alpha)$ and

$$|J(j)|^{-1} = \left|1 \pm \frac{\hbar k'}{2E'}\cdot\nabla_q\,\omega(q,j)\right|^{-1} \qquad (4.16)$$

As will be indicated later, the expression for the Jacobian J may be simplified for certain specialised types of scan with a triple axis spectrometer.

4.2 Neutron Spectrometry

4.2.1 Triple Axis Spectrometers

Any experiment in which coherent inelastic scattering of neutrons is to be measured must have facilities for the selection of incident neutrons of known wavevector and the simultaneous energy and wave vector analysis of the scattered neutrons. Spectrometers which have these capabilities may be divided into two major types - triple axis and time of flight, although hybrids also exist (see Dolling 1974 for review). Time of flight spectrometers usually consist of a large number of fixed detectors set at known angles and distances from the target. With this instrument a large number of neutrons may be recorded simultaneously but it is difficult to preselect the point in $(q\omega)$ space to be investigated. The triple axis spectrometer, by comparison is quite wasteful of neutrons but it is possible to accurately choose the region of (q,ω) space to be examined before the scan is performed. This leads to two main advantages over time of flight instruments for the investigation of dispersion curves in crystals:

i) It is possible to measure the curves along chosen high symmetry

i) contd.

directions in the Brillouin zone thus enabling a useful classification of phonons by group theoretical labels to be made.

ii) Intensities of phonon peaks measured at equivalent points in the structure factor repeat volume may be compared. Thus the mode may be identified by correlating these intensities with those predicted from structure factor calculations based on a dynamical model.

Fig.4.1 shows a schematic plan of a triple axis spectrometer (Brockhouse, 1961) and corresponding reciprocal space diagram. Neutrons of energy E are selected from the continuous spectrum by Bragg reflection:

$$G = 2|k| \sin\theta_M \qquad (4.17)$$

from the monochromating crystal. The energies of neutrons scattered by the sample through an angle ϕ are similarly examined by Bragg reflection from an analysing crystal. The relative positions of the monochromator sample and analyser tables enable the wave vector directions to be determined.

The particular choice of analyser and monochromator crystals and collimator $C_{(i)}$ used depends on the experiment to be performed (i.e. resolution desired, neutron energies involved etc). Monochromator crystals are large single crystals with good scattering characteristics - no absorption or incoherent scattering but large coherent scattering cross sections. However crystals with small mosaic spread less than $\sim\frac{1}{4}^\circ$ (Iyengar 1965) reject too large a fraction of the incident neutron intensity. The mosaic spread of such crystals may be increased by thermal or mechanical distortion. Metallic crystals have high reflectivity and the right order of mosaic spread. The wavelength range 0.5-2Å can be covered using reflections from copper, lead

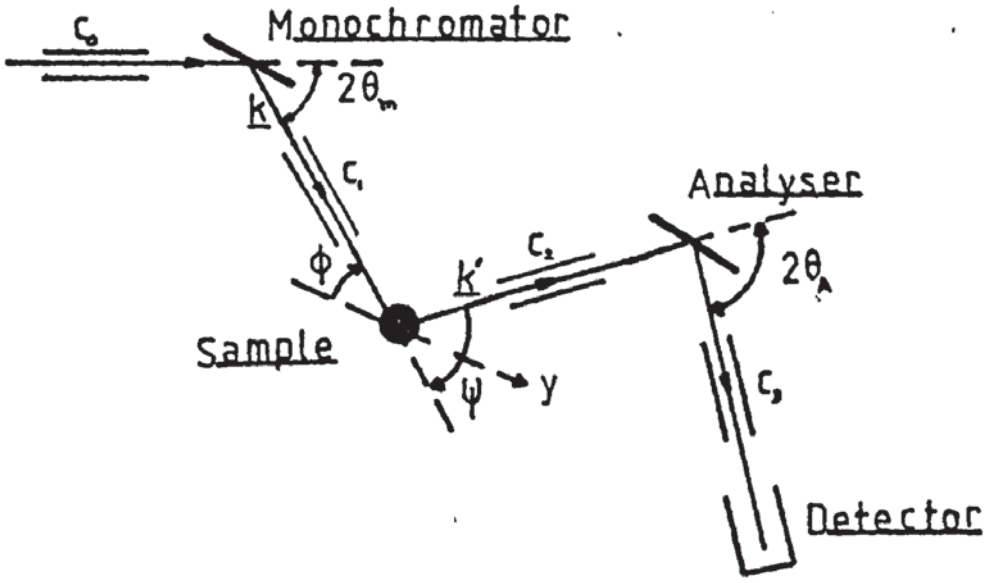

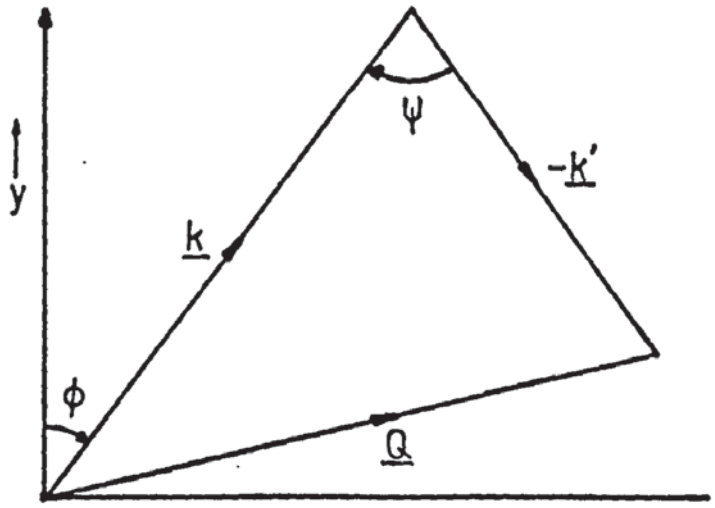

Triple-Axis Spectrometer: Scheme and Vector Diagram

Fig 4.1

and aluminium crystals. One problem is order contamination in the chosen wavelength due to multiple Bragg scattering. This may be avoided by use of reflections from crystals for which the structure factor of the second order is zero e.g. Ge(111),(222) absent.

The detector usually consists of an array of $^{10}BF_3$ or ^3He gas detectors. Neutrons undergo reactions with the gas nuclei to produce charged particles that are detected by the ionization generated as the particles move through the gas. The latter detectors are favoured because of the higher cross section of the (n,p) reaction involved, and smaller physical dimensions.

The monochromater table is situated in a fixed position either at the end of a hole in the reactor shielding or at the end of a guide tube. The other crystal tables and detector unit interconnected, as in fig.4.1 by a beam and rail assembly as in the original model (Brockhouse, 1961) or in the tanzboden (dance floor) type mounted on platforms that rise on air pads from the laboratory floor for positioning, connected by beams.

Triple axis spectrometers operate in the plane of the incident and scattered neutrons. The conservation equations (4.6) and (4.7) then only involve components of the vectors Q,,k,k' in the scattering plane. The components of Q given in terms of the measured quantities are

$$\begin{aligned} Q_1 &= -|k|\sin\psi - |k_1|\sin(\phi-\psi) \\ Q_2 &= |k|\cos\psi - |k_1|\cos(\phi-\psi) \end{aligned} \qquad (4.18)$$

where the quantities are defined as positive by the arrows in fig.4.1. Equations (4.18) with the conservation of energy constitute a set of three relations containing four unknown quantities. To specify an experimental point it is usual to fix the value of either the incident or scattered energy of the neutrons. In performing a scan in a particular direction in (q,ω) space the instrumental quantities required are calculated in the computer "controlling" the experiment.

Triple axis spectrometers allow the use of two powerful modes of scan. The constant energy or constant E (Sinclair and Brockhouse, 1960) scan is particularly useful for measurement of dispersion curves with steep gradients. The energy exchange is fixed while the change in wavevector Q is varied in a set direction equivalent to scanning across a range of q values. For the constant wave vector or constant Q scan (Brockhouse, 1961), however, Q is maintained at a set value while the energy exchange is varied over a given range. From (4.6) it can be seen that this method maintains q at a constant value. Figures 4.2 and 4.3 illustrate these modes for fixed incident neutron energy. The equation for the measured cross section (4.15) is simplified for these scan modes as the Jacobian for the constant energy scan is given by

$$|J| = \left|\frac{\hbar k}{2E}, \cdot \nabla_q \omega(q,j)\right| \qquad (4.19)$$

while for the constant Q scan it is simply unity.

4.2.2 Resolution and Focussing.

When the spectrometer is set to measure the scattered intensity from a particular point in (Q,ω) space, scattering from adjacent points will also be detected. This is a result of the finite resolution of the instrument due, in large part to the imperfect definition of neutron path by the collimators and the mosaic spread of the monochromator and analyser crystals. The problems of triple axis resolution have been reviewed by Nielsen and Bjerrum Moller (1969). If the collimator transition probabilities and crystal mosaic spread are assumed to have Gaussian distribution a suitable resolution function may be given by (Cooper and Nathans, 1967)

$$R = R_0 \exp\left(-\tfrac{1}{2} \sum_{ij} M_{ij} X_i X_j\right) \qquad i,j = 1,2,3,4 \quad (4.20)$$

with the X_i corresponding to ΔQ_x, ΔQ_y, ΔQ_z and $\Delta\omega$. The elements to M_{ij} are obtained from the spectrometer specification. This function is the probability of detecting scattering from points around the

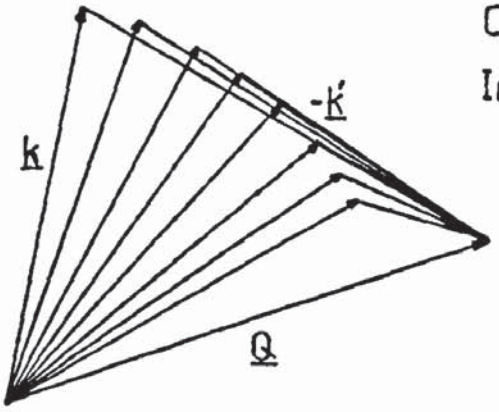

Fig 4.2 Vector Diagram-Constant Q Scan

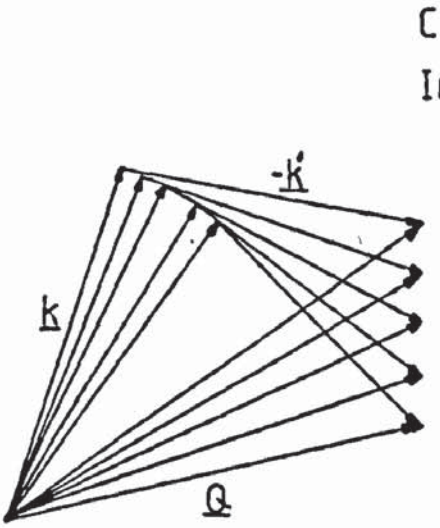

Vector Diagram-Constant Energy Scan

Fig 4.3

position in (Q,ω) space at which the spectrometer has been set. The intensity of the peak is given by convolving $R(\Delta Q,\Delta\omega)$ with the scattering cross section of the sample. From (4.20) it is seen that contours of R are ellipsoids in (Q,ω) space. The dimensions and orientation of the ellipsoids are determined by the fineness of the mosaic structure, the collimation and the configuration of the spectrometer.

In certain situations finite resolution has the effect of displacing the centre of the observed peak from the true phonon coordinates (Q,ω). For example, as most of the measured intensity is from scattering in the plane of the spectrometer, vertical collimation is relatively relaxed. Thus for two phonons which are degenerate in the scattering plane shifted or split peaks may be observed if the degeneracy is removed as Q moves out of the plane. (Cowley and Pant 1970).

An increase in peak height relative to the background, referred to as focussing, may be obtained by an optimized arrangement between the orientation of the resolution ellipsoid and the slope of the dispersion curve. Assuming the dimensions and orientation of the ellipsoid are unaltered during the small changes of configuration of the spectrometer during a scan it may be seen from fig.4.4 that the sharpness of the peak obtained is proportional to the "rate" at which the ellipsoid traverses the curve. Particularly for steep curves with gradients similar to that of the long axis of the ellipsoid the curve will be most rapidly crossed using a suitable constant energy scan. The diagram also shows that although the total cross section, i.e. integrated intensity for a constant Q scan is independent of the gradient of the dispersion curve, the measured peak shape may be drastically affected. Graphical and numerical methods have been developed which enable focussed configurations to be predicted before performing the scan. (Peckham et al. 1967).

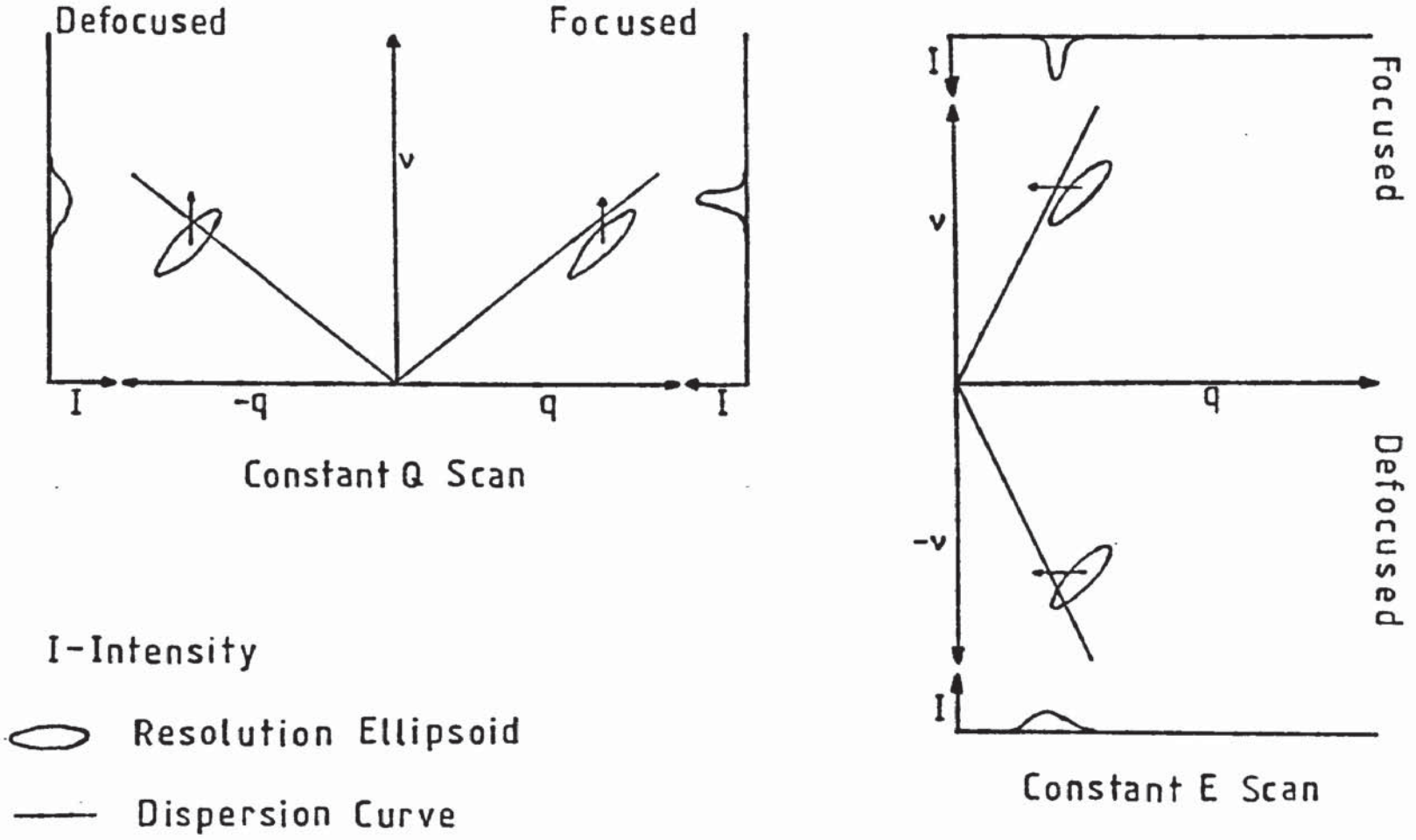

Fig 4.4 Effects of Focusing

4.2.3 Order Contamination.

Order contamination in the neutron wavelength brought about by multiple Bragg scattering has already been discussed. Spurious peaks may also occur in one phonon coherent inelastic scattering experiments by another process which may be easily eliminated. Bragg scattering may occur in the specimen which produces a reflected beam in the direction of the analyser. These neutrons can then be detected even when the analyser is not set to measure this wave vector (Dolling, 1974). A similar process starting with diffuse scattering from the monochromator which is then Bragg reflected by the other crystals also occurs. The measured peak often has a similar intensity to the phonon peaks but is usually sharper. This peak will in general disappear if the same scan is performed with a different incident or scattered wavelength.

4.3 Experimental Measurements.

Magnesium aluminate, $MgAl_2O_4$, is a particularly straight forward spinel on which to perform neutron scattering experiments as the constituent nuclei have very small or zero incoherent scattering lengths and none of the ions are magnetic. The scattering lengths for aluminium ($0.345\ 10^{-12}$ cm) and oxygen ($0.577\ 10^{-12}$ cm) are well established and may be obtained from the International Tables for Crystallography.

However over the years there has been some discrepancy in the value reported for magnesium:

$b_{COH}/10^{-12}$cm	$b_{inc}/10^{-12}$cm	
0.520	0.155	International Tables (1972)
0.537	0.089	Koester (1977)

The estimate of the incoherent scattering length has thus decreased and is taken here to be zero.

As neutron-phonon interactions are fairly weak and neutron beam

intensities low counting rates must be improved by the use of large single crystals as samples. The specimen employed had an approximate volume of 5×10^4 mm^3 and was roughly cylindrical about a [110] growth axis. The only previous neutron scattering measurements of this material were made by Thompson and Grimes (1978) on the same sample. Using the rotating crystal time of flight spectrometer at AWRE Aldermaston most of their data was collected at 523K. Present measurements were made at room temperature with the IN3 triple axis spectrometer at the Institute Laue-Langevin (I.L.L) during 22-26 August 1977. This spectrometer, of the Tanzboden type, has the sample and analyser crystal tables and the detector mounted on air pads that raised these components from a marble floor for position changes. Experiments are controlled by a computer linked to the I.L.L. Carine system. The spectrometer was set up to use the (111) reflection from copper as the monochromator and the (002) reflection from pyrolytic graphite for the analyser. The detector consisted of an array of five helium three (^{3}He) counters grouped together as a unit.

Six Bragg reflections from an aluminium oxide powder ($A\ell_2O_3$) were used to align the instrument and determine various offsets. The energy resolution was obtained from a scan of the incoherent inelastic scattering from a vanadium standard, the half width at half maximum, 0.32 THz, is taken as an indication of the resolution (fig.4.5).

Initially measurements were performed with the [001] axis of the sample crystal vertical so that phonons could be measured in the reciprocal plane perpendicular to this direction. Thus access was gained to previously unmeasured modes with wave vectors in the [110] direction with polarisations essentially transverse in [110] directions. As it proved impossible to unravel the optic modes in the [110] and [100] directions the majority of measurements were taken with the [1$\bar{1}$0] axis of the sample vertical. For simplicity attention was con-

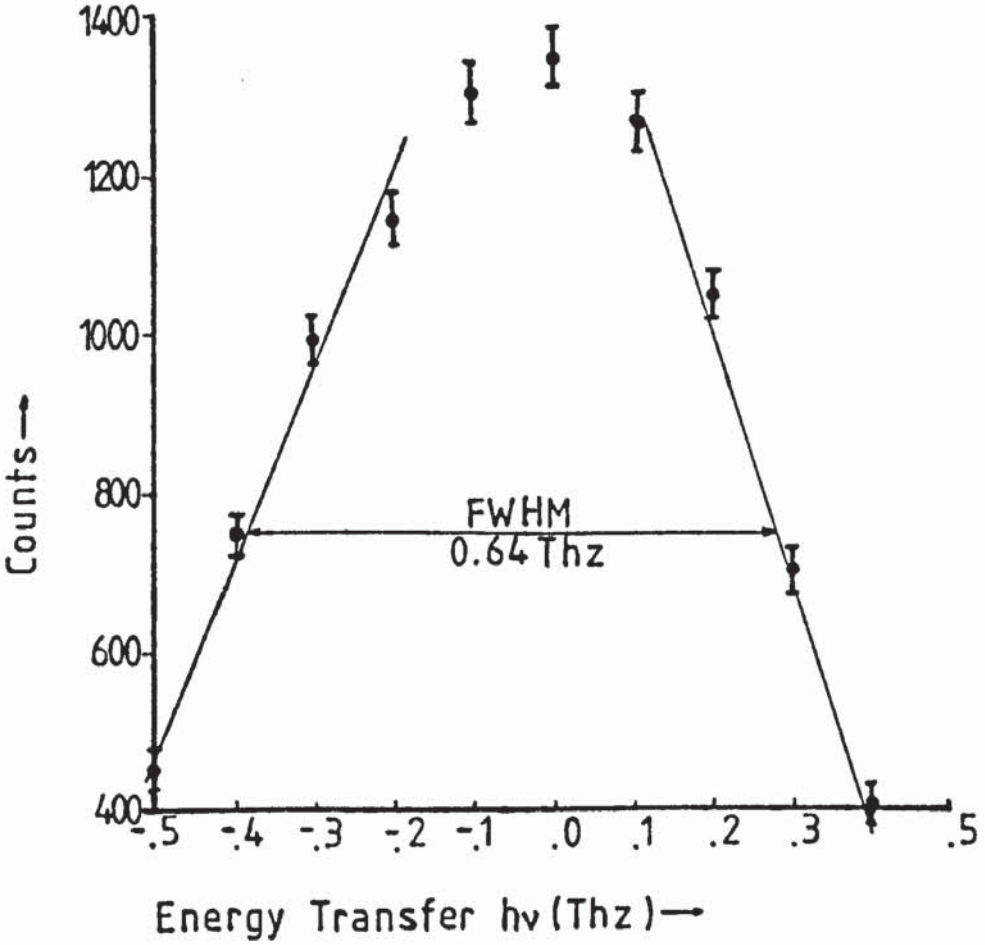

Energy Resolution - Vanadium Scan

Fig 4.5

centrated on phonon curves with propagation vectors in <111> directions. Figures 4.6(a)-4.6(d) show a selection of measured peaks, the effect of focussing is apparent in 4.6(a). As the flux intensity from the reactor fluctuates in time intensities are recorded over the interval in which a monitoring counter in the incident beam detects a preset number of events rather than over a given time period. Measurements were usually taken with the magnitude of the scattered wave vector k' maintained constant at 2.65 or 2.8 $\mathring{A}^{-1}$. However a few were made at other wavelengths and some with constant incident wave vector at 3 or 3.3$\mathring{A}^{-1}$. Constant k' has the advantage that the integrated intensity is a direct measure of the scattering power of the crystal because the k^{-1} factor in equation (4.15) is essentially cancelled by the 1/(velocity) efficiency of most detectors.

The effect of contamination in the incident and scattered wavelengths is to replace equations (4.6) and (4.7) by

$$\begin{aligned} Q &= rk - sk' \\ \hbar\omega &= \frac{\hbar^2}{2m}((rk)^2-(sk')^2) \end{aligned} \qquad (4.20)$$

where r and s are integers that are not simultaneously equal to unity. Only small values of these integers need to be considered as the intensity of the neutron spectrum decreases with increase of energy. Regions of (Q,ω) space in which (4.20) are satisfied may be avoided by the use of diagram such as fig 4.7 and the corresponding one for fixed incident energy. Lines corresponding to k = 2k', $^3/_2$k' etc. are plotted on a diagram of E' against energy transfer $h\nu$. Wavelengths related to energies that are removed from these lines and less than the maximum energy transfer (for IN3 17THz for zero E or E') may be used to avoid spurious peaks.

Considering only long wavelength acoustic modes wherein all atoms in adjacent unit cells vibrate in phase the dynamical structure factor in equation (4.13) may be approximated to

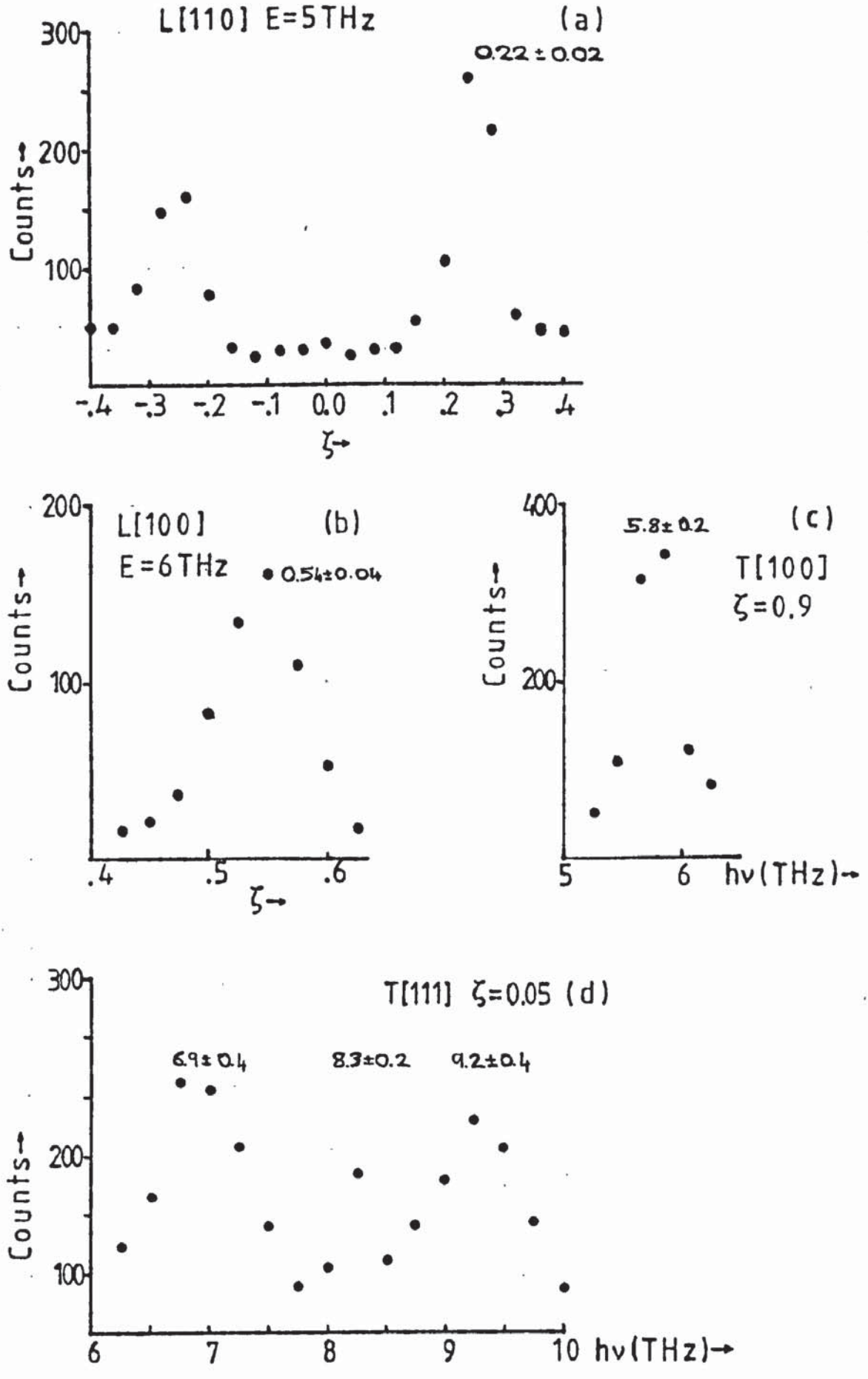

Fig 4.6 Some Observed Phonon Peaks

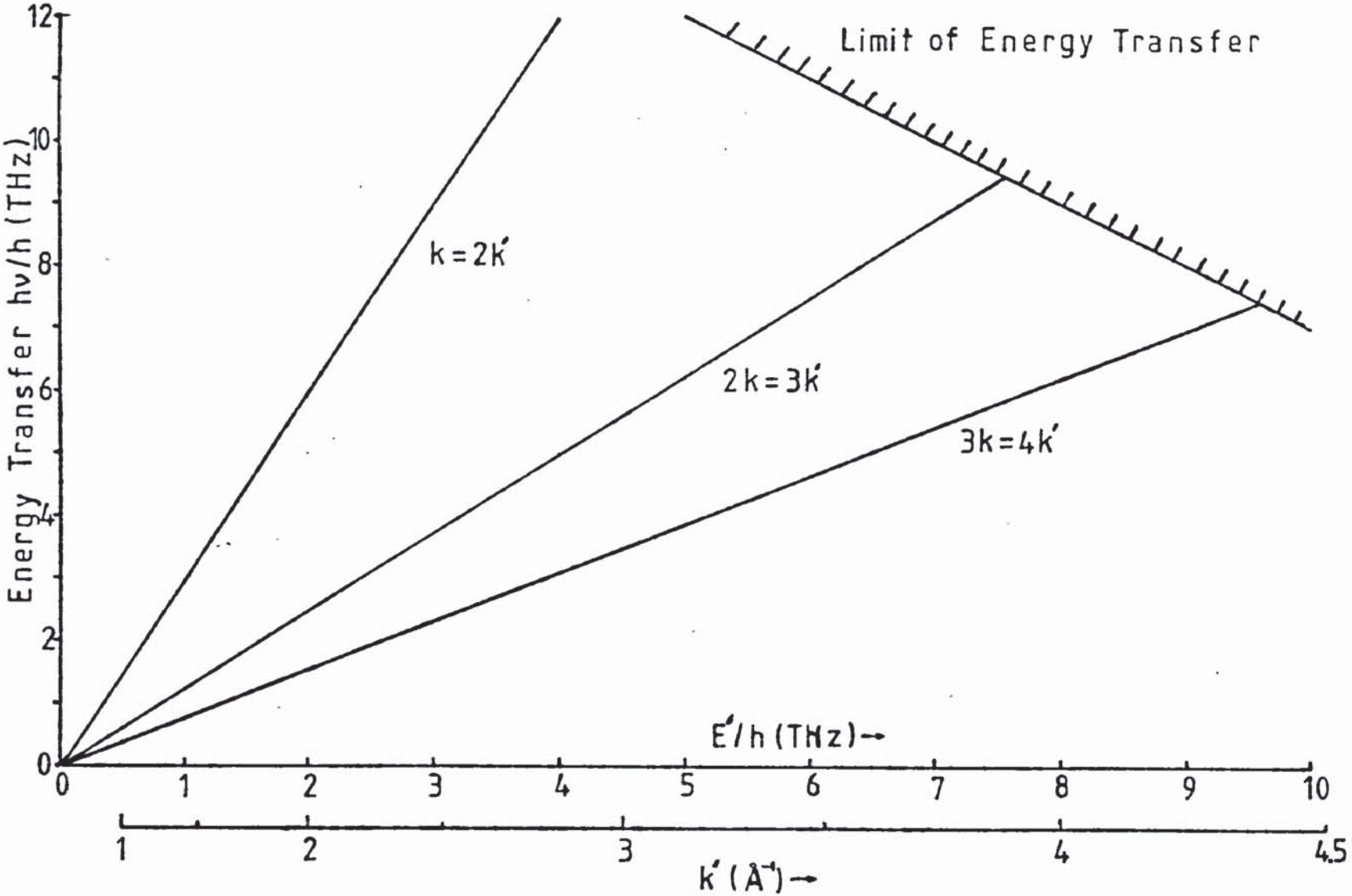

Fig 4.7 Order Contamination (for details see text)

$$\left| Q.e(\kappa,qj) \sum_{\kappa} \bar{b}(\kappa)\exp(iQ.r(0,\kappa))m_{\kappa}^{-\frac{1}{2}} e^{-W_{\kappa}} \right|^2 \qquad (4.21)$$

Neglecting the Debye Waller factor the terms to the right of the summation are merely the static structure factor. Calculations show that this term is maximum at the reciprocal lattice points (440), (400) and (444) in descending order. The Brillouin zone which has the greatest structure factor for a particular mode is now determined by Q.e where, for acoustic modes, the eigenvectors may be taken as purely longitudinal or transverse. This approximation, however, was not applicable for optic modes. The zones used for the measurement of X point frequencies and one of the transverse optic modes in the [111] direction were found by trial and error. Table 4.1 lists the zones used for the measurements of modes in some high symmetry directions in the Brillouin zone. The labels L and T refer to the spectrometer configurations used which would have been ideal if the mode were purely longitudinal or transvers respectively. Some phonons gave rise to peaks in both configurations. Table 4.2 contains lists of the phonons measured here, following Brokchouse and Stewart (1956) the error is taken as one quarter of the full width at half maximum. These are diagrammed in fig.4.8 where the drawn lines are guides to the eye only.

4.4. Discussion of Results.

The results obtained (table 4.2) are in good agreement with those of Thompson and Grimes (1977). There is no discernible difference between their measurements at elevated temperatures (usually 523K) and the corresponding measurements on the triple axis spectrometer at room temperature. The majority of the results are extensions of these same modes. However, the frequencies of the lower"transverse" acoustic mode T_2 in the [110] direction and the partial optic branches in the

TABLE 4.1 Zones Used for Observation of Phonons.

Brillouin Zone	Mode Type
400	T[ζ00] L[ζ00] T[ζζ0]
422	T[ζζζ]
440	T[ζζ0]
444	T[ζζζ] L[ζζζ]
640	L[ζζ0]

L and T refer to configurations of the spectrometer to measure longitudinal and transverse modes.

TABLE 4.2 - Observed Phonons in Magnesium Aluminate

ζ-Reduced Wave Vector

ν-Mode Frequency

Longitudinal [ζζζ]	
ζ	ν(THz)
0.05	6.9±0.5
0.05	8.1±0.2
0.05	9.3±0.4
0.07±0.02	5.5
0.09±0.02	8.5
0.10±0.04	2.5
0.1	7.5±0.4
0.1	8.7±0.3
0.12±0.04	3
0.15±0.04	3.5
0.16±0.03	8
0.17±0.04	4
0.20±0.03	4.5
0.2	8.7±0.5
0.22±0.02	5
0.23±0.03	5.5
0.25	9.6±0.2
0.27±0.03	6
0.27±0.03	7.5
0.32±0.03	7
0.36±0.03	8
0.36±0.03	8.5
0.37±0.03	9
0.43±0.04	9.5

Brillouin Zone Point	ν(THz)
Γ	6.5±0.5
Γ	7.7±0.2
Γ	9.2±0.3
L	4.4±0.3
L	6.5±0.3
L	8.6±0.3
X	5.9±0.3
X	6.8±0.2
X	9.8±0.3

Transverse [ζζζ]	
ζ	ν(THz)
0.05	6.9±0.4
0.05	8.3±0.2
0.05	9.2±0.4
0.15	5.5±0.3
0.15	6.84±0.14
0.2	6.5±0.14
0.2	7.5±0.3
0.25	6.2±0.1
0.25	7.4±0.2
0.3	6.3±0.25
0.3	7.1±0.2
0.35	5.5±0.1
0.35	6.90±0.15
0.4	6.6±0.3
0.4	4.0±0.25
0.45	6.5±0.2
0.45	4.4±0.2

Longitudinal [ζ00]	
ζ	ν(THz)
0.35±0.05	4
0.44±0.04	5
0.54±0.04	6
0.67±0.04	7
0.70±0.04	7.5
0.9	10.0±0.4

Transverse [ζ00]	
ζ	ν(THz)
0.3	2.3±0.2
0.4	3.1±0.2
0.5	3.8±0.3
0.6	4.5±0.3
0.7	5.0±0.3
0.8	5.5±0.2
0.9	5.8±0.2

Longitudinal [ζζ0]	
ζ	ν(THz)
0.20±0.04	4
0.25±0.04	5
0.32±0.05	6
0.4	6.5±0.2
0.5	6.6±0.4
0.5	8.4±0.2
0.6	6.8±0.2
0.7	7.1±0.3
0.9	5.9±0.3
0.9	6.8±0.3

Transverse [ζζ0] (T_1)	
ζ	ν(THz)
0.2	1.6±0.13
0.3	2.34±0.14
0.4	3.1±0.2
0.5	3.8±0.2
0.6	4.45±0.15
0.7	5.0±0.2
0.8	5.4±0.2
0.9	5.6±0.3
0.9	6.8±0.3

Transverse [ζζ0] (T_2)	
ζ	ν(THz)
0.2	2.15±0.15
0.4	4.4±0.2
0.5	5.4±0.2
0.6	6.4±0.3
0.7	6.9±0.3
0.7	8.0±0.3

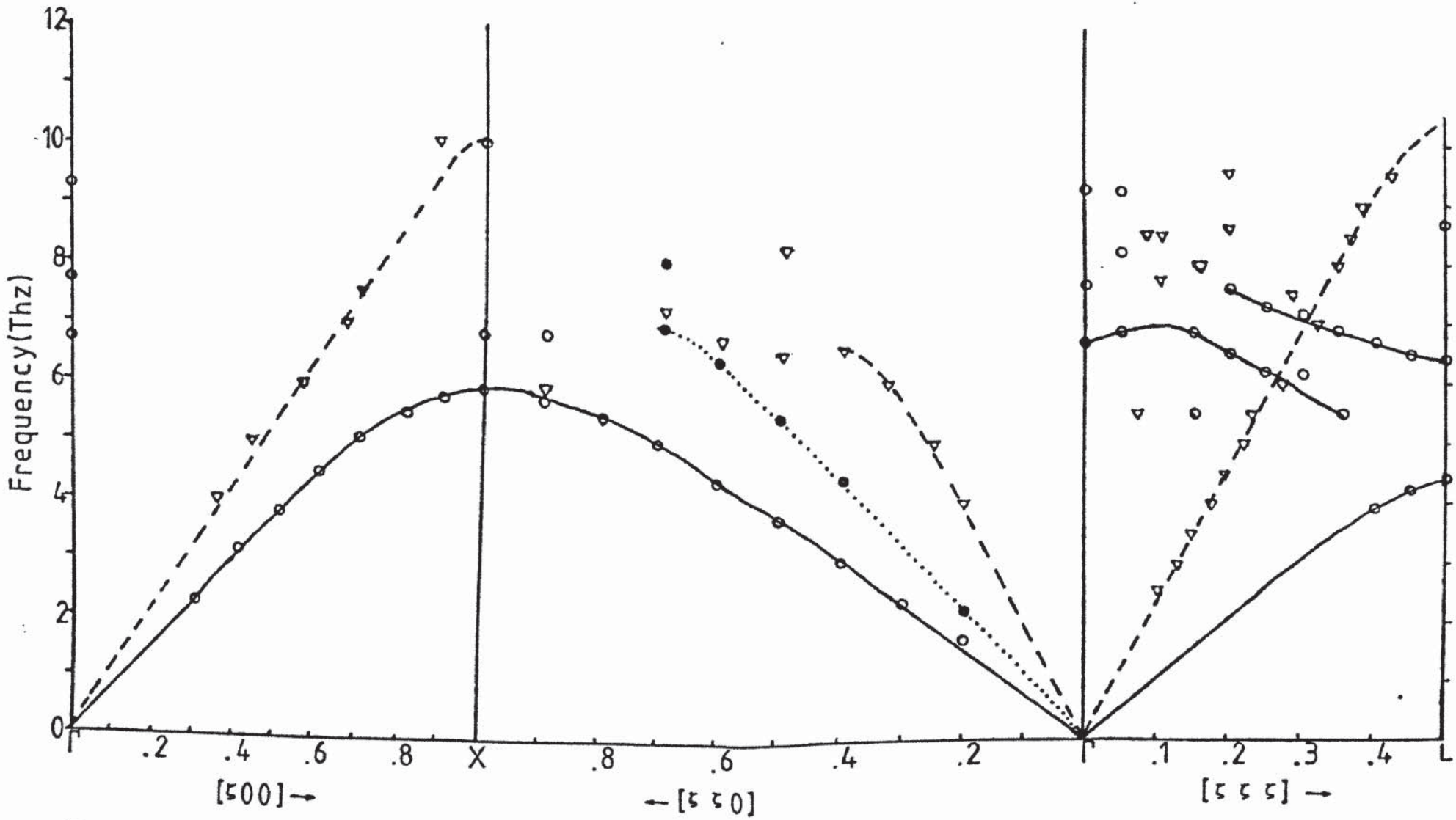

Fig 4.8 Low Energy Phonons in Spinel

[111] direction were previously unrecorded. The effects of the dynamical structure factor are particularly apparent for the latter curves as neither optic branch could be completely traced out in a single Brillouin zone. Calculations of the structure factor reveal great variation in intensity throughout the zone, even for acoustic modes. Fig.4.9 illustrates this for the lowest Λ_1 modes in the (444) zone, the calculations having been performed using eigenvectors for the best fit shell model (see Chapter 5). In principle calculations of this sort enable Brillouin zones to be chosen in which maximum intensity may be expected for any given mode. However, in practice calculations from the eigenvectors proved inconsistent and inconclusive. The curves in fig.4.9 were obtained using a program written in Algol and are completely at variance both in trend and order, with those calculated by an equivalent Fortran program. The problem lies in the actual calculation of the eigenvectors (see section 5.4.3), it appears impossible to calculate these accurately for a 42 x 42 complex matrix.

Table 4.3(b) compares the sound velocities obtained from the initial slopes of the neutron curves to those deduced from elastic constants given by Chang and Barsh (1973). The relations connecting the elastic constants and acoustic velocities are given in table 4.3(a). In all cases the quantities from the ultrasonic method are lower, hence the elastic constants deduced from neutron data would be larger. Similar effects have been observed for other materials including magnetite (Samuelson and Steinsvoll, 1974) but in general the discrepancies from either method do not give consistently higher or lower velocities. The two types of elastic constant have different thermodynamic natures. Ultrasonic measurements are made in the first sound region wherein the frequency of the probe is much less than the reciprocal lifetime of the phonon. Thus the phonons may be considered as a gas in thermal equilibrium. On the other hand neutron measure-

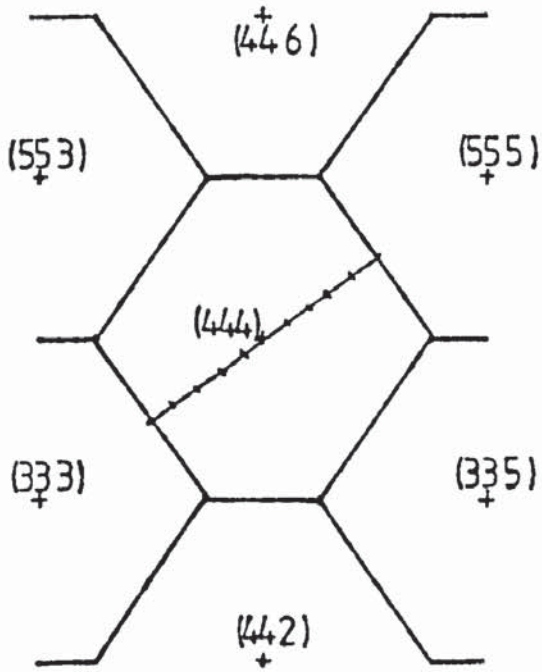

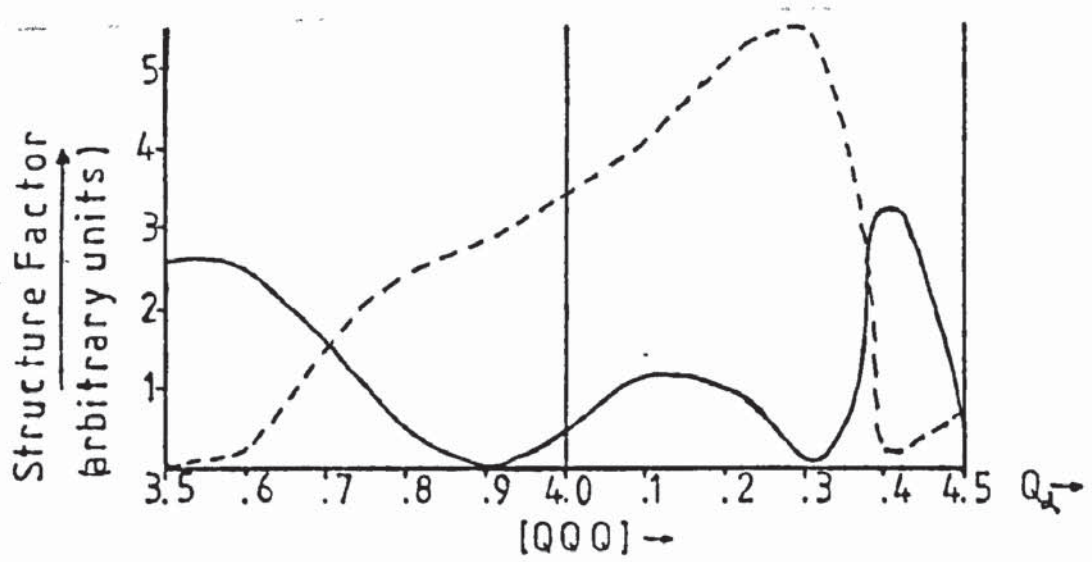

Dynamic Structure Factor for Δ_1 Modes in the (444) Zone

Fig 4.9

Mode Polarization [Direction]	Elastic Wave Velocity
L[100]	$\sqrt{C_{11}/\rho}$
T[100]	$\sqrt{C_{44}/\rho}$
L[110]	$\sqrt{(C_{11}+C_{12}+2C_{44})/(2\rho)}$
T_1[110]	$\sqrt{(C_{11}-C_{12})/(2\rho)}$
T_2[110]	$\sqrt{C_{44}/\rho}$
L[111]	$\sqrt{(C_{11}+2C_{12}+4C_{44})/(3\rho)}$
T[111]	$\sqrt{(C_{11}-C_{12}+C_{44})/(3\rho)}$

For $MgAl_2O_4$ $\rho = 3.581$ g/cm^3

TABLE 4.3a - Mode Elastic Velocities

Probe	Elastic Constants (10^{11}dynes/cm^2)		
	C_{11}	C_{44}	C_{12}
Ultrasonics (Chang and Barsch,1973)	2.808	1.547	1.523
Neutrons	3.86	1.57	2.3

TABLE 4.3b - Elastic Constant Measurements

ments are made with a higher frequency probe in the region known as zero sound (Liebfried and Ludwig 1961). Here the phonons have insufficient time for collisions to occur during each period of the sound wave. Cowley (1967) has considered these effects in detail, particularly with respect to the symmetry of the indices of the elastic constant tensors. In a harmonic solid these constants would be equal but if anharmonicity is significant they may be markedly different. For a cubic crystal the two elastic constants, isothermal (for neutrons), adiabatic (for ultrasonics) are related by

$$c^{AD} = c^{ISO} + (TV/C)\alpha^2 \qquad (4.22)$$

where C is the heat capacity and α the coefficient of expansion. Thus in general the ultrasonic measurements are expected to be greater than the neutron elastic constant by $(TV/C)\alpha^2$ which is a positive quantity. Thus although Samuelson and Steinsvoll have suggested that the discrepancies in their results for the spinel Fe_3O_4 may be accounted for by the difference in elastic constants this does not seem to be the case for $MgAl_2O_4$ where the expected inequality is violated.

The difference then is probably due, in this case, to the effects of the resolution function and scattering cross section. As already indicated the measured intensity is given by convolving the resolution function with the scattering cross section. For small wave vector acoustic modes the latter, in particular is a rapidly varying quantity. Computer calculations (e.g. Fujii et al. 1974 on Argon) have shown that peak positions for these phonons may be offset by about 5% of their observed values. This effect may then contribute to the observed differences in the results from the two different techniques. In all cases however the differences are within the error of the neutron measurements.

CHAPTER 5

RESULTS FROM MODEL CALCULATIONS.

5.1 Simplifying Assumptions.

The intention is to use rigid ion and shell models, outlined in Chapter 2, to describe the dynamical behaviour of magnesium aluminate. The number of adjustable parameters that could be used is very large. However, apart from the difficulties of refining vastly complex models, any sensible interpretation of the results requires simplification of the problem so that the important quantities may be elucidated. Various assumptions are made to reduce the number of parameters. From Chapter 1 it is apparent that the properties of magnesium aluminate are probably most accurately assigned to the space group $F\bar{4}3m$ rather than Fd3m. However the latter was assumed for model calculations as the differences in ionic positions between the two structures are minute and the higher symmetry ensures a reduction in the number of independent interactions. Taking $MgAl_2O_4$ to be completely normal the fourteen ions in the basis, which give rise to a dynamical matrix of order 42 x 42, are labelled according to table 5.1.

As magnesium aluminate is one of the more ionic spinels (see section 1.3.6) it is convenient to use shell models equivalent to early models for alkali halides (Cowley et al. 1963). The bonding is taken as completely ionic therefore the valence states are assumed to be at their nominal values ($Z_{Al} = 3e$, $Z_{Mg} = 2e$, $Z_{ox} = -2e$). Further, because of the larger size of the anions compared to the cations only the oxygen ions are considered polarizable. Matrices S and T of equation (2.54) are set equal to the inter-ion short range matrix R at all values of wave vector thus representing all short range interactions as acting through the shells. In comparison it is usual in studies of materials in which covalent bonding is thought significant to assume these matrices to be related by a numerical factor determined during model refinement.

In alkali halides all anions are at sites of cubic symmetry and therefore the intra-ion core-shell interactions are isotropic.

Ion	Label κ	Position
Aℓ	1	$0,0,0$
Aℓ	2	$0,\frac{1}{4},\frac{1}{4}$
Aℓ	3	$\frac{1}{4},0,\frac{1}{4}$
Aℓ	4	$\frac{1}{4},\frac{1}{4},0$
Mg	5	$\frac{3}{8},\frac{3}{8},\frac{3}{8}$
Mg	6	$\frac{\overline{3}}{8},\frac{\overline{3}}{8},\frac{\overline{3}}{8}$
Ox	7	$\frac{\overline{1}}{4}+\delta,\frac{\overline{1}}{4}+\delta,\frac{\overline{1}}{4}+\delta$
Ox	8	$\frac{\overline{1}}{4}+\delta,-\delta,-\delta$
Ox	9	$-\delta,-\delta,\frac{\overline{1}}{4}+\delta$
Ox	10	$-\delta,\frac{\overline{1}}{4}+\delta,-\delta$
Ox	11	$\frac{1}{4}-\delta,\frac{1}{4}-\delta,\frac{1}{4}-\delta$
Ox	12	$\frac{1}{4}-\delta,\ \delta,\ \delta$
Ox	13	$\delta\ ,\frac{1}{4}-\delta,\ \delta$
Ox	14	$\delta\ ,\ \delta\ ,\frac{1}{4}-\delta$

Labelling of Ionic Positions in the Basis

TABLE 5.1

Consequently the shell charge Y and short range intra-ion core-shell force constant K matrices are diagonal. In spinel, however this condition is not imposed by symmetry. As shown in fig.1.3 the oxygen site is trigonal with the unique axis lying along the Mg-O bond. In general the 3 x 3 submatrix of the dynamical matrix of type $D_{\alpha\beta}(8,8,q=0)$ has a form similar to

$$\begin{pmatrix} A & B & B \\ B & A & -B \\ B & -B & A \end{pmatrix} \qquad (5.1)$$

which when referred to a set of principal axes at that ion site reduces to the diagonal form

$$\begin{pmatrix} D & 0 & 0 \\ 0 & C & 0 \\ 0 & 0 & C \end{pmatrix} \quad \text{where } D = A + 2B, \quad C = A - B \qquad (5.2)$$

The submatrices of Y and K (and also the polarizability tensor for an oxygen ion then, by symmetry have a minimum of two independent parameters each. In general when referred to the cubic axes these matrices have both on and off diagonal terms and different but related forms depending on the relative orientation of the site. This complexity was avoided by arbitrarily assuming the core-shell to be isotropic (i.e. setting D = C), thus making (5.1) and (5.2) equal regardless of anion site. This is expected to be a fair approximation for magnesium aluminate as the measured value of δ (0.012)'' is very close to the value (δ = 0.0125) at which the Mg-O and Al-O distances are equal, although of course, the charges on the neighbouring cations emphasize the uniaxial symmetry. Alternatively the cations may be considered as lying in the interstices of the surrounding oxygen ions. The oxygen intra-ion interaction may then be greatly influenced by the effects of the surrounding oxygen shells. As the oxygen ion arrangement is almost perfect face centre cubic packing the anions may be thought to lie in sites of effectively diagonally cubic symmetry. Therefore the Y and K matrices may reasonably be taken as diagonal.

The rigid ion models are taken to be limiting cases of the corresponding shell models with Y = 0 and K = 10^{10}, these values having been found to give the same frequencies as a "pure" rigid ion model to an accuracy of at least 0.01 THz. Note that it is necessary to set both the Y and K parameters to the values given above simultaneously. For instance setting Y = 0 only, yields a shell model with uncharged shells and somewhat "soft" ions which has quite different eigenvalues to those of the rigid ion model.

5.2 Matrix Elements.

5.2.1 Elements of the Short Range Interaction Matrix R.

The short range inter ion interactions are given in terms of the parameters A and B defined by equations (2.41), one pair A,B assigned to each independent distance. For the cations the interaction is considered to occur only between the metal ions and their nearest neighbour oxygen ions. The short range interactions with magnesium then only involve the four anions at distance d_t which form the tetrahedron about the cation site, fig.5.1. Similar conditions exist for aluminium ions which lie at the centre of oxygen octahedra, fig.5.2. The six oxygen ions surrounding each aluminium site are equidistant from the centre (distance d_o) even though the octahedron is distorted when the oxygen δ is greater than zero. The short range interactions assumed for the oxygen ions are more complicated to account for the expected electron cloud overlap effects due to their large diameters. Therefore not only the nearest neighbour cation interactions are included (fig.1.3) but also those of the surrounding twelve anions. In an ideal spinel structure (δ = 0) the neighbouring oxygens would be equidistant. The effect of having a non-zero δ is to separate these ions into three groups at slightly different distances from the central oxygen. These anions of index A,B,C say are at the nearest neighbour distance d_1. Another three ions, equivalent to the

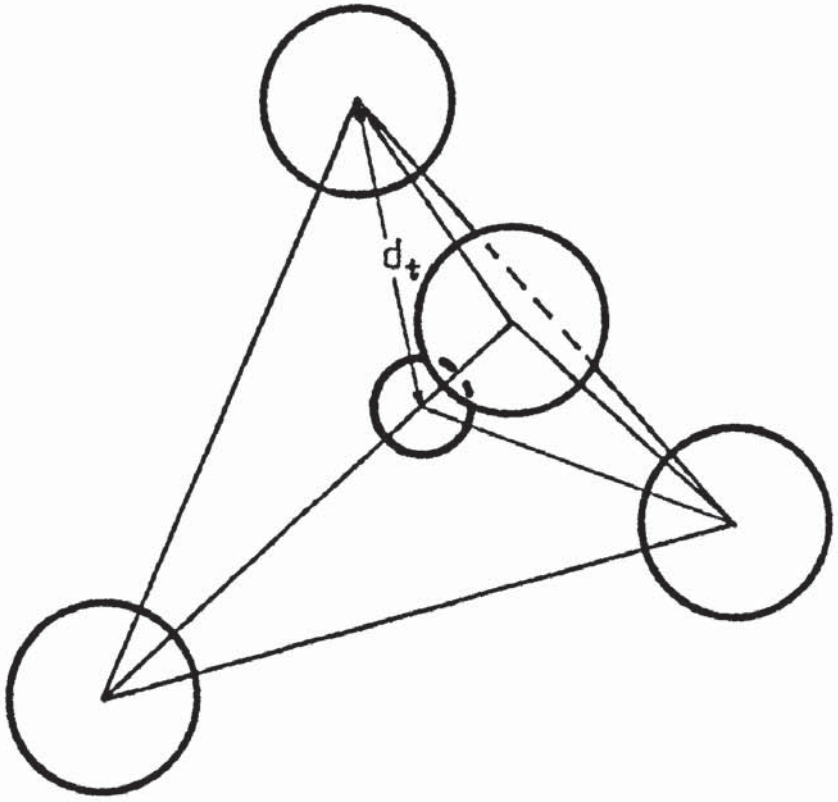

Fig 5.1 Tetrahedral Ion Environment

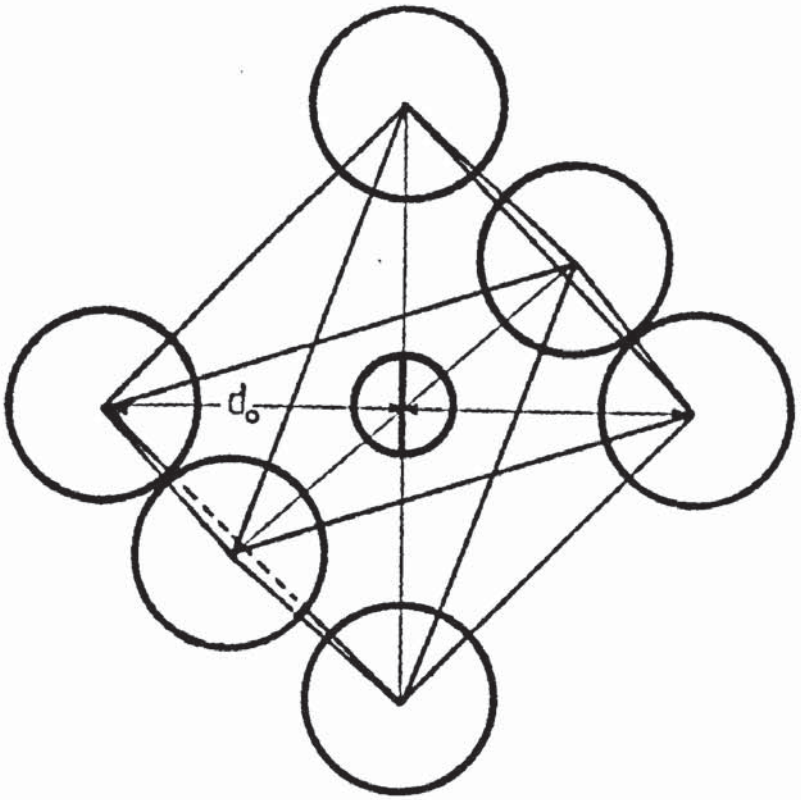

Fig 5.2 Octahedral Ion Environment

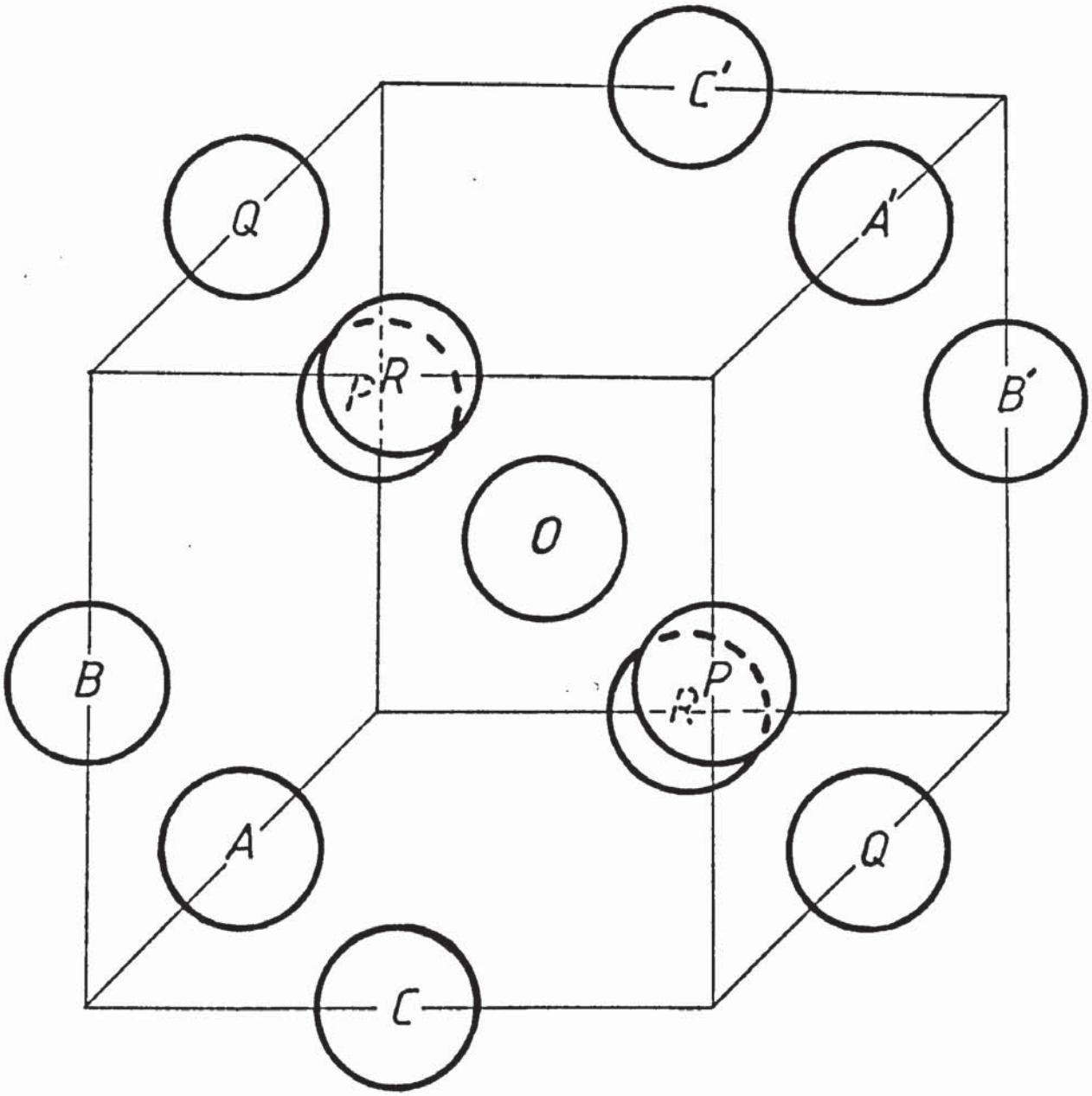

Distance	O - A, B, C	d_1
	O - A', B', C'	d_3
	O - P, Q, R	d_2

Oxygen-Oxygen Environment

Fig 5.3

Interaction	Separation Distance	Associated Parameters
Aℓ - O	$d_o = a\sqrt{\frac{1}{16} - \delta/2 + 3\delta^2}$	A_o, B_o
Mg - O	$d_t = a\sqrt{3}(\frac{1}{8} + \delta)$	A_t, B_t
O1 - O1	$d_1 = a\sqrt{2}(\frac{1}{4} - \delta)$	A_1, B_1
O2 - O2	$d_2 = a\sqrt{\frac{1}{8} + 4\delta^2}$	A_2, B_2
O3 - O3	$d_3 = a\sqrt{2}(\frac{1}{4} + \delta)$	A_3, B_3

a = lattice parameter

Interionic Distances and Associated
Short Range Interaction Parameters

TABLE 5.2

above by face centred translations lie at the greatest oxygen neighbour distance d_3. The remaining six are in sites at an intermediate distance d_2. Fig.(5.3) displays the oxygen-oxygen environment. The short range parameters and inter ion distances are summarized in table 5.2. In total there are five pairs of parameters A,B corresponding to the five distinct distances.

The dimensionless elements of the matrix R are now readily given in terms of these parameters by substituting equation (2.43) in equation (2.44). The translational invariance terms are given by

$$R_{\alpha\beta}(\kappa\kappa,q) = - \delta_{\kappa\kappa'} \sum_{\kappa'} R_{\alpha\beta}(\kappa\kappa',q=0) \qquad (5.3)$$

and are always regular. The independent elements at q=0 are given in Appendix I in terms of the adjustable parameters and interaction distances of table 5.2.

5.2.2 Coulomb Coefficients.

The Coulomb coefficients are the elements of the dimensionless matrix C in the equations of motion (2.57). Unlike the short range matrix these coefficients are completely determined by the crystal structure and form of the potential (see equations (2.39) and (2.40)) and do not depend on any adjustable parameters. Each coefficient may be evaluated by a device due to Ewald (see Born and Huang 1954) in which the slowly convergent summation of equation (2.40) is replaced by two rapidly convergent series, one in real space the other in reciprocal space as given below

$$C_{\alpha\beta}(\kappa\kappa' q)=4\pi\sum_{G}\frac{(G_\alpha+q_\alpha)(G_\beta+q_\beta)}{|G+q|^2}\exp(-G+q)^2/4c^2)\exp(i(G+q).[r(\kappa)-r(\kappa')])$$

$$-\frac{c^3}{4}\left\{\frac{4\delta_{\alpha\beta}}{3\sqrt{\pi}}+\sum_{\ell'}{}' H_{\alpha\beta}(c\ x(\ell',\kappa',\kappa))\exp[iq.x(\ell'\kappa',\kappa)\ ]\right\} \qquad (5.4)$$

where

$$H_{\alpha\beta}(y)=\frac{y_\alpha y_\beta}{|y|^5}\left[3\mathrm{erfc}(|y|)+(4|y|^3+6|y|\ \frac{\exp(-y^2)}{\sqrt{\pi}}\right]-$$

$$-\frac{\delta_{\alpha\beta}}{|y|^3}\left[\mathrm{erfc}(|y|)+\frac{2}{\pi}|y|\exp(-y^2)\right], \qquad (5.5)$$

erfc(x) is the complementary error function

$$\mathrm{erfc}(x)=1-\frac{2}{\sqrt{\pi}}\int_0^x\exp(-\rho^2)d\rho \qquad (5.6)$$

and c is the parameter chosen to obtain fast convergence of both series to give the final result. A value of 3.0 gave approximately equal rates of convergence on both series for spinel.

$C_{\alpha\beta}(\kappa\kappa' q)$ is not regular at q=0 as it contains the term $q_\alpha q_\beta/q^2$, the limit of which as q tends to zero depends on the direction from which the origin of the Brillouin zone is approached. The non regular term is related to the macroscopic electric field which lifts the degeneracy of threefold infrared T_{iu} modes predicted by group theory. However, it is still possible to consider the q=0 dynamical matrix where the first term of the reciporcal space series of equation (5.4) has been omitted, since its inclusion only affects the predicted frequencies of infrared modes with dipole moments in the direction of the considered wave vector.

It is of interest to note that whereas the translation invariance terms of ZCZ in the equation of motion are given by

$$-\delta_{\kappa\kappa'}\ Z_\kappa\sum_{\kappa}Z_{\kappa''}\ C_{\alpha\beta}(\kappa\kappa'',q=0) \qquad (5.7)$$

the translation invariance terms for the shell terms ZCY, YCZ and YCY may be shown to be identical (Stirling 1972a, Venkateraman et al.1975)

$$- \delta_{\kappa\kappa'} Y_{\kappa} \sum_{\kappa''} Z_{\kappa''} C_{\alpha\beta}(\kappa\kappa'', q=0) \qquad (5.8)$$

5.3 Central Forces.

The short range forces given so far in terms of force constants defined by equation (2.41) are known as axially symmetric forces. Cochran (1971a) has shown that use of these forces without restraints is equivalent to the inclusion of a volume dependent term in the expression for the potential. This may be removed by using central forces and the imposition of the static equilibrium conditions. The short range forces may be made central if the parameter B is redefined in terms of the first derivative of the potential function as

$$B = \frac{2v_a}{e^2} \frac{1}{r} \frac{\partial \phi(r)}{\partial r} \qquad (5.9)$$

The Coulomb forces are already central in nature.

The static equilibrium conditions are a balance between the essentially attractive Coulomb forces in the crystal and the essentially repulsive short range forces. This is achieved by minimizing the crystal potential energy with respect to both constant volume distortions of the whole crystal (macroscopic strain) and with respect to any internal position parameters (internal strain) as all atoms are assumed to be at their equilibrium positions. The second condition may be shown to be equivalent to the imposition of rotational invariance on the crystal potential function (Boyer 1974).

In spinel the potential energy ϕ is a function of both the lattice parameter a and the oxygen position parameter δ. Therefore the static equilibrium conditions are given in terms of derivatives of ϕ with respect to these quantities. In principle the potential function includes electronic polarization effects and so for spinel

contains an extra structural parameter to describe the symmetry allowed displacements of the oxygen shells relative to their cores. However as Coulomb contributions to crystal statics are usually well accounted for in terms of the nominal ionic charges and the actual displacement is unknown this possibility will not be considered. The alternative is to replace the oxygen core positions in the Coulomb coefficients of the type core-core and core-shell by positions of the type (u-R,u-R,u-R) and re-evaluating and replacing K_{ox} by $K_{ox} \exp(iq.R)$ where R is a parameter to be determined by model refinement. This method was used by Cran and Sangster (1974a) to model MnF_2. As the calculation of the Coulomb coefficients is a fairly lengthy process this method besides introducing an extra parameter would be prohibitively expensive in computer time for a structure of the complexity of spinel. It is worthwhile to point out that although it may be thought that the shell displacements relative to the cores could be obtained by comparison of neutron and X-ray data (e.g. as suggested by Smit (1968) this would be difficult to achieve in practice as X-rays in general, are insensitive to the distortion of the valance electron arbitals.

The potential energy per formula unit for spinel, first given by Striefler and Barsch (1972) is

$$\phi^c + 4\phi_t(d_t) + 12\phi_0(d_0) + 6\phi_1(d_1) + 12\phi_2(d_2) + 6\phi_3(d_3) \qquad (5.10)$$

where the Coulomb contribution in terms of the Madelung constant per formula unit M is given by

$$\phi^c = -\frac{e^2}{a} M \qquad (5.11)$$

The corresponding static equilibrium conditions in terms of B and M are

$$M + 8\alpha_t^2 B_t + 24\alpha_0^2 B_0 + 12\alpha_1^2 B_1 + 24\alpha_2^2 B_2 + 12\alpha_3 B_3 = 0 \qquad (5.12)$$

$$\frac{\partial M}{\partial \delta} - \frac{24}{\sqrt{3}} \alpha_t B_t + 24(\tfrac{1}{4} - 3\delta)B_0 + 24\sqrt{2}\alpha_1 B_1 - 96\delta B_2 - 24\sqrt{2}\alpha_3 B_3 = 0 \qquad (5.13)$$

where $\alpha_i = d_i/a$.

M may be calculated from the Ewald transformation of the series (Born and Huang 1954)

$$M = \tfrac{1}{2} \times \tfrac{1}{2} \sum_{\ell\kappa\kappa'}{}' \frac{aZ_\kappa Z_{\kappa'}}{|r(\ell'\kappa')-r(\ell\kappa)|} \qquad (5.14)$$

Thompson and Grimes (1977a) have calculated M for several values of δ taking one of the factors $\frac{1}{2}$ to the right of the summation and using a/2 as a reference length. In comparison I used the expression as given and obtained the following expression for M in terms of the ionic charges

$$M=\tfrac{1}{2} \times (3.9685Z^2_{A\ell}+3.2131Z^2_{Mg} +1.2561Z^2_{ox}-2.0254Z_{A\ell}Z_{Mg}-29.7349Z_{A\ell}Z_{ox} - 11.3614Z_{Mg}Z_{ox}) \qquad (5.15)$$

which is quite different from theirs at $\delta = 0.012$:-

$$M = -0.0792Z^2_{A\ell}+1.0905Z^2_{Mg}-7.624Z^2_{ox}-3.0760Z_{A\ell}Z_{Mg}-23.118Z_{A\ell}Z_{ox}-9.80\mathfrak{Z}Z_{Mg}Z_{ox} \qquad (5.16)$$

although both give the same answer 132.65. The coefficients are not different by a factor of 2 as the convergence factor in the Ewald transform has also to be changed with reference length to make the result independent of this parameter.

The derivative of M with respect to δ was evaluated by taking a $\pm$ 0.0001 variation in $\delta = 0.012$. As expressions like the above are too inaccurate for this purpose the Ewald transformation was used in full to give

$$\left(\frac{\partial M}{\partial \delta}\right)_{\delta=0.012} = 299.9 \pm 0.4 \qquad (5.17)$$

which is in fair agreement with the Striefler and Barsch value of 300.16 but shows that Thompson's (1977) value of 301.6 is quoted to too many significant figures.

5.4 Refinement of Models

5.4.1 The Models

The equation of motion with the approximations mentioned included is given by

$$4\pi^2\left(\frac{v_a}{e^2}\right)\nu^2 U = M\left\{R+ZCZ+2_T-[R+ZCY+Y_T][R+K+YCY+Y_T]^{-1}[\tilde{R}^*+YCZ+Y_T]\right\}\times MU \tag{5.18}$$

Z_T and Y_T are matrices that include the translation invariance terms for the associated ionic and shell Coulomb terms. M,Z,Y,K are 42 x 42 diagonal matrices containing the reciprocal square root of the ionic masses, the ionic charges the shell charges and the short range core-shell force constants respectively. The values of all the elements of M and Z and those of K and Y pertaining to metal ions are held fixed for all models. Only in the shell models are the elements of Y and K for the anions variable, having values Y_{ox} and K_{ox} for all eight oxygens in the basis, otherwise these are set at rigid ion values Y = 0, K = 10^{10}.

Inspection of Appendix I shows that at q=0 the oxygen-oxygen parameters A_1,A_3 and B_1,B_3 of the matrix R always occur together. Thus at the Γ point in the Brillouin zone A_3,B_3 may be set to zero and A_1,B_1 adjusted to give the same eigenfrequencies. Although these pairs of parameters are decoupled at finite wavevectors it is reasonable to reduce the number of parameters by imposing the above condition for two reasons (i) the short range interactions are expected to decrease exponentially in strength with increasing distance, thus A_3 and B_3 are expected to be much smaller than A_1 and B_1 (ii) most of the experimental data to which the models are refined is concentrated at or near the zone centre. Any separate refinement of these pairs of parameters is then unreliable because the decoupling phase factors in this region are small.

Striefler and Barsch (1972) used the argument of decreasing influence with distance also to set A_2, B_2 to zero. However, investigation revealed that these parameters had the greatest influence on the highest frequency T_{2g} Raman mode for several sets of short range parameter and thus were retained. Consequently the most generalised shell model has ten disposable parameters: $A_o, A_t, A_1, A_2, B_o, B_t, B_1, B_2, Y_{ox}$ and K_{ox}.

Two pairs of models were investigated, each pair consisting of a shell model and corresponding rigid ion model enabling the effects of polarization to be directly ascertained. The first pair used central forces with equations (5.12) and (5.13) solved for B_1 and B_2. The imposition of the static equilibrium conditions would not then unrealistically effect model refinement as these parameters are usually the smallest. In comparison the second pair were optimized without imposing any restrictions. It is possible in principle to impose stability constraints which are of similar form but inequivalent to the equilibrium conditions. However this was not undertaken. Despite their unphysical nature models of this type are expected to indicate the degree to which the assumption of central forces is appropriate.

5.4.2 Refinement.

The models were optimized to fit the observed A_{1g}, E_g, T_{2g} Raman frequencies, the two highest frequency infrared absorption modes and the acoustic modes. The last mentioned were taken at two sets of positions in the Brillouin zone, firstly close to the origin at (0.05,0.05,0.05),(0.05,0.05,0.0),(0.05,0.0,0.0) and then approximately half way to the zone boundary at (0.25,0.25,0.25),(0.4,0.4,0.0) (0.5,0.0,0.0). Although group theory predicts four infrared modes the Kramers-Kronig analysis of single crystal reflectance data only reveals three. At present it is uncertain to which of the two lower modes the lowest observed frequency corresponds. It is reasonable to assume the

modes used are actually the highest infrared bands as the Kramers-Kronig analysis shows the largest longitudinal-transverse splittings for these modes (O'Horo et al. 1973) in qualitative agreement with the rigid ion models of both Striefler and Barsch and Thompson.

Refinement to room temperature data is inconsistent as the models are based on the assumption that the crystal is at OK (section 2.1). Leibfried (1963) has argued that the temperature variation of the experimental data be extrapolated to OK and the models refined to the resulting quantities. However this is not common practice and is impossible here where the data temperature dependence is unknown.

The refinements were performed using a non-linear least squares fitting procedure following a method given by Dolling (1976), minimizing the function χ given by

$$\chi = (N-V)^{-1}\ \chi' \tag{5.19}$$

where

$$\chi'^2 = \left[\frac{\omega^2_{CALC} - \omega^2_{OBS}}{2\omega_{OBS}\ \Delta\omega_{OBS}}\right] \tag{5.20}$$

$\Delta\omega$ is the error on the observed frequency, N and V are the number of experimental frequencies used and the number of adjustable parameters respectively. To achieve stable models it was necessary to weight the acoustic mode frequencies. A disparity of say $(-1)^2(THz)^2$ for these modes compared to say $(\pm 6)^2(THz)^2$ for an optic mode has much less effect on the fitting parameter but may result in vibration amplitudes that increase exponentially in time.

5.4.3 Numerical Calculations

The necessary calculations were performed with programs written in Fortran and Algol 60 evaluated on the CDC 7600 computer at the University of Manchester Regional Computer Centre. Matrix manipulations were performed using the appropriate subroutine of the Numerical Algorithms Group subroutine library.

Before diagonalisation the 42 x 42 dynamical matrix was block diagonalised by a similarity transformation with the appropriate symmetry coordinate matrix obtained from Warren and Worlton's (1974) group theory program. The largest block that then had to be diagonalised was a 14 x 14 matrix for the Λ_3 modes.

As the Coulomb coefficient matrix C and the elements of the symmetry coordinates are independent of the disposable parameters these quantities were calculated once, stored and used throughout the refinements.

As mentioned previously the numerically evaluated eigenvectors of the full dynamical matrix unfortunately have proved unreliable. It transpires that in the subroutine used, F02AXA/F, orthogonal eigenvectors are always produced the elements of which may be particularly sensitive to small changes in the dynamical matrix.

5.4.4 Results.

Table 5.3 lists the values of the refined parameters for the models together with those of previous workers. Quantities in square brackets are either held fixed for the model, such as the Y and K parameters in the rigid ion models or determined by static equilibrium conditions. The errors quoted were obtained from the non linear least squares procedure. The fitting parameters are given with $\Delta\omega$ set to unity, all weighting removed from the acoustic modes and evaluated for fit half way through the Brillouin zone. The zone centre frequencies are given in table 5.4 together with the experimental values where known. Again quantities in brackets were not used in refinement. The longitudinal infrared frequencies, labelled T'_{1u} are those of the corresponding mode in the [qqq] direction evaluated at $|q/q_{max}| = 0.05$. In view of the irregularity of the macroscopic electric field contribution this choice of direction is arbitrary. However these frequencies are approximately central between the corresponding eigen-

	MODELS					
	Central Force		Unrestrained		Previous	
Parameters	Rigid Ion	Shell	Rigid Ion	Shell	SB*	Thompson
A_o	435.5 ±0.3	431.2±0.3	449.0±0.2	463.3±0.3	437.42	425
A_t	319.9 ±0.2	325.7±0.04	305.2±0.2	304.0±0.2	296.52	190
A_1	-16.1±0.2	3.6±0.2	-39.9±0.3	1.8±0.2	75.04	135
A_2	15.1±0.3	11.2±0.4	10.4±0.2	2.4±0.4	-	-10
A_3	-	-	-	-	-	43
B_o	-68.9±0.2	-67.9±0.3	-77.5±0.4	-76.8±0.4	-73.71	-42
B_t	-90.1±0.5	-90.5±0.6	-82.8±0.3	-80.4±0.5	-50.24	-17.5
B_1	[-21.33]	[-21.93]	29.8±0.3	14.2±0.2	-8.0	-5
B_2	[9.37]	[9.22]	5.5±0.6	5.9±0.4	-	-9
B_3	-	-	-	-	-	-
K_{ox}	[10^{10}]	1027.5±0.1	[10^{10}]	948.5±0.1	-	-
Y_{ox}	[0]	-2.21±0.03	[0]	-2.6±0.03	-	-
Z_o	[3]	[3]	[3]	[3]	[3]	2.95
Z_t	[2]	[2]	[2]	[2]	[2]	1.14
Z_{ox}	[-2]	[-2]	[-2]	[-2]	[-2]	-1.76
χ'	9.99	4.96	8.67	3.42	-	-
χ	1.25	0.83	1.44	0.86		

*SB - Striefler and Barsch Model

TABLE 5.3 - Model Parameters

		MODELS					
		Central Force		Unrestrained		Previous	
Mode	Expt. (THz)	Rigid Ion (THz)	Shell (THz)	Rigid Ion (THz)	Shell (THz)	SB* (THz)	Thompson (THz)
A_{1g}	23.16	26.69	22.88	24.59	21.83	30.94	35.03
E_g	12.30	6.68	7.43	12.04	12.20	12.23	16.32
T_{1g}	-	5.63	4.51	13.87	11.73	7.91	9.77
A_{2u}	-	20.53	19.86	18.84	20.16	23.65	27.36
	-	31.53	29.07	30.67	27.88	32.62	34.96
E_u	-	11.11	10.73	12.63	12.96	11.68	13.56
	-	25.54	21.92	26.35	20.31	26.01	25.45
T_{2u}	-	5.42	5.17	4.77	4.99	4.58	5.84
	-	12.13	11.00	17.16	14.67	11.73	12.09
T_{2g}	9.32	9.37	9.50	9.19	9.12	10.04	8.68
	14.75	13.10	13.19	12.02	12.85	12.07	14.09
	20.12	26.79	22.07	26.94	21.11	28.15	28.43
T_{1u}	[9.15]	5.12	5.42	5.43	5.69	9.23	10.62
	-	12.95	12.70	12.80	13.45	12.54	17.25
	14.54	14.29	14.63	14.47	15.56	17.25	20.68
	20.09	21.87	21.72	21.81	22.16	21.78	23.46
T'_{1u}	[9.15]	9.47	9.22	9.48	9.34	10.96	11.03
	-	14.30	14.61	14.45	15.37	17.21	20.37
	[18.89]	20.93	20.76	20.94	22.05	21.12	23.12
	[25.63]	37.00	30.42	36.91	29.12	37.08	36.08
$\Pi \frac{\omega_L^2}{\omega_T^2}$	[2.75]	25.61	15.13	23.30	12.20	11.54	4.45
$\epsilon(\infty)$	[2.95]	1	1.47	1	1.75	1	1
$\epsilon(0)$	[8.42]	25.6	22.24	23.3	21.3	11.54	4.45

*SB - Striefler and Barsch Model

TABLE 5.4 Zone Centre Frequencies and Dielectric Constants

Key to Fig 5.4 and Figs 5.5

———	Δ_5	Σ_4	Λ_3
- - - - -	Δ_1	Σ_1	Λ_1
.....	Δ_2'	Σ_3	
— - —	Δ_2	Σ_2	Λ_2
— · —	Δ_1'		

Lines

▽ Longitudinal

○ Transverse

● Transverse

⊙ Unknown

Phonon Polarization

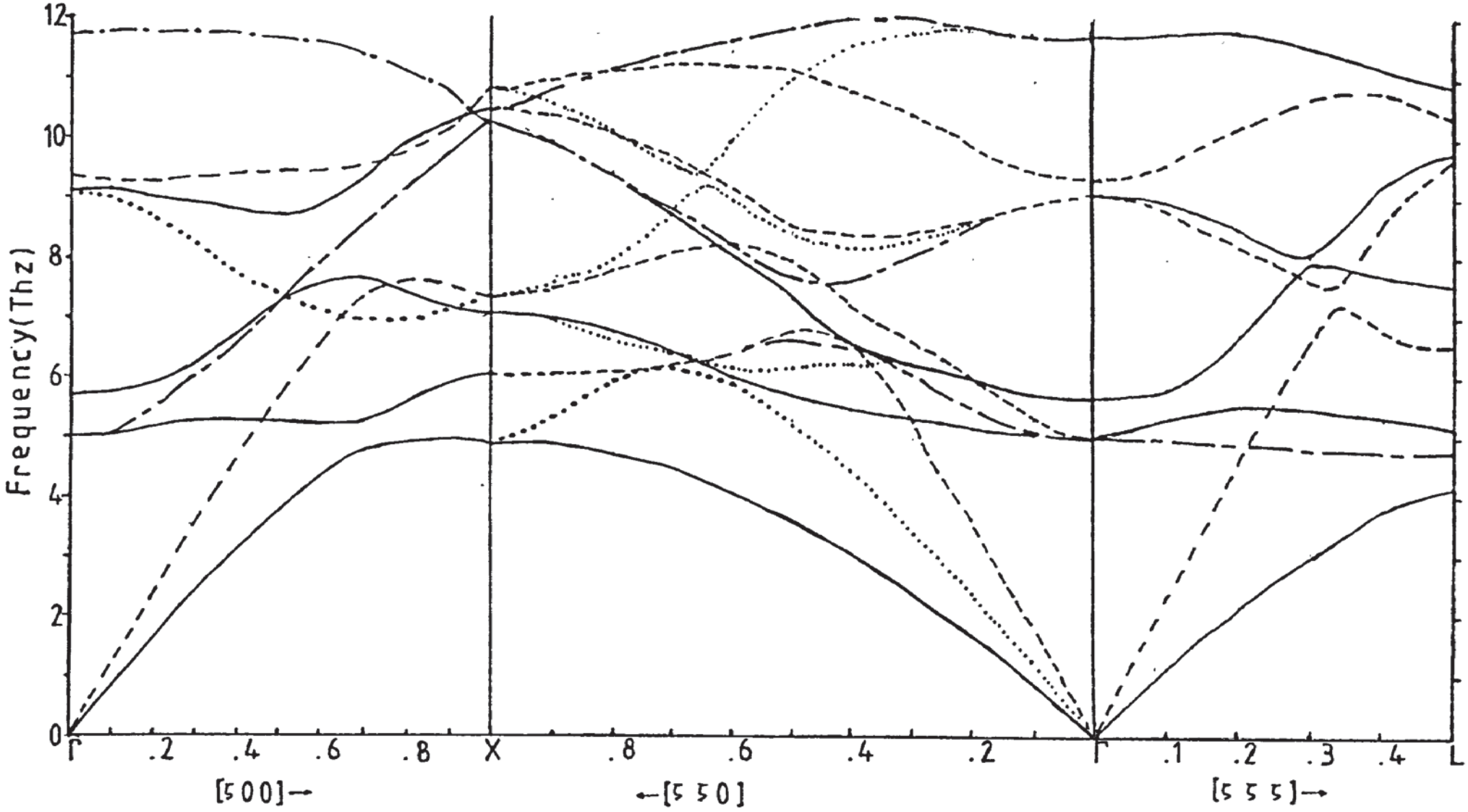

Fig 5.4 Low Energy Dispersion Curves-Unrestrained Shell Model

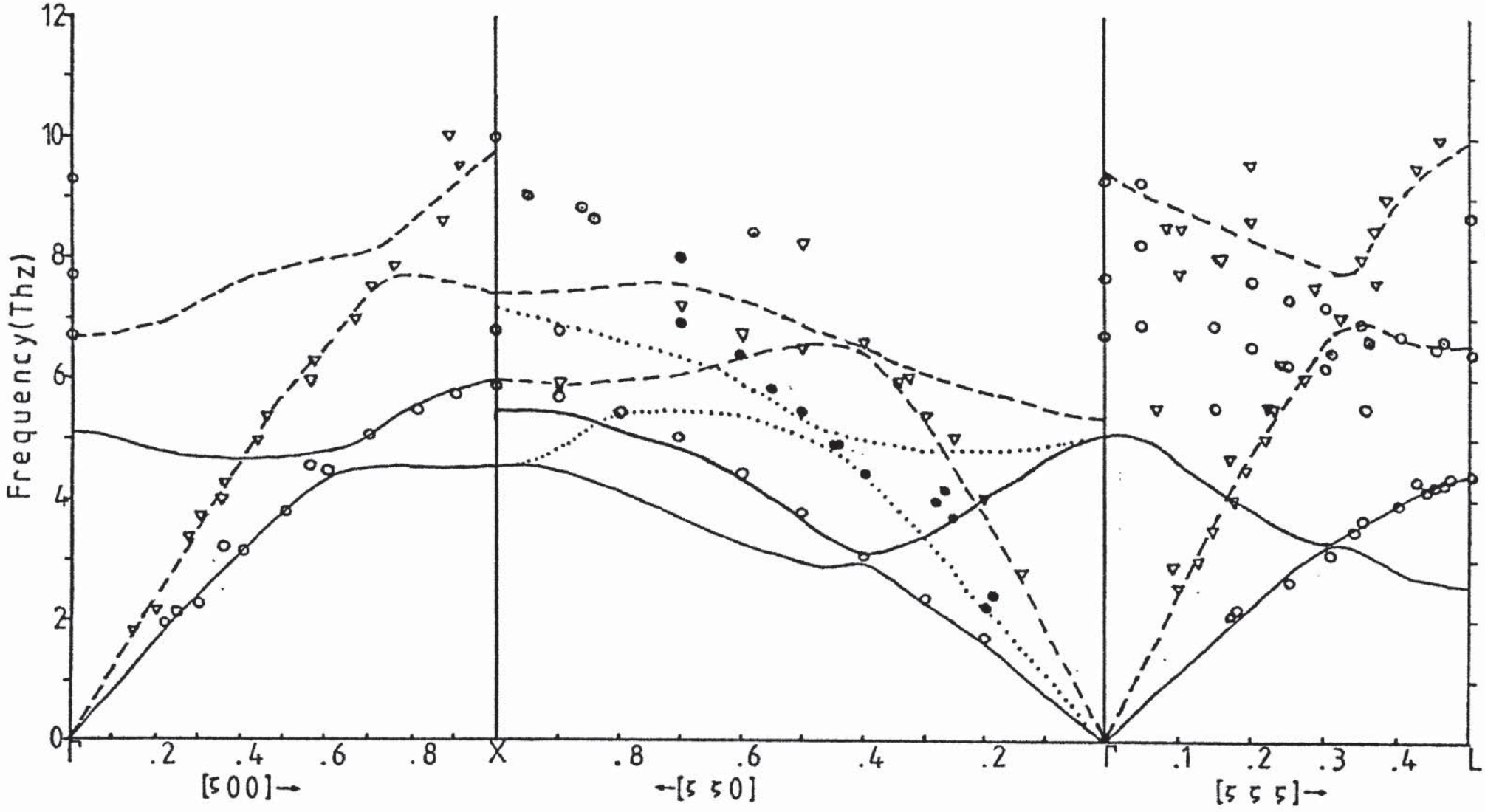

Fig 5.5a Acoustic Mode Fit-Cental Force Rigid Ion Model

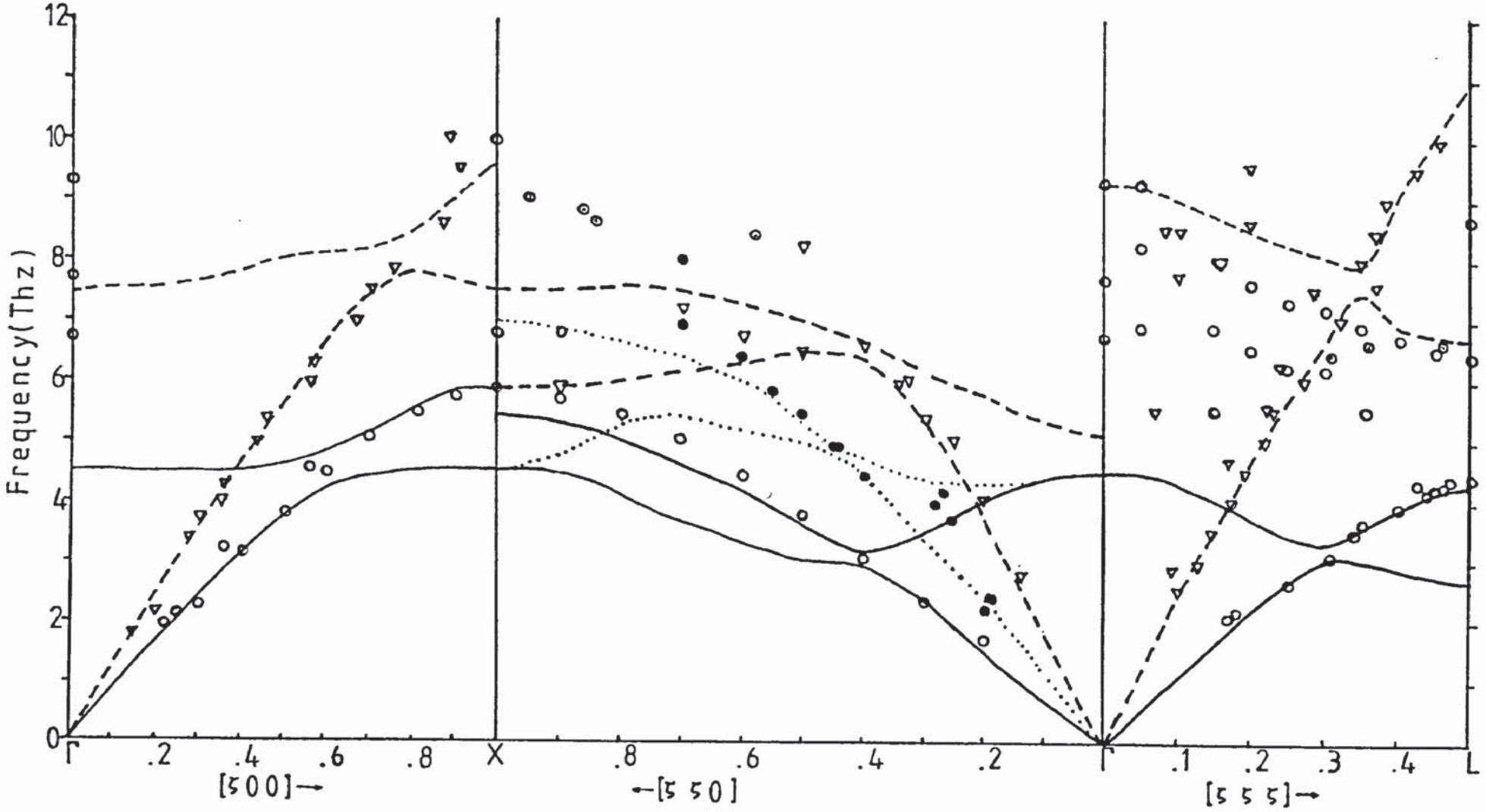

Fig 5.5b Acoustic Mode Fit-Central Force Shell Model

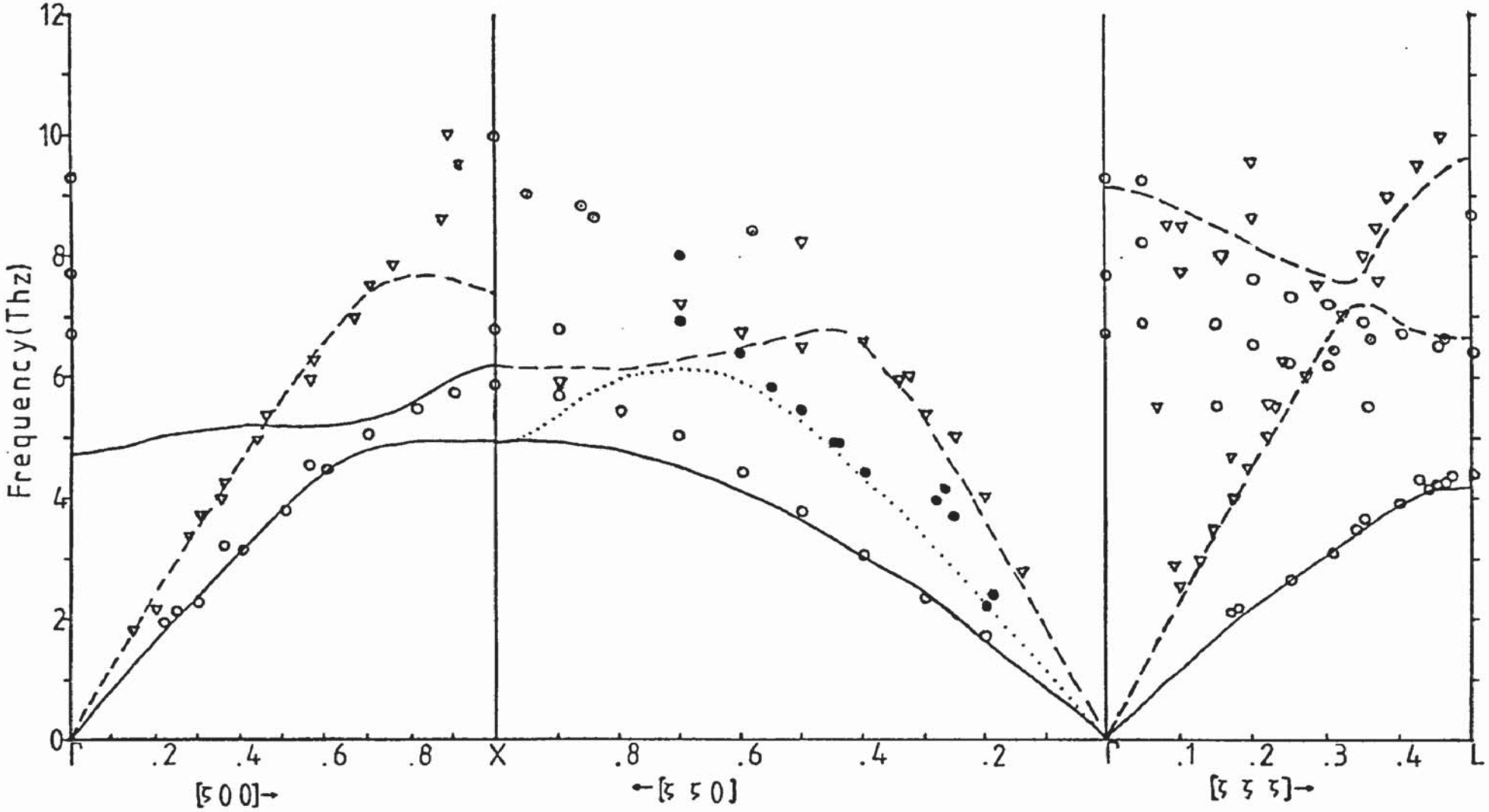

Fig 5.5c Acoustic Mode Fit-Unrestrained Rigid Ion Model

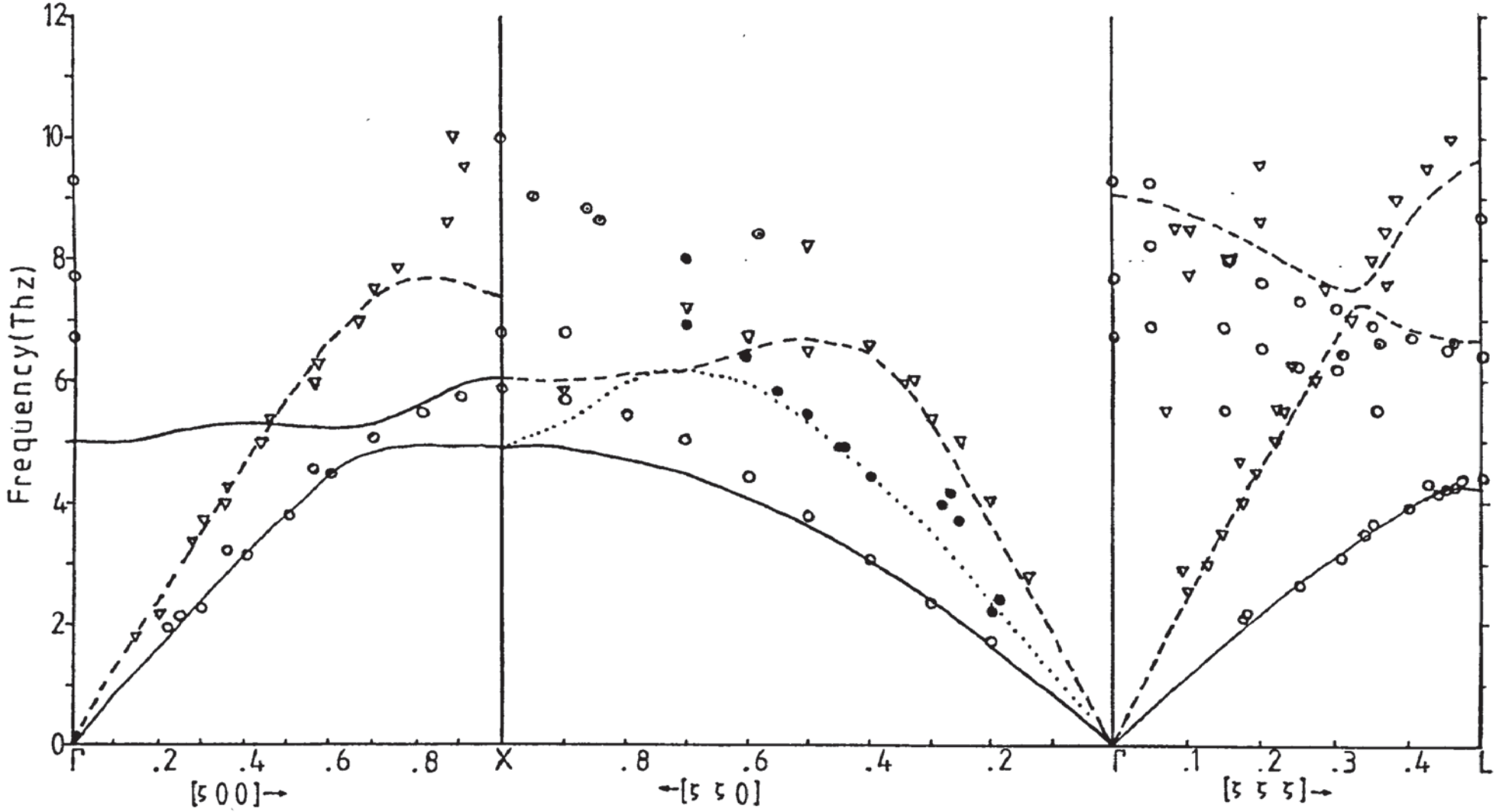

Fig 5.5d Acoustic Mode Fit-Unrestrained Shell Model

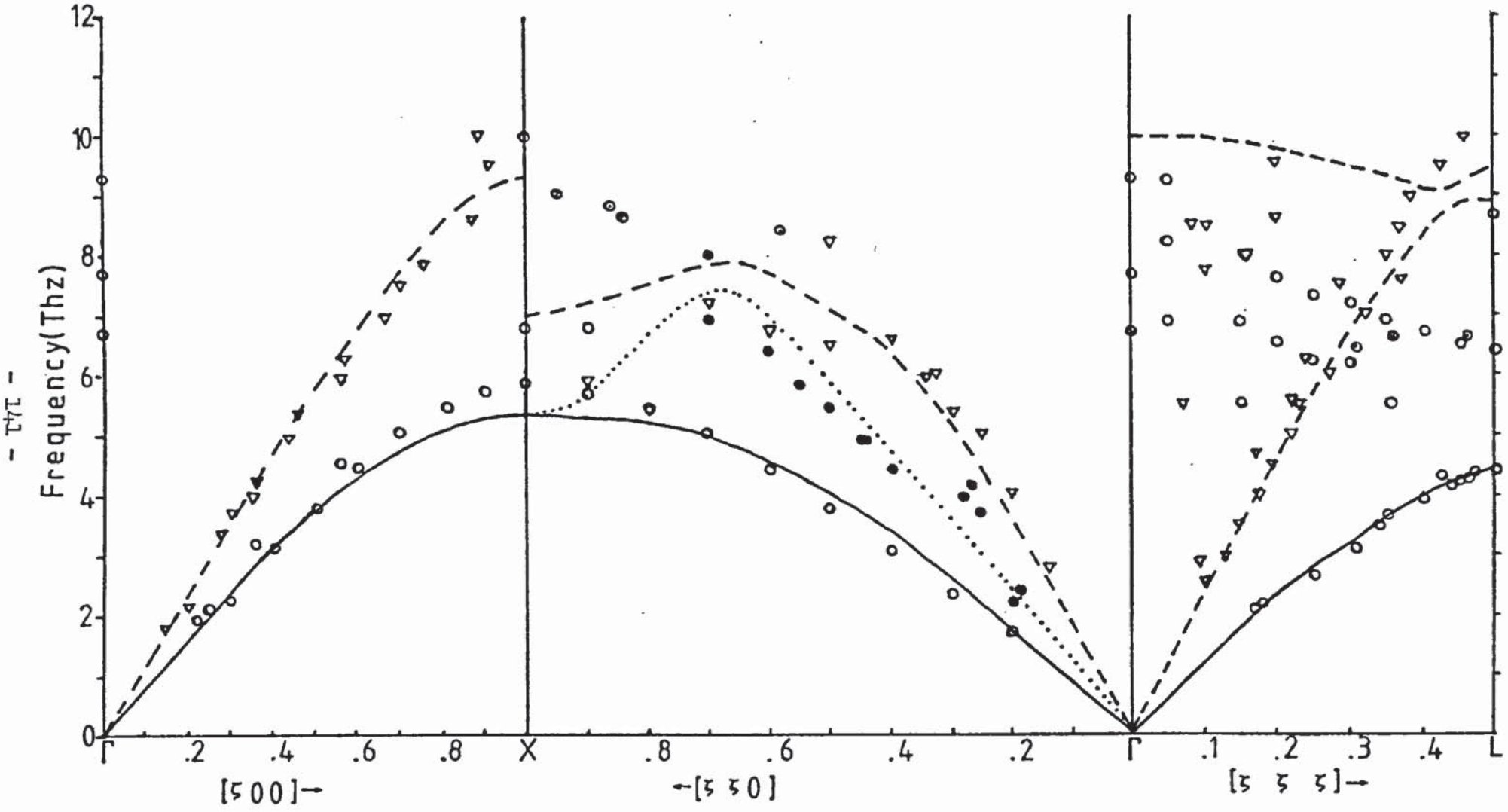

Fig 5.5e Acoustic Mode Fit-Striefler and Barsch Model

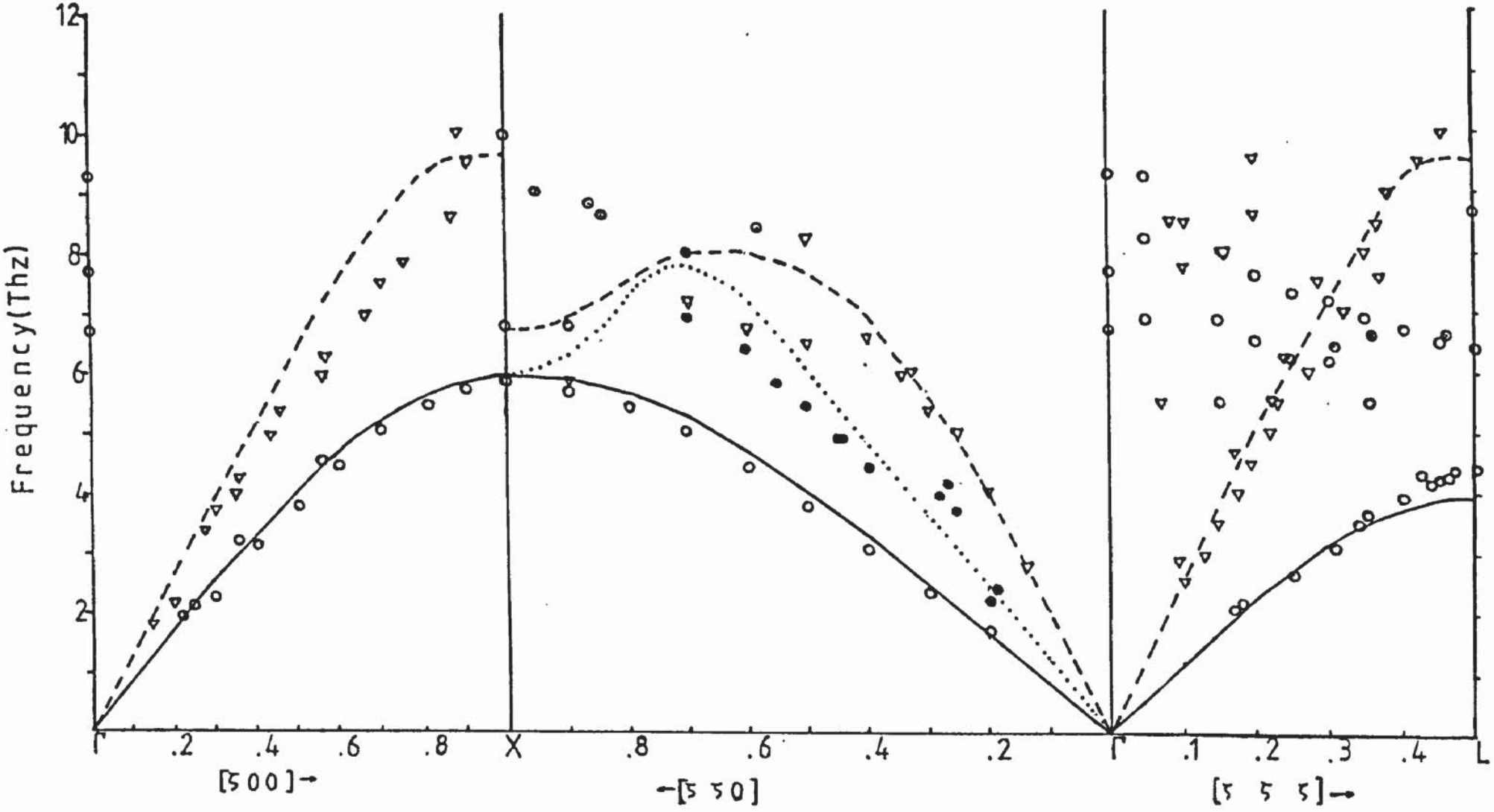

Fig 5.5f Acoustic Mode Fit-Thompson Model

values for the [qqq] and [q00] directions. The high and low frequency dielectric constants are also included in this table, the former evaluated from (2.67), the latter from the Lyddane-Sachs-Teller relation.

The complexity of the phonon spectrum is revealed in the diagram of the low energy dispersion curves of the unrestrained shell model (fig.5.4). Connectivities of points of the Brillouin zone boundaries were established using the comptatability relations and extrapolation. The available symmetry coordinates did not fully block diagonalise the dynamical matrix at these points. The fit to the acoustic modes is shown in fig.5.5a-5.5f. For clarity only the relevant modes have been drawn.

5.5 Elastic Constants

For a cubic material the three non zero elastic constants are given from equation (2.63) by

$$C_{11} = C_{11\ 11} = [\alpha\alpha,\alpha\alpha] + (\alpha\alpha,\alpha\alpha) \tag{5.21}$$

$$C_{12} = C_{11,22} = 2[\alpha\beta,\alpha\beta] - [\alpha\alpha,\beta\beta] - (\alpha\alpha,\beta\beta) \tag{5.22}$$

$$C_{44} = C_{23,23} = [\alpha\alpha,\beta\beta] - (\alpha\beta,\alpha\beta) \tag{5.23}$$

where the equivalent constant in Voigt notation is given on the far left. The square bracket terms have been calculated using Born and Huang (1954) explicit expressions as corrected by Cowley (1962a). Their contribution to the elastic constants may be given as the sum of the following short range and Coulomb expressions

$$\left(\frac{v_a a}{2e^2}\right) C_{11}^{SR} = 8(\tfrac{1}{4}-\delta)^2 A_0 + {}^8/_3(A_t+2B_t)(\tfrac{1}{8}+\delta)^2 + 4(A_1+B_1)(\tfrac{1}{4}-2\delta)^2 + 4(A_3+B_3)(\tfrac{1}{4}+2\delta)^2 + \tfrac{1}{2}(A_2+B_2) \tag{5.24}$$

$$\left(\frac{v_a a}{2e^2}\right) C_{12}^{SR} = -8B_0(\tfrac{1}{4}-\delta)^2 + {}^8/_3 A_t(\tfrac{1}{8}+\delta)^2 - \tfrac{32}{3} B_t(\tfrac{1}{8}+\delta)^2 + (2A_1-6B_3)(\tfrac{1}{4}+2\delta)^2 + (2A_3-6B_3)(\tfrac{1}{4}+2\delta)^2 + \tfrac{1}{4}A_2 - \tfrac{5}{4}B_2 \tag{5.25}$$

$$\left(\frac{v_a a}{2e^2}\right) C_{44}^{SR} = 8B_0(\tfrac{1}{8}-\delta)^2 + {}^8/_3(A_t+2B_t)(\tfrac{1}{8}+\delta)^2 + 2(A_1+B_1)(\tfrac{1}{4}+2\delta)^2 + 2(A_3+B_3)(\tfrac{1}{4}+2\delta)^2 + \tfrac{1}{4}(A_2+3B_2) \tag{5.26}$$

$$\left(\frac{v_a a}{2e^2}\right) C_{11}^{C} = -2.021Z_t^2 - 4.454Z_0^2 + k_1 Z_{ox}^2 + 2.533Z_0 Z_t + k_2 Z_t Z_{ox} + k_3 Z_0 Z_{ox} \tag{5.27}$$

where the oxygen dependent coefficients k_1, k_2, k_3 are given in table 5.5 for a range of δ values. It may be shown from the explicit expressions and the definition of the Madelung constant that the remaining Coulomb contributions may be obtained from

$$C_{11}^c = -2C_{44}^c \qquad (5.28)$$

$$C_{11}^c + 2C_{12}^c = -\frac{2}{3}M \qquad (5.29)$$

The above expressions (from (5.22) onward) differ from earlier work by Thompson and/or Striefler and Barsch although some of the discrepancies may be merely typing errors. The expressions given are believed to be correct (5.24)-(5.26) have been confirmed

(i) By computer calculation of the generalised terms. The small discrepancies which occur are due to the approximations made in obtaining the expressions, mainly occurring in the coefficients of A_o and B_o. In view of this, the full Born and Huang expressions were used in all calculations presented here.

(ii) The corresponding results for $F\bar{4}3m$ symmetry were derived by setting the δ's in $F\bar{4}3m$ to give an $Fd3m$ situation the same expressions are obtained.

(iii) As there are only three ions at each distance d_1 and d_3 from a central anion but six at d_2 it is expected that if δ is set to zero and the relevant A and B terms set equal to A_2 and B_2 the sum of the d_1 and d_3 terms equals the d_2 term. Inspection of the expressions shows that this holds.

Similarly it has been found that equation (5.27) holds for the coefficients of similar expressions for the Coulomb contributions C_{12}^c and C_{44}^c. Sammis (1971) also gives equations equivalent to (5.28) and (5.29) whereas those used by Striefler and Barsch are quite different.

k_1	k_2	k_3	δ
-8.666	-1.477	11.528	0.020
-8.283	-2.008	12.059	0.016
-7.981	-2.556	12.441	0.012
-7.764	-3.121	12.691	0.008
-7.633	-3.699	12.826	0.004
-7.589	-4.289	12.861	0.000
-7.633	-4.888	12.813	-0.004
-7.764	-5.494	12.696	-0.008

Oxygen Dependent Coefficients of the Expression for C_{11}^{c}

TABLE 5.5

Unfortunately it is not possible to give explicit expressions for the round bracket terms because of the matrix inversion involved in their definition (equation (2.65)).

An alternative method is to use expressions for the velocities of the acoustic modes (table 4.3a)with a least squares fitting procedure to obtain the values of the elastic constants. This method had to be resorted to for the shell models.

Table 5.6 compares the elastic constants obtained, the terms formula and curve refer to the use of equations (5.21)-(5.23) and the method outlined in the previous paragraph respectively. Also included is a comparison of the Striefler and Barsch results as given in their paper (1972,text) and as given by my calculations from the general formulae (formula). The acoustic data is that of Chang and Barsch (1973).

The two values quoted for C_{44} of the unrestrained rigid ion model when calculated from equations (5.21)-(5.23) are results obtained for different sets of indices that should be equivalent to 44. In section 5.3 on central forces it was mentioned that the minimisation of the crystal potential with respect to internal strain, to which the round bracket terms correspond, is identical to the imposition of rotational invariance. Therefore, as this constraint was not applied to the model in question the index equivalent mentioned was illusory. Rotational invariance does not affect the symmetry of the square bracket terms in a cubic material.

Overall there is closer agreement with the neutron values of the elastic constant than those obtained by ultrasonics; certainly the difference from the Cauchy - like condition $C_{44} = C_{12}$ is emphasized. This accord is not unexpected as the model acoustic modes are dependent on the fit to the experimental data obtained by neutron spectrometry. Taking into account the fit of these models to the acoustic mode data, particularly at low q, these results may be

		Elastic Constants (10^{12} dynes/cm)		
		C_{11}	C_{44}	C_{12}
Experiment Ultrasonics		2.808	1.547	1.532
Neutrons		3.86	1.57	2.3
Rigid Ion (CF)	Curves	3.31	1.58	1.86
	Formula	3.34	1.58	1.87
Shell (CF)	Curves	3.28	1.60	1.90
Rigid Ion(U)	Curves	3.32	1.56	1.69
	Formula	3.35	1.57(2.2)	1.06
Shell (U)	Curves	3.36	1.57	1.76
SB*	Text	3.49	1.63	1.68
	Formula	3.45	1.64	1.72

CF - Central Force Model

U - Unrestrained Model

*SB - Striefler and Barsch Model

TABLE 5.6 - Elastic Constants

taken as more accurate estimates of the isothermal elastic constants than those obtained directly from neutron data which are greatly affected by scatter of data points.

5.6 Heat Capacity Calculations

The accuracy of dynamical models cannot be reliably tested by comparison of predicted and measured molar heat capacities as these quantities are well known to be insensitive to the form of the normal mode frequency distribution. However these computations are a useful null test in that any large discrepancy in the comparison of these values would indicate a major error in the model.

At constant volume the molar heat capacity in terms of the frequency distribution $g(\nu)$ is given by (Born and Huang 1954)

$$C_v = \frac{N_A}{Nn} k_B \int_0^{\infty} (z\nu)^2 \exp(z\nu)(\exp(z\nu)-1)^{-2} g(\nu) d\nu \qquad (5.30)$$

where $z = h/k_B T$ with k_B as Boltzmann's constant, N_A = Avogadro's number, n the number of molecules per basis and N the number of unit cells of the crystal. The frequency distribution is normalised by

$$\int_0^{\infty} g(\nu) d\nu = 3sN \qquad (5.31)$$

where s is the number of particles in the basis. Using this and the high temperature approximation for the exponentials in equation 5.30 it is easily shown that the molar heat capacity tends to the classical value $\frac{3s}{n} N_A k_B$, which is 174.6 J/K for spinel.

In computations overflow errorswhich may occur where high frequency and low temperature are taken together were avoided by taking advantage of Stirling's (1972a) hint to rewrite $e^a(e^a-1)^2$ as $e^{-a}(1-e^{-a})^{-2}$.

To obtain the frequency distribution the full 42 × 42 Hermitian dynamical matrix was diagonalised over a grid of wave-vectors

in the irreducible $1/48^{th}$ of the Brillouin zone. By symmetry this irreducible zone may be taken to be in the quadrant for which q_x, q_y and q_z are positive. The wave vectors on this zone may then be taken as those which satisfy the following conditions:-

$$\begin{aligned} 1 \geq q_x \geq q_y \geq q_z \geq 0 \\ q_x + q_y + q_z \leq {}^{3}/_{2} \end{aligned} \qquad (5.31)$$

In the calculations the principal axes were divided into eighths and the dynamical matrix diagonalised for the resulting 29 wave vectors of the type $(h_x, h_y, h_z)\frac{2\pi}{8a}$. The frequency distribution for the whole Brillouin zone was obtained by weighting the contributions from each wave vector according to the following scheme.

Wavevector Indices	Weight (w)
$h_x = h_y = h_z \neq 0$	8
$h_x = h_y \neq h_z = 0$	12
$h_x = h_y \neq h_z \neq 0$	24
$h_x \neq h_y = h_z = 0$	6
$h_x \neq h_y = h_z \neq 0$	24
$h_x \neq h_y \neq h_z = 0$	24
$h_x \neq h_y \neq h_z \neq 0$	48

with the following applied in turn to account for sharing of points with other zones

$$\begin{aligned} h_x + h_y + h_z = 1.5 \times 8 \qquad {}^{w}/_{2} \\ h_x = 8 \qquad {}^{w}/_{2} \end{aligned}$$

There are then a total of 511 points on this mesh for the whole zone. This number is also taken to be the number of unit cells N in the crystal. The complete frequency distribution $g(\nu)$ was therefore compiled from $511 \times 42 = 24{,}462$ frequencies.

The origin has been excluded as the calculations would have of necessity ignored the effect of the macroscopic electric field on the infrared modes making them all threefold degenerate. The effect of the omission is not serious as the associated weighting factor, value

one, is the lowest in the whole zone.

Although the grid is very coarse (even Kellermann, 1940 used 56 wavevectors in the irreducible segment) it is believed to be of sufficient density for heat capacity calculations. The parameter which decided the grid size used, was the required program execution time. For example Algol 60 programs for rigid ion models use more than eighteen minutes core time to calculate the frequency distribution.

The distributions obtained for the models are shown in figs. 5.6a-5.6f plotted as histograms of number of frequencies against frequency. The frequency range has been divided into "bins" of 1THz width, the curve shown being obtained by connecting the midpoint of each bin.

Equation (5.30) has been used to determine the heat capacity from each of the models for a range of temperatures. This, of course, uses the tacit assumption that the normal mode frequencies are temperature invariant.

Table 5.7 compares the molar heat values for the models with those obtained from experiment. The experiment values of C_v are those given by Grimes (1972b) derived from the measurements of heat capacity at constant pressure by King (1955). Although there is no difference between these quantities in the harmonic approximation it is conventional to relate the model calculated quantities to C_v.

In all models the classical value for heat capacity is attained in the temperature range 1300-1500K.

Temperature (K)		300	260	220	180	140	100	60
Cp(J/K)	Experiment (a)	116.16	103.29	87.45	68.05	45.35	22.71	6.14
	Experiment (b)	114.53	102.16	86.78	67.72	45.19	22.70	6.14
	Rigid Ion (CF)	116.14	105.54	92.44	76.27	56.60	33.89	12.28
	Shell (CF)	120.34	109.58	96.08	79.29	58.87	35.39	12.28
Cv(J/K)	Rigid Ion (U)	110.29	98.58	84.27	67.01	47.05	26.13	8.19
	Shell (U)	115.28	103.26	88.23	69.86	48.55	26.49	8.13
	SB*	110.37	99.52	85.81	69.09	48.99	26.35	6.80
	Thompson	102.11	90.00	75.64	58.90	40.08	20.74	5.49

(a) King (1955)

(b) Grimes (1972b)

CF - Central Force Model

U - Unrestrained Model

*SB - Striefler and Barsch Model

TABLE 5.7 - Heat Capacities

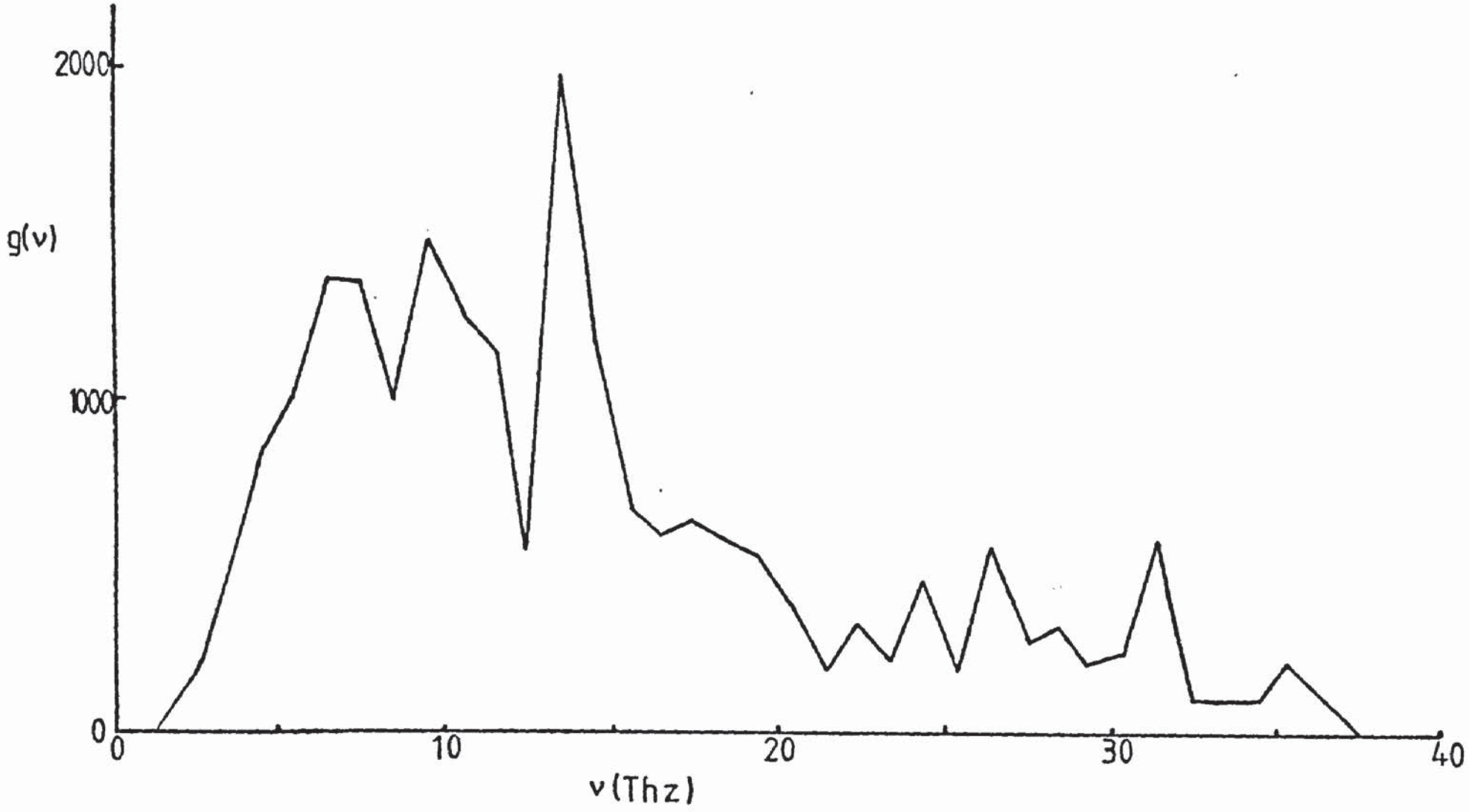

Fig 5.6a Frequency Distribution - Central Force Rigid Ion Model

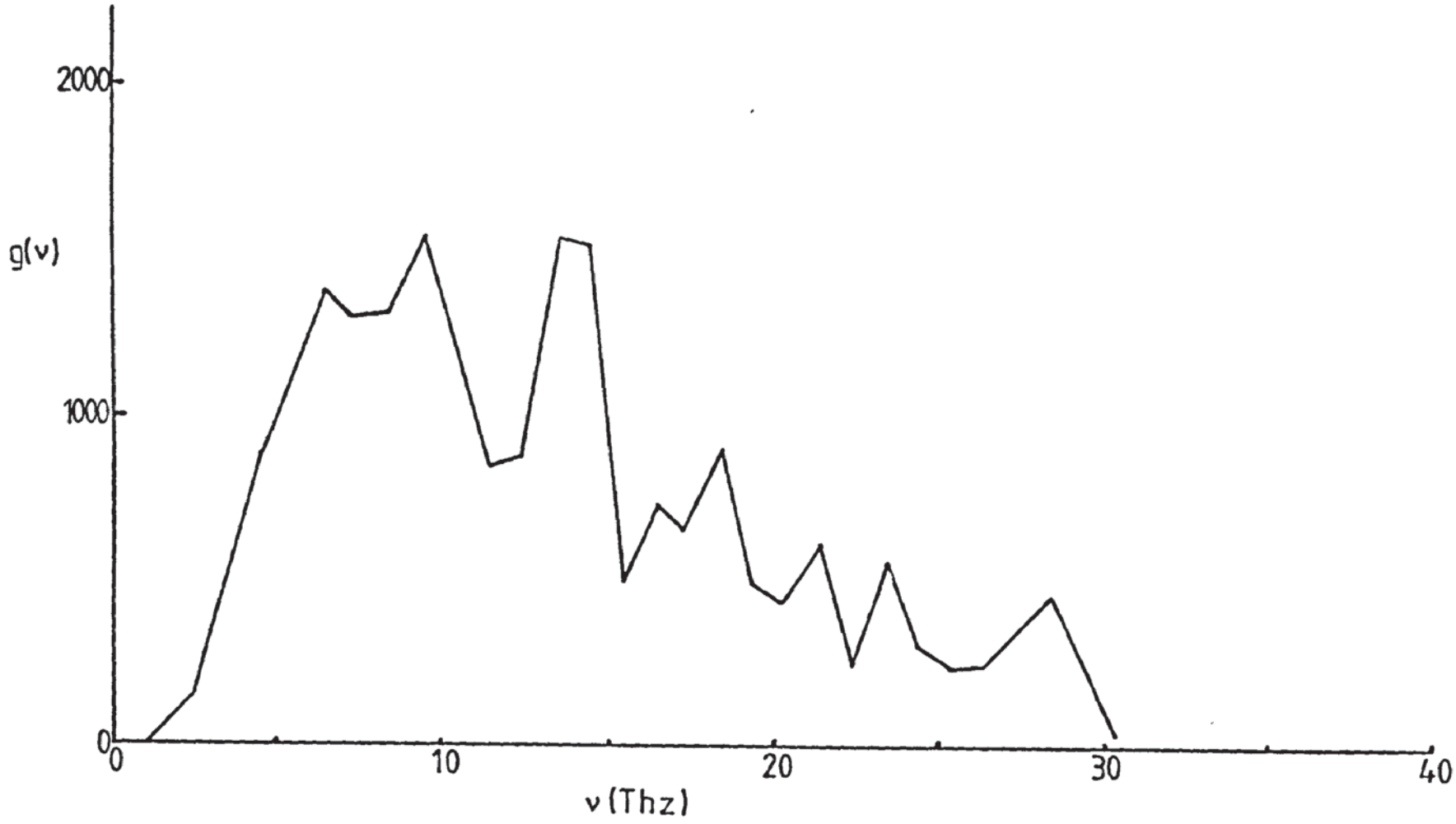

Fig 5.6b Frequency Distribution-Central Force Shell Model

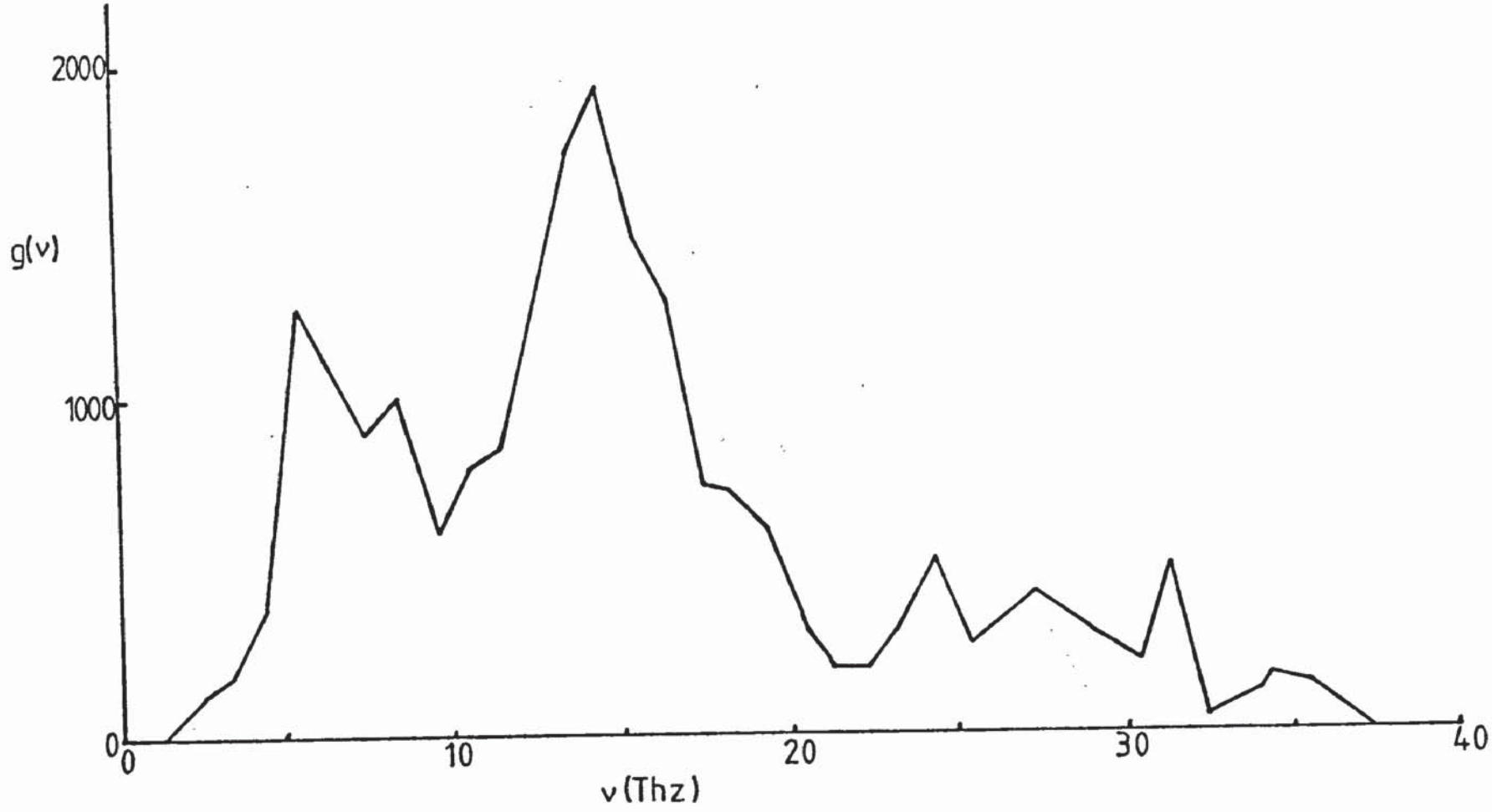

Fig 5.6c Frequency Distribution-Unrestrained Rigid Ion Model

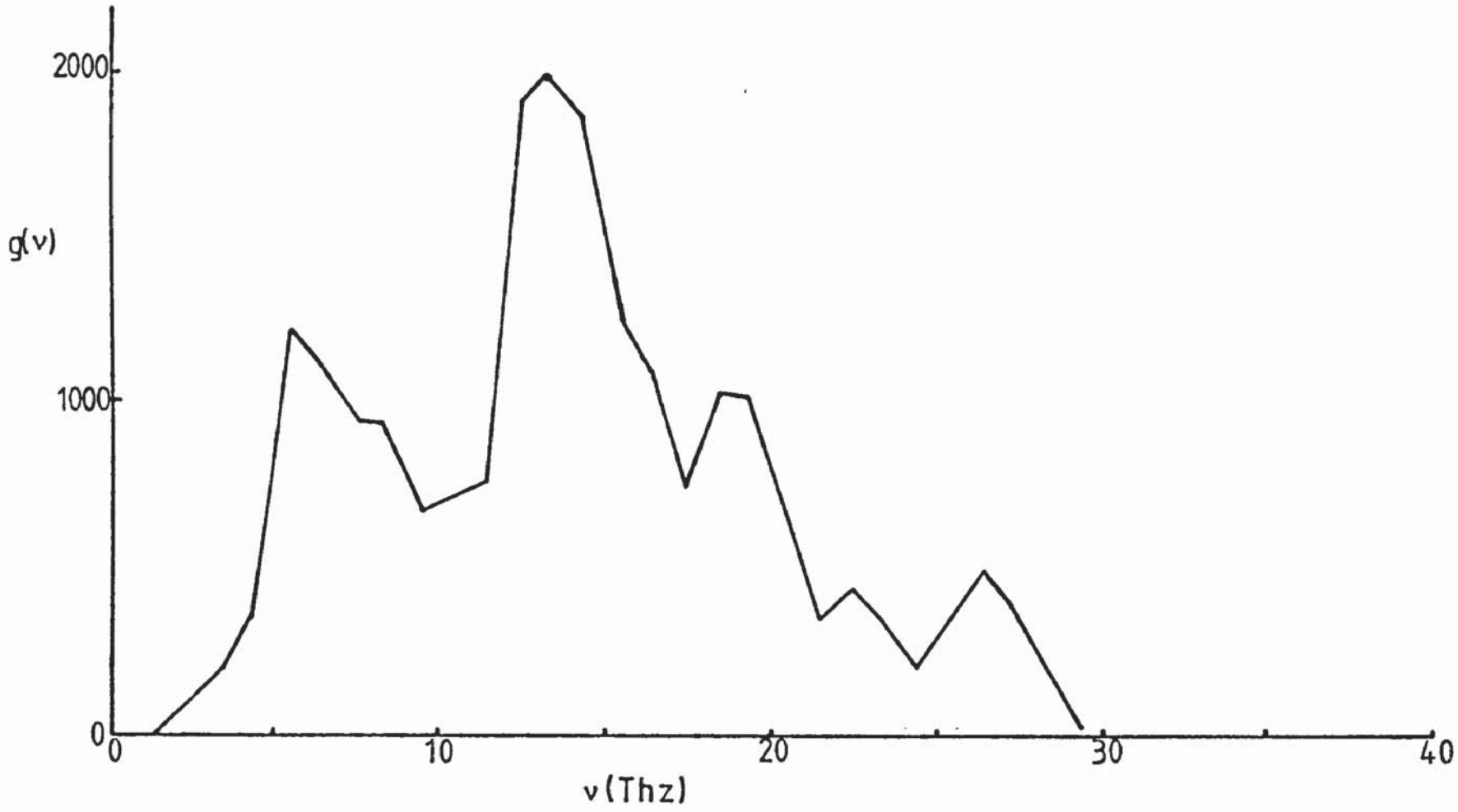

Fig 5.6d Frequency Distribution-Urestrained Shell Model

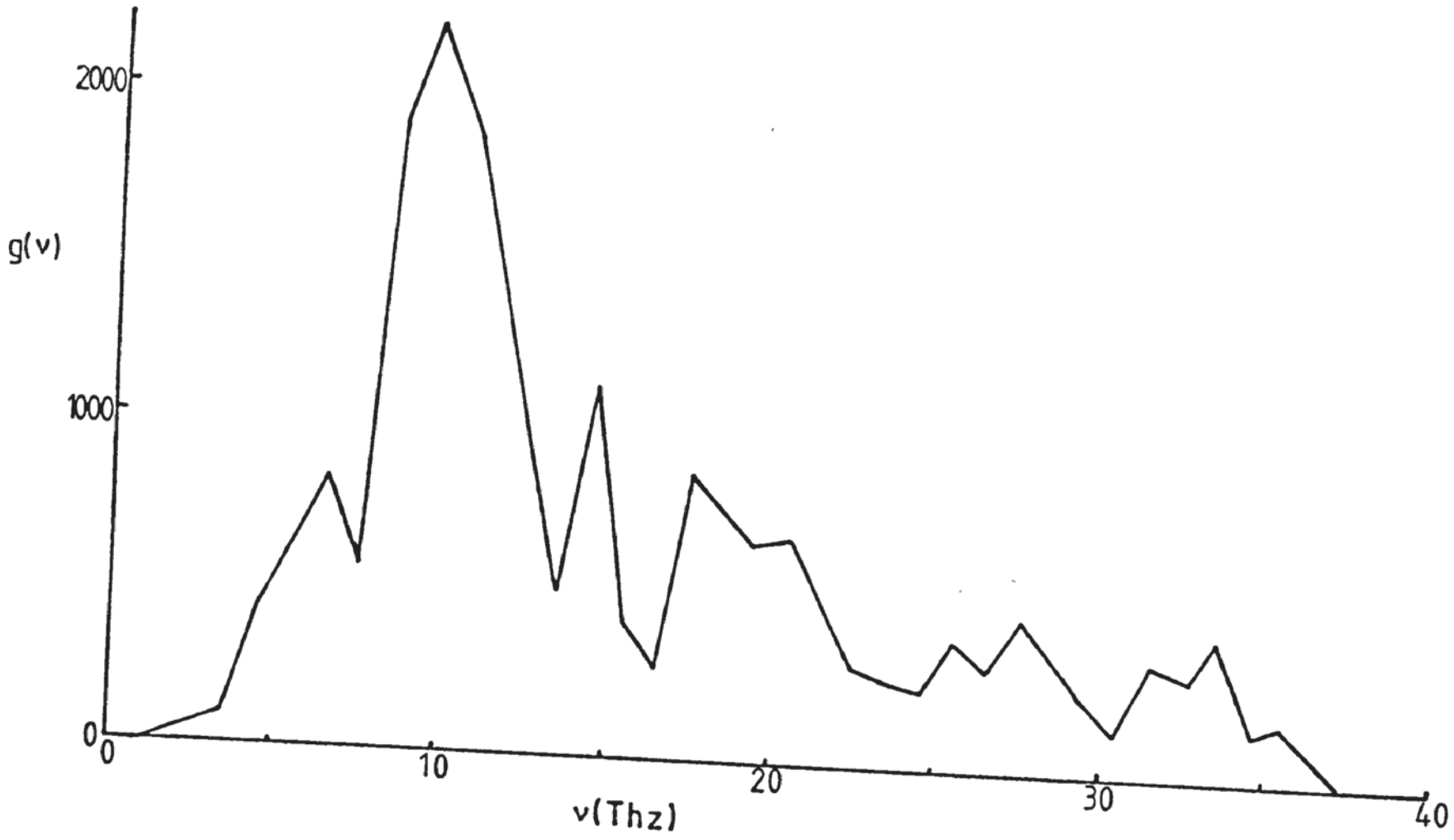

Fig 5.6e Frequency Distribution - Striefler and Barsch Model

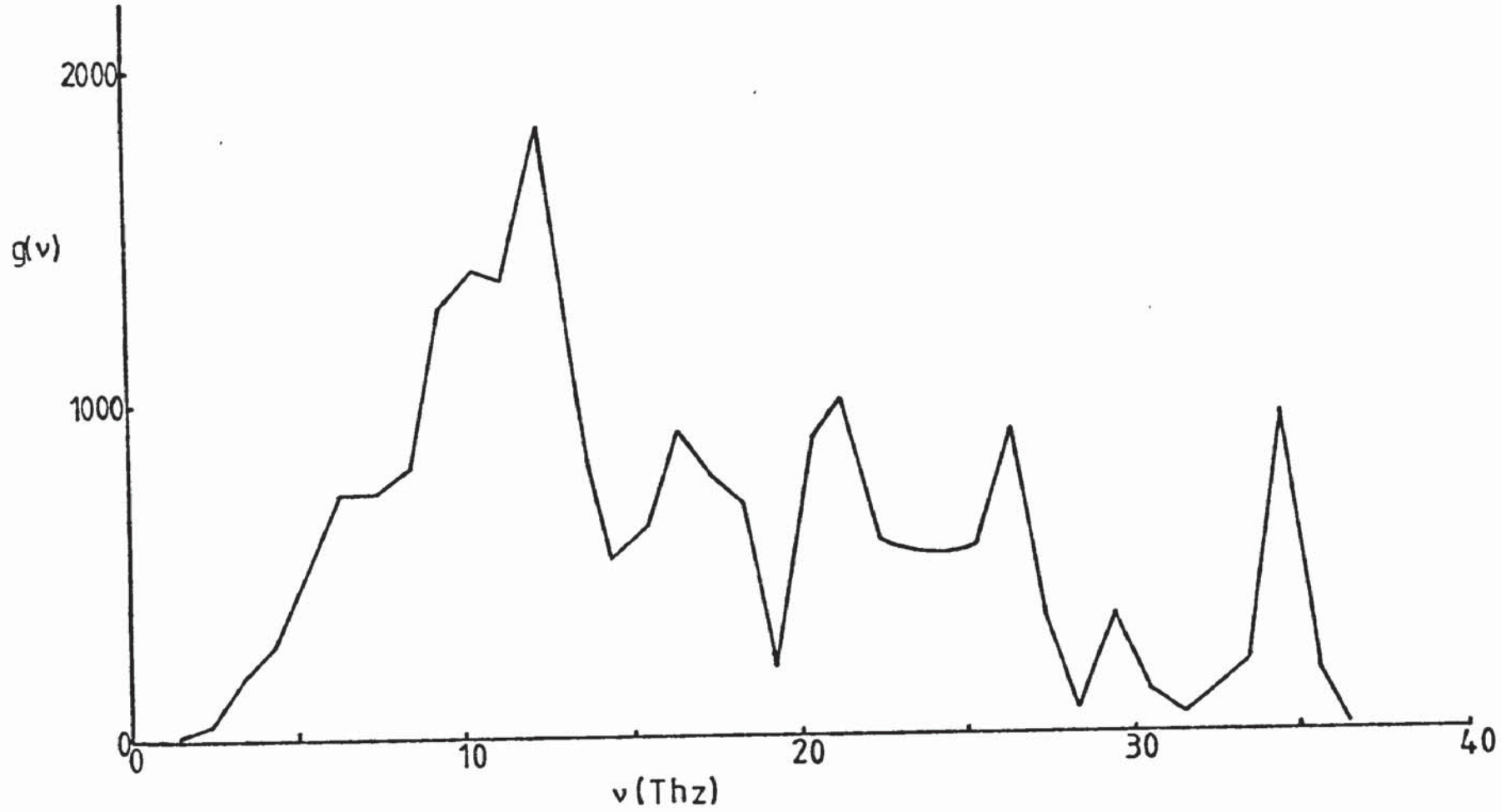

Fig 5.6f Frequency Distribution-Thompson Model

CHAPTER 6

DISCUSSION OF RESULTS

6.1 The Force Constants

It has been shown (Leigh et al. 1971, Cochran 1971b) that, even in principle, it is impossible to obtain the force constants of a solid from consideration of lattice frequencies alone. The set of force constants so obtained will not be unique regardless of the number of independent frequencies taken into account and the degree of accuracy to which the model fits the data. Dolling et al. 1965 have reported such a case where two different sets of parameters fit the data almost equally well.

To obtain a unique and correct set of force constants it is necessary to measure the eigenvectors of some of the normal modes. This is possible using inelastic neutron spectrometry (Harada et al. 1970) although rarely performed. The eigenvectors are expanded in terms of the symmetry coordinates and the coefficients deduced from measurements of intensity of the same mode in different Brillouin zones within the inelastic scattering cross section repeat volume. However in materials such as spinel which do not have every ion at a centre of symmetry the coefficients cannot all be taken as real. This raises a problem similar to that in crystallography where structure factors of crystals without a centre of symmetry have to be obtained from intensity measurements. In both cases phase information has been lost and the problem consequently made more complicated.

An alternative is to use isotopic substitution thus changing the atomic masses but not the force constants. However neither method is believed to be particularly accurate.

Bearing this in mind and also Cochran's comment that "it seems improbable in practice that there ever will be an equivalent set of force constants having a shorter range than the correct set" it is nevertheless of interest to compare the parameters of the various models and examine their implications.

Table (5.3) lists the parameters for the models used in this work together with those of Striefler and Barsch (1972) and Thompson (1977). As the latter model gives markedly low values for heat capacity (table 5.7) and in general does not agree with the optic mode frequencies (table 5.4) it will not be considered further.

The Striefler and Barsch model (SB) assumed central forces with short range potentials of the type

$$\phi_i = G_i \exp(-r_i/\rho_i) \qquad (6.1)$$

where r_i is the i^{th} independent distance. The A and B parameters are then obtained from equations (2.41) and (5.9). It was further assumed that the ρ_i for the Al–O and Mg–O interactions were equal. The remaining G_o, G_t, G_1 and ρ_o, ρ_t parameters were determined from the static equilibrium conditions (5.12) and (5.13), the E_g mode and fitting to the two lowest infrared absorption frequencies as given by O'Horo et al. (1973).

All models have similar values for A_o, A_t and B_o. Amongst my models the value of B_t is greater in magnitude than B_o whereas the opposite is true for SB which may reflect the difference in data used for optimization.

There is much less agreement amongst the oxygen force constants. However in all models the magnitude of the oxygen-oxygen interaction parameters are less than the cation-oxygen parameters, even among the central force models where B_1 and B_2 are obtained from the static equilibrium conditions. This seems reasonable as the inter-oxygen distances are greater than anion-oxygen intervals, also in view of the tight oxygen packing it is not expected that these repulsive interactions would be large.

Expressing the central force model parameters in terms of potentials of the form of (6.1), the following values of ρ are obtained:

	Rigid Ion	Shell Model	SB
ρ_o(Å)	0.305	0.304	0.325
ρ_t(Å)	0.540	0.533	0.325
ρ_1(Å)	-3,42	15.7	0.275
ρ_2(Å)	-1.78	-2.35	-

The value of the octahedral parameter ρ_o agrees well with that found by Striefler and Barsch and is typical of values found in other structures (Catlow et al. 1977). ρ_t in my models was not set equal to ρ_o and its greater magnitude may reflect the larger magnesium ion radius (Aℓ = 0.53Å, Mg = 0.58Å and oxygen has a radius of 1.42Å, Shannon and Prewitt, 1968). The negative sign on most oxygen parameters and their magnitude indicates the short range repulsion actually rapidly increases with distance. However, as these parameters are in part determined by the central force conditions it may not be physically meaningful to compare them with the independent parameters ρ_o and ρ_t.

The values of Y_{ox} obtained imply that the core of the oxygen has a small positive charge. But this parameter by itself has no clear physical interpretation as demonstrated in models for other materials where anomalously large value of Y are found e.g. -4.44e for F^- in MnF_2 from Cran and Sangster (1974a). Often Y and K are combined to give the electronic polarizability of the ion using equations such as

$$\alpha = \frac{Y_{ox}^2 \, v_a}{K_{ox}+R_{xx}(77,q=0)} \quad m^3 \qquad (6.2)$$

However as pointed out in section 2.5 the polarizability of particular ions may only be formally expressed in this manner for diagonally cubic crystals. Although, the very concept has been challenged, for example, by Pantelides (1975) who shows that even for alkali halides the high frequency dielectric constant is determined by inter-ion rather than intra-ion interactions. Hence the idea of associating a polarizability with individual ions is meaningless, although in covalent crystals the converse appears to be true. Neverthless an

experimental value for the polarizability of the oxygen ion in $MgAl_2O_4$ has been given by Brun and Hafner (1962) as $0.75\mathring{A}^3$. Using equation (6.2) comparable values of $0.77\mathring{A}^3$ for the shell model and $0.54\mathring{A}^3$ for the central force shell model are obtained. Continuing the fiction of diagonally cubic oxygen sites it is instructive to apply the Clausius-Mosotti relationship:

$$\frac{4\pi}{3v_a} \sum_i \alpha_i = \frac{\epsilon(\infty)+1}{\epsilon(\infty)+2} \qquad (6.3)$$

where the summation is over the oxygen ions in the basis. Substituting the experimental value of $\epsilon(\infty)$ (from Vedam et al. 1975) the result for α_{ox} is $1.55\mathring{A}^3$, twice as large as either the experimental or shell model results. On the other hand substitution of the shell model polarizability gives $\epsilon(\infty) = 1.73$ in good agreement with the value calculated from equation (2.67), $\epsilon(\infty) = 1.75$. Therefore as equations (6.2) and (6.3) work well with only oxygen polarizable it appears that the contribution to the dielectric susceptibility from the cations is significant if made polarizable. Emphasizing Pontelides' conclusions, Bilz et al. (1975) have shown that it may be important to parameterize very small cations, such as Al here, in terms of K and Y in shell models. The argument is that regions of heavy anion shell overlap are equivalent to placing dipoles at cation sites. A similar conclusion was reached by Cowley et al. (1963) who pointed out that this situation arises because the shell model does not take into account the deformability of the electron clouds.

The value of the dielectric constant substituted in equation (6.3) must be wholly real but in real crystals anhamonicity leads to complex constants and therefore multiphonon contributions which have been ignored here.

A different way in which the effect of the shell model parameters may be revealed, for any structure, is through the apparent

charge matrix. It is common in rigid ion models, for example, to have the ionic charges as variable parameters to account for possible polarizability of the ions. In the models presented here the ionic charges are maintained at their nominal values to represent an ionic solid and by comparison to determine the effect of polarizability. The apparent charge matrix may be evaluated by the following equation (Cowley, 1962c)

$$X = Z - B^{(o)}D^{(o)-1}Y \qquad (6.4)$$

where the matrices are defined in section 2.5. The product of this charge with the macroscopic electric field provides the extra restoring force which raises the longitudinal infrared modes above the transverse. As rigid ion models are well known to give too high values for the frequencies of the longitudinal infrared modes it is expected that the apparent charges are less than the nominal charges. For the unrestrained shell model the value of the apparent charge on the long diagonal for the oxygen ion is -1.63e and for the central force shell model -1.74e. However in both cases the sum of the elements on any row for the anions must equal -2e as the oxygen is the only ion polarizable. In neither case does the magnitude of the off diagonal elements exceed 0.15e. It should be noted that the apparent charge given by equation (6.4) is not the effective charge of Szigeti (1949,1950). That quantity may only be defined for diagonally cubic materials and for these substances may be related to the apparent charge matrix via the high frequency dielectric constant (Cochran 1969).

Although a 25% reduction from the nominal charge has been effected resulting in a drop of up to 7THz in the highest frequency infrared mode (Table 5.4) it is insufficient as these modes are still 5THz too high compared to experimental values.

6.2 Comparison with Experimental Data

From the fitting parameters in table 5.3 it can be seen that the superior agreement with the refinement data of the unrestrained models is insufficient to justify the use of two extra parameters. Comparison of the acoustic mode graphs (figs.5.5) and the zone centre frequencies (table 5.4) reveals that the inferior fit of the central force models can be almost entirely attributed to the 50% discrepancy in the E_g mode frequency. Striefler and Barsch (1972) have shown that if the central force model is extended to include three body forces of the type of Basu and Sengupta (1968) about the magnesium ion the A_{1g} and highest T_{2g} frequencies may be varied without affecting the infrared modes. Although it is now known that the top T_{2g} mode is greatly influenced by the A_2 and B_2 parameters it is expected that the inclusion of such forces could improve the central force models by allowing readjustment of the E_g frequency without detriment to the fit of the other modes.

All models fit the acoustic dispersion curves from neutron data fairly well, particularly in the Λ and Δ directions. Along these high symmetry lines the curves are almost linear to the zone boundary. This type of behaviour is not unexpected for complex crystals which tend to have large unit cells and hence smaller Brillouin zone volumes with consequently less space in which to exhibit dispersion phenomena. In figs.5.5 calculated curves of the same representation have been drawn conventionally in that these do not cross each other. However as these points do not in general disappear with small changes of the parameters but simply move I believe these regions to be areas of actual curve crossing. Therefore the fit of the models to the neutron data must often be considered in terms of two modes of a given irreducible representation and not just the lowest or acoustic mode as diagrammed. Referring back to the Γ point the interfering modes are usually the T_{2g} mode for the Λ direction

and the T_{2u} along the Δ line. Together with the lowest E_u mode the latter frequency was often found to be imaginary in the process of model refinement. Striefler and Barsch also reported a similar difficulty with this optically inactive mode. In Chapter 3 it has been shown that the T_{2u} will be soft for a second order transition to the tetragonal space group $I\bar{4}2d$. However although such a transition has been reported for $CuCr_2O_4$ none has yet been reported for $MgAl_2O_4$.

Agreement in the Σ direction is not as good, particularly the lowest transverse Σ_4 mode at the zone boundary. The lack of data for the other acoustic modes inhibits discussion of the fit towards the zone boundary.

Considering the simplicity of the SB model and its determination of parameters from zone centre data only the fit to the acoustic modes is impressive. In comparison to the other models the acoustic curves are somewhat steeper as reflected in the larger elastic constants (table 5.6). Using the method given by Striefler and Barsch (1972) I am in agreement with these authors that the internal strain contributions to the elastic constants for c_{11} and c_{12} depend on the A_{1g} and E_g modes and for c_{44} depends only on T_{2g} modes. However care must be taken with the non-rotationally invariant (unrestrained) models as the T_{1g} mode which transforms as an antisymmetric second rank tensor will also contribute to c_{44}.

Although the calculated elastic constants for all models do not agree well with those from ultrasonic data this does not imply that they are incorrect. As explained in section 4.4 the elastic constants from neutron data, which the models reflect, are of a different thermodynamic nature to the ultrasonic measurements. The disparity between the two data sets is due to the presence of anharmonic effects.

Examining table 5.4 it is noticeable that the lowest A_{2u}, E_u, T_{2u} and T_{1u} modes have similar values for all models even though these were not used in model optimization. This is a result of the refinement

of the cation-oxygen parameters to coincidentally almost equal values particularly those relating to the aluminium oxygen interaction. In contrast modes such as E_g and T_{1g} which are known from group theory only to involve oxygen motions (table 3.2) vary markedly between models.

The effect of polarizability is apparent for all high frequency models, not only the longitudinal T'_{1u} modes where it produces a reduction of up to 7THz but also Raman active modes A_{1g}, the highest T_{2g} modes and the inactive E_u and to a greater extent A_{2u} modes.

In all models including SB there is agreement that an infrared absorption band exists in the region 12.5-13.5 THz. This was expected for the SB model which was refined to that frequency, however this is not the case for the models presented here. There has been some doubt that the experimental mode at 12.8 THz was a pure one-phonon mode in view of its low intensity and the absence of a corresponding discontinuity in the Kramers-Kronig analysis. But in all my models the ratio of the longitudinal to the transverse frequency for this mode has the smallest value of the four infrared bands. Therefore it seems reasonable to conclude that the mode at 12.8 THz is in fact a one-phonon mode for $MgAl_2O_4$.

Grimes et al. (1978) have shown that the ratio of the experimental values of the dielectric constants $\epsilon(\infty)$ and $\epsilon(0)$ is very close to that of the product of the ratios $(\omega_L/\omega_T)^2$ for the infrared frequencies - that is, the Lyddane-Sachs-Teller (LST) relation holds. As discussed in the previous section the calculated values of $\epsilon(\infty)$ from the shell models are about 50% low. The static dielectric constants from the LST relation (equation (2.68)) have values about 23 compared to 8.4 (Wang and Zanzucchi 1971). Among the calculated values the greatest contribution to the product of the frequency ratios is from the splitting of the lowest T_{1u} mode (table 5.4). Ignoring this contribution the values obtained $\epsilon(0)$ are in the range 7.6-8. Thus it would

appear that the infrared mode found experimentally at 9.23 THz is also of one phonon origin and the lowest infrared band in $MgAl_2O_4$, although the models predict a much lower value.

The two lowest infrared bands had been excluded from the data used for model refinement because the existence of the higher of this pair was in doubt and the speculation by Striefler and Barsch (1972) that there may be an infrared mode lower than that at 9.23 THz. In retrospect it appears that the model parameters may have been improved if this data had been included.

6.3 Heat Capacity: Comparison with Experiment and Grimes Interpretation.

As the models have been refined to room temperature data comparison should only be made to the experimental value at 300K. In general agreement is good with the exception of Thompson's model which predicts a value about 10% less than that measured (table 5.7). As heat capacity is insensitive to details in the frequency distribution of the normal modes this difference demonstrates that the Thompson model is unsatisfactory. The low value is produced by over population of the high frequency end of the density of states.

If the assumption of thermally insensitive normal modes is valid the temperature variation of heat capacity is well accounted for by the unrestrained and SB models. However my central force models consistently predict high values with decrease of temperature.

The frequency distributions of each model pair (figs.5.6) are very similar, the shell model spectra terminating approximately 7THz lower than the corresponding rigid ion model. All spectra have two major prominences at 5.5 THz and about 14 THz. Another common feature which is more distinct in the central force models is a peak at about 10 THz. The breadth of this feature produces the characteristically higher heat capacities for this type of model. It is interesting to note that the Thompson's time of flight spectra from inelastic neutron scattering

reveals a region of intensity between 10 to 30 THz corresponding to unresolved optic modes with the highest peak at 13-15 THz. This data however is unsatisfactory because resolution and structure factor variation effects are unknown.

Comparing with Grimes (1972b) distribution, fig. 1.6 produced from Einstein and Debye functions at the infrared absorption frequencies the highest frequency peak does not have a counterpart in these spectra. From table 5.4 it is found that although it may be possible to relate the first two mentioned peaks to the first and third infrared bands this is purely fortuitous. For example the T_{2g},T_{2u} and T'_{1u} modes have similar frequencies.

To account for heat capacities up to room temperature any proposed density of states need only be essentially correct below the frequency equivalent of 300K ie. 6.25 THz as the population factors for modes of higher frequency will be less than unity. Therefore the contribution of peaks at frequencies higher than that of the lowest infrared absorption mode at 9.23 THz (equivalent to 443K) will be small and decrease with reduction of temperature.

To obtain the proposed density of states Grimes showed that the acoustic modes intercepted the zone boundary at frequencies approximately half that of the infrared modes when calculated from elastic constants and assuming a linear q dependence. This variation has now been shown by experiment to be essentially true. Then if the modes at the zone boundary are supposed to interact with themselves the infrared spectra could be explained in terms of two phonon modes. This is a tacit assumption of at most $F\bar{4}3m$ symmetry for an Fd3m structure does not allow overtone states. However it may not be necessary to make this simplification. Consider table 6.1 of the X point frequencies for the unrestrained shell mode. The selection rules of Gashimzade and Rustamov (1975) show that the only groupings of irreducible represen-

Time of Flight Spectra (after Thompson, 1977).

Fig 6.1

Mode Frequencies			
X_1(THz)	X_2(THz)	X_3(THz)	X_4(THz)
7.41	10.31	4.91	6.08
10.87	12.09	7.08	10.54
15.39	17.46	11.91	14.31
17.68		13.18	16.40
18.59		14.98	23.29
24.18		16.85	
26.48			

X Point Frequencies of the Unrestrained Shell Model

TABLE 6.1

tations that do not produce combination states are-X_4X_4, X_3X_3 and X_1X_2. Acoustic modes intersect the zone boundary from the [100] direction at X_1 and X_3 points and from the [110] direction at X_3 and X_4 modes. These may then interact with each other to give similar sum frequencies, for example,

$$X2.X3 = 4.91 + 10.31 = 15.22 \text{ THz}$$

$$X1.X3 = 4.91 + 10.87 = 15.78 \text{ THz}$$

$$X4.X3 = 4.91 + 10.51 = 15.42 \text{ THz}$$

which are approximately the same as the third infrared absorption band for the model at 15.56 THz (table 5.4).

Therefore Grimes' calculation for c_v appears to work because

i) The insensitivity of the heat capacity to the form of the frequency distribution.

ii) The proposed frequency distribution need only be reasonably accurate below the frequency of the first infrared to account for heat capacities over a temperature range up to room temperature.

iii) The approximation of linear acoustic modes is good. However because of the large number of optic modes and allowed transitions it is virtually possible to combine any zone boundary frequency with the others to produce sum or difference modes approximately equal to the infrared absorption frequencies.

6.4 Four Force Constant Model.

The models discussed so far describe magnesium aluminate as a completely ionic crystal. Partial covalent bonding may be represented in this formalism by allowing the core charges to be variable. While this is a common paramaterization it is somewhat difficult to separate such effects from those due to polarizable atoms. To enable a quick comparison to be made between ionic and co-valent effects the zone

centre frequencies have been calculated using the four force constant model described in the introduction (section 1.3.5). As the matrix elements given by Bruesch and D'Ambrogio (1972) were used the model describes $MgAl_2O_4$ as a covalent, normal spinel with δ set to zero. The eigenfrequencies and force constants are given in table 6.2.

In comparison to the ionic models the fit to the higher frequency T_{2g} and T_{1u} modes is improved although the value obtained for A_{1g} is somewhat low. Attempts to fit all four infrared modes resulted in imaginary values for the frequencies of the E_u and A_{2u} modes. Unlike the models of covalent spinels described in Chapter 1 the ratio $f_1:f_3$ is far removed from 2:1. The near zero value of f_3 results in modes involving aluminium-oxygen bond stretching such as E_u and A_{2u} having low frequencies. The high value of f_4, the aluminium-oxygen bond bending constant, raises the frequencies of modes such as T_{2u} above that found in ionic models. Thus it would appear that the likelihood of phase transitions by either of the A_{2u} or T_{2u} modes predicted in Chapter 3 depends on the degree of covalency present in $MgAl_2O_4$.

6.5 Conclusions and Suggestions for Possible Further Work.

The lattice dynamics of magnesium aluminate are well described by models in which the crystal is treated as completely ionic. Cation-oxygen interactions dominate the lower frequency spectra and Madelung energy. The inclusion of polarizability for the oxygen ions improves the fit of the higher frequency modes but is insufficient to completely describe the materials dielectric behaviour.

The unrestrained models are in closer agreement with experimental data than those employing central forces. The optimization parameters, however indicate that the improvement does not justify the increased number of parameters. It is doubtful that this is an accurate conclusion as the number of parameters used is comparable to the

Mode	Experimental (THz)	Four Force Constant Model (THz)
A_{1g}	23.16	20.96
E_g	12.3	12.31
T_{1g}	-	9.39
A_{2u}	-	4.29
	-	21.17
E_u	-	4.13
	-	21.14
T_{2u}	-	13.47
	-	14.79
T_{2g}	9.32	7.87
	14.75	14.80
	20.12	20.53
T_{1u}	9.15	11.97
	-	14.67
	14.54	15.68
	20.09	20.91

Force Constant (mdyn./Å)	f_1	f_2	f_3	f_4
	0.697	0.222	-0.072	0.498

Four Force Constant Model: Zone Centre Frequencies and Parameters

TABLE 6.2

number of data points. The greatest disparity between these models lies in the predicted frequency of the E_g Raman modes probably due to the difference in oxygen-oxygen short range parameters.

Of the previous models that of Striefler and Barsch describes the low frequency region of the spectrum well. However Thompson's generalised rigid ion model is unsatisfactory because of its failure to fit the heat capacity data to a reasonable degree of accuracy. The success of Grimes formula for these quantities is due to the essential validity of the assumption of linear acoustic modes and the fact that it is only necessary to get the frequency distribution correct at low frequencies. The four force constant model works fairly well for this compound but reasonable interpretation of its parameters is impossible because of the neglect of Coulomb effects. However it does show that the possible phase transition to the $F\bar{4}3m$ structure brought about by the softening of an A_{2u} mode is probably due to short range effects.

Two soft modes are predicted for possible second order phase transitions to tetragonal structures - T_{1g} $(I4_1/a)$, $T_{2u}(I\bar{4}2d)$. The latter being the only structure of the two that has been reported and its soft mode T_{2u} has often been found to be unstable during the refinement of the ionic models. As this mode has a higher frequency in the four force constant model this transition - if it is to occur in $MgAl_2O_4$ is probably due to long range Coulomb effects.

The models presented here could doubtless be improved by the introduction of extra parameters to account for covalent and further polarization effects. However the lack of experimental data and the vast amount of computer time required for optimization would not make the task worthwhile. The best that could probably be done for $MgAl_2O_4$ is to re-optimize the models presented here to include the two lower reported infrared modes that are now known to have a one-phonon origin. Although even this is unlikely to increase understanding of the dynamics much further. In view of the linear acoustic modes and fairly flat

optic modes it would probably be more profitable to construct models to represent the zone centre behaviour for a series of spinels.

APPENDIX I

Independent Elements of the Short Range R and Coulomb C Interaction Matrices at the Brillouin Zone Centre

The elements given below include translational invariance terms for the short range matrix but not for the Coulomb matrix. In both cases, elements of the type $M_{\alpha\beta}(\kappa\kappa')$ for the magnesium ions ($\kappa,\kappa'=5,6$) are zero when $\alpha \neq \beta$. For general labelling of ions and short range parameters see Tables 5.1 and 5.2 in main text.

κ	κ'	α	β	$\frac{v_a}{e^2} C_{\alpha\beta}(\kappa\kappa')$	$\frac{v_a}{e^2} R_{\alpha\beta}(\kappa\kappa')$ *
1	1	1	1	-4.189	A_o+2B_o
1	2	1	1	4.479	0
1	3	1	1	-8.523	0
1	5	1	1	-4.189	0
1	7	1	1	-4.189	0
1	8	1	1	-39.006	$-A_o/2$
1	9	1	1	13.220	$-B_o/2$
5	5	1	1	-4.189	$\frac{2}{3}(A_t+2B_t)$
5	6	1	1	-4.189	0
5	7	1	1	-4.189	0
5	11	1	1	-4.189	$-\frac{1}{6}(A_t+2B_t)$
7	7	1	1	-4.189	
7	8	1	1	5.158	$-\frac{1}{2}(B_1+B_3)$
7	9	1	1	-8.862	$-\frac{1}{4}(A_1+A_3+B_1+B_3)$
7	11	1	1	-4.189	0
7	12	1	1	-4.257	$-B_2$
7	13	1	1	-8.411	$-\frac{1}{2}(A_2+B_2)$
1	1	1	2	0.0	$2(A_o-B_o)\delta/(\frac{1}{4}-\frac{3}{2}\delta)$
1	2	1	2	0.0	0
1	5	1	2	3.374	0
1	7	1	2	-0.965	0
1	8	1	2	-2.868	$-(\delta/2)(A_o-B_o)/(\frac{1}{4}-\delta)$
1	9	1	2	-0.124	≈ 0
5	7	1	2	3.009	0
5	11	1	2	-18.604	$-\frac{1}{6}(A_t-B_t)$
7	7	1	2	0.0	
7	8	1	2	0.0	0
7	9	1	2	-15.446	$-\frac{1}{4}(A_1+A_3-(B_1+B_3))$
7	11	1	2	-0.183	0
7	12	1	2	0.0	0
1	3	1	3	-14.461	0
7	13	1	3	14.242	$\frac{1}{2}(A_2-B_2)$

*Only terms linear in δ have been retained in the expressions for the elements of the short range matrix R. It is to be noted however that the translational invariance term $R_{12}(11)$ contains a linear contribution for the sum of elements equivalent to $R_{12}(19)$. These terms which are

almost zero when taken alone do contribute significantly to the translation invariance term in summation.

APPENDIX II

Expressions for the Elements of the Block Diagonalised Matrix for the Optically Active Modes in Rigid Ion Models

All elements are quoted in units of e^2/v_a.

Z_o, Z_t, Z_{ox} are the charges on the octahedral tetrahedral and oxygen ions respectively in units of e.

Similarly the ionic masses are given by m_o, m_t, m_{ox}.

Mode: A_{1g}

$$D(1,1) = Z_{ox}Z_o(7.461)+Z_{ox}Z_t(39.57)+Z_{ox}^2(96.365)+$$
$$+A_t/2+B_o+A_o/2 -\frac{2\delta}{(\frac{1}{4}-\delta/2)}(A_o-B_o)+2(A_1+A_3)+2B_2$$

$$\text{Frequency of } A_{1g} = \sqrt{D(1,1)} \times \frac{5.157}{m_{ox}} \text{ THz}$$

Mode: E_g

$$D(1,1) = Z_{ox}Z_o(21.402)+Z_{ox}Z_t(-7.218)+Z_{ox}^2(4.787)+$$
$$+ B_t/2+B_o\left(1 - \frac{\delta}{(\frac{1}{4}-\delta/2)}\right) +A_o\left(\frac{1}{2} + \frac{\delta}{(\frac{1}{4}-\delta/2)}\right) + \tfrac{1}{2}(A_1 +A_3)+$$
$$+ \tfrac{3}{2}(B_1+B_3)+2B_2$$

$$\text{Frequency of } E_g = \sqrt{D(1,1)} \times \frac{5.157}{m_{ox}} \text{ THz}$$

Modes: T_{2g}

$$D(1,1) = \tfrac{2}{3}(A_t+2B_t)/m_t$$
$$D(1,2)=(Z_tZ_{ox}(61.13) + \sqrt{\tfrac{2}{3}}(A_t-B_t))/\sqrt{m_tm_{ox}}$$
$$D(1,3)=\tfrac{1}{3}(A_t+2B_t)/\sqrt{m_tm_{ox}}$$
$$D(2,2)=\{Z_oZ_{ox}(12.108)+Z_tZ_{ox}(23.973)+Z_{ox}^2(63.135)+ \tfrac{1}{6}(2A_t+B_t)+$$
$$+B_o\left(1 +\frac{\delta}{(\frac{1}{4}-\delta/2)}\right)+A_o\left(\frac{1}{2} -\frac{\delta}{(\frac{1}{4}-\delta/2)}\right)+A_1+A_2+A_3+B_1+B_2+B_3\Big\}/m_{ox}$$
$$D(2,3)=\{Z_oZ_{ox}(-6.572)+Z_tZ_{ox}(22.05)+Z_{ox}^2(-40.8)+\sqrt{2}(\tfrac{1}{6}(A_t-B_t)-$$
$$-\frac{\delta}{(\frac{1}{4}-\delta/2)}(A_o-B_o)-A_2+B_2)\}/m_{ox}$$

$$D(3,3)=\{Z_oZ_{ox}(16.755)+Z_tZ_{ox}(8.378)+Z_o^2(33.509)+\tfrac{1}{6}(A_t+2B_t)+$$
$$+B_o+A_o/2+4B_2+2A_2\}/m_{ox}$$

Taking the three eigenvalues of this symmetric matrix to be f_i, the corresponding frequencies ν_i are given by

$$\nu_i = 5.157\sqrt{f_i} \quad \text{THz}$$

Modes: T_{1u}

$$D(1,1)=\left\{Z_o^2(37.01)+Z_oZ_t(1.63)+Z_oZ_{ox}(47.16)+A_o\left(1+\frac{2\delta}{(\frac{1}{4}-\frac{3}{2}\delta)}\right)+\right.$$
$$\left.+2B_o\left(1-\frac{\delta}{(\frac{1}{4}-\frac{3}{2}\delta)}\right)\right\}/m_o$$

$$D(1,2)=\left\{Z_tZ_o(-9.543)+Z_oZ_{ox}(19.304)+\frac{2\sqrt{2}\delta}{(\frac{1}{4}-\frac{3}{2}\delta)}(A_o-B_o)\right\}/m_o$$

$$D(1,3) = Z_oZ_t(13.496)/\sqrt{m_tm_o}$$

$$D(1,4) =\left\{Z_oZ_{ox}(48.049)+A_o/\sqrt{2}\right\}/\sqrt{m_om_{ox}}$$

$$D(1,5) =\left\{Z_oZ_{ox}(-13.65)-\frac{2\delta}{(\frac{1}{4}-\delta)}A_o-B_o)\right\}/\sqrt{m_om_{ox}}$$

$$D(2,2)=\left\{Z_tZ_o(8.378)+Z_o(8.378)+Z_oZ_{ox}(33.51)+A_o+2B_o\right\}/m_o$$

$$D(2,3) = Z_oZ_t(-11.848)/\sqrt{m_tm_o}$$

$$D(2,4) =\left\{Z_oZ_{ox}(9.294)+\frac{2\delta}{(\frac{1}{4}-\delta)}(A_o-B_o)\right\}/\sqrt{m_om_{ox}}$$

$$D(2,5) =\left\{Z_oZ_{ox}(-23.695)-\tfrac{1}{2}(A_o-B_o)\right\}/\sqrt{m_om_{ox}}$$

$$D(3,3) =\left\{Z_t^2(-8.378)+\tfrac{2}{3}(A_t+2B_t)\right\}/m_t$$

$$D(3,4) =\left\{Z_tZ_{ox}(-44.109)-\sqrt{\tfrac{2}{3}}(A_t-B_t)\right\}/\sqrt{m_tm_{ox}}$$

$$D(3,5) =\left\{Z_tZ_{ox}(-16.756)-\tfrac{1}{3}(A_t+2B_t)\right\}/\sqrt{m_tm_{ox}}$$

$$D(4,4) =\left\{Z_oZ_{ox}(12.108+Z_tZ_{ox}(23.973)+Z_{ox}^2(18.125)+\tfrac{1}{6}(2A_t+B_t)+\right.$$
$$\left.+B_o\left(1+\frac{\delta}{(\frac{1}{4}-\delta/2)}\right)+A_o\left(\tfrac{1}{2}-\frac{\delta}{(\frac{1}{4}-\delta/2)}\right)+A_1+A_3+B_1+B_3+4B_2\right\}/m_{ox}$$

$$D(5,5) = \left\{ Z_o Z_{ox}(16.755) + Z_o Z_t(8.378) + \tfrac{1}{6}(A_t + 2B_t) + B_o + A_o/2 \right\} \Big/ m_{ox}$$

Taking the five eigenvalues of this symmetric matrix to be f_i, the corresponding frequencies ν_i are given by

$$\nu_i = 5.157\sqrt{f_i} \quad \text{THz}$$

APPENDIX III

Symmetry Coordinates at the Point Γ and Along Lines Λ, Δ, Σ

The symmetry coordinates are tabulated in such a fashion as only to show those parts of each forty two dimensional vector that are not necessarily zero. As no symmetry operation may interchange inequivalent ions only the sublocks shown in fig.III-1 for each ion type have been given. For clarity even amongst these, zero value elements are represented by a dot. All other elements are given by a symbol (eg.g) equivalent to the complex exponential of a given angle, for example

$$g = \exp(i\theta).$$

The angles given in the tables refer to the symmetry coordinates at $q/q_{max} = 0.05$ for each direction, except of course at the Γ point. The asterisks indicate complex conjugation and i retains its usual meaning, $\sqrt{-1}$.

The elements are listed in the order of the labelling of the ions in Table 5.1: $r_\alpha(\kappa), \alpha = 1,2,3; \kappa = 1,2 \ldots 14; \alpha$ changing most rapidly.

To block diagonalise the dynamical matrix the coordinates have to be first normalised and arranged in order of the repetition index for each representation varies before the part or index. The coordinates given then have to be multiplied by phase factors $\exp(-iq.r(\kappa))$ to agree with the form of the dynamic matrix used in this thesis.

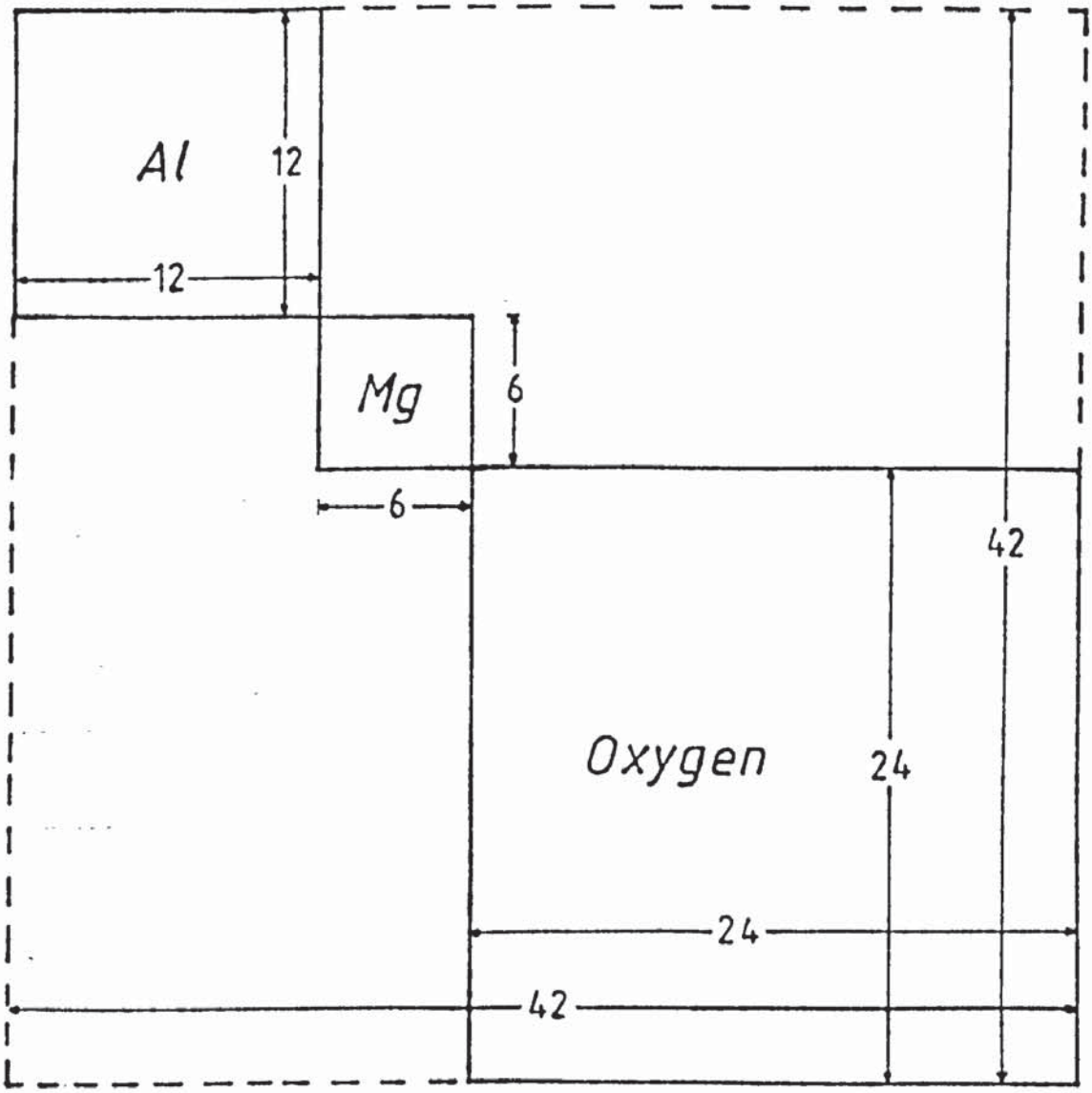

Non-Zero Blocks for Symmetry Co-ordinate Matrix

Fig III-1

Γ Modes: Symmetry Coordinates

Symbol	Angle
a	-60°
b	-90°
1	0°

Representation	A_{2u}	T_{2u}			T_{1u}						E_u	
Partner	1	1	2	3	1		2		3		1	2
	1	1	-1	.	1	.	1	.	.	1	-ia	ia*
	1	-1	.	1	1	.	.	1	1	.	-ia*	ia
	1	.	1	-1	.	1	1	.	1	.	b	b*
	1	-1	1	.	-1	.	-1	.	.	1	-ia	ia*
	-1	-1	.	-1	1	.	.	1	-1	.	ia*	-ia
	-1	.	1	1	.	1	1	.	-1	.	b*	b
	-1	1	1	.	1	.	-1	.	.	1	ia	-ia*
	1	1	.	-1	-1	.	.	1	-1	.	-ia*	ia
	-1	.	-1	-1	.	1	-1	.	1	.	b*	b
	-1	-1	-1	.	-1	.	1	.	.	1	ia	-ia*
	-1	1	.	1	-1	.	.	1	1	.	ia*	-ia*
	1	.	-1	1	.	1	-1	.	-1	.	b	b*
Repetition	1	1	1	1	1	2	1	2	1	2	1	1

Octahedral Ions

Representation	T_{2g}			T_{2u}		
Partner	1	2	3	1	2	3
	.	.	1	.	.	1
	.	1	.	.	1	.
	1	.	.	1	.	.
	.	.	-1	.	.	1
	.	-1	.	.	1	.
	-1	.	.	1	.	.
Repetition	1	1	1	3	3	3

Tetrahedral Ions

Γ Point Modes

Representation	A_{2u}		T_{2g}						T_{2u}			T_{1g}		
Partner	1	1	1		2			3	1	2	3	1	2	3
	1	1	1	.	1	.	.	1	1	-1	.	1	-1	.
	1	1	1	.	.	1	1	.	-1	.	1	-1	.	1
	1	1	.	1	1	.	1	.	.	1	-1	.	1	-1
	1	1	-1	.	-1	.	.	1	-1	1	.	-1	1	.
	-1	1	1	.	.	1	-1	.	-1	.	-1	-1	.	-1
	-1	-1	.	1	1	.	-1	.	.	1	1	.	1	1
	-1	-1	-1	.	1	.	.	1	-1	-1	.	-1	-1	.
	-1	-1	-1	.	.	1	1	.	1	.	1	1	.	1
	1	1	.	1	-1	.	-1	.	.	-1	1	.	-1	1
	-1	-1	1	.	-1	.	.	1	1	1	.	1	1	.
	1	1	-1	.	.	1	-1	.	1	.	-1	1	.	-1
	-1	-1	.	1	-1	.	1	.	.	-1	-1	.	-1	-1
	-1	1	-1	.	-1	.	.	-1	1	-1	.	-1	1	.
	-1	1	-1	.	.	-1	-1	.	-1	.	1	1	.	-1
	-1	1	.	-1	-1	.	-1	.	.	1	-1	.	-1	1
	-1	1	1	.	1	.	.	-1	-1	1	.	1	-1	.
	1	-1	-1	.	.	-1	1	.	-1	.	-1	1	.	1
	1	-1	.	-1	-1	.	1	.	.	1	1	.	-1	-1
	1	-1	-1	.	1	.	.	-1	1	1	.	-1	-1	.
	-1	1	1	.	.	-1	1	.	1	.	-1	-1	.	1
	1	-1	.	-1	1	.	-1	.	.	-1	-1	.	1	1
	1	-1	1	.	-1	.	.	-1	-1	-1	.	1	1	.
	1	-1	1	.	.	-1	-1	.	1	.	1	1	.	-1
	-1	1	.	-1	1	.	1	.	.	-1	1	.	1	-1
Repetition	1	2	2	3	2	3	2	3	2	2	2	1	1	1

Anions

Γ point Modes

Representation	T_{1u}						E_g		E_u	
Partner	1		2		3		1	2	1	2
	1	.	1	.	.	1	a	a*	-ia	ia*
	1	.	.	1	1	.	a*	a	-ia*	ia
	.	1	1	.	1	.	1	1	b	b*
	-1	.	-1	.	.	1	a	a*	-ia	ia*
	1	.	.	1	-1	.	-a*	a	ia*	-ia
	.	1	1	.	1	.	-1	-1	b*	b
	-1	.	1	.	.	1	-a	-a*	ia	-ia*
	-1	.	.	1	1	.	-a*	-a	-ia*	ia
	.	1	-1	.	-1	.	1	1	b	b*
	1	.	-1	.	.	1	-a	-a*	ia	-ia*
	-1	.	.	1	-1	.	a*	a	-ia*	ia
	.	1	-1	.	1	.	-1	-1	b*	b
	1	.	1	.	.	1	-a	-a*	-ia	ia*
	1	.	.	1	1	.	-a*	-a	-ia*	ia
	.	1	1	.	1	.	-1	-1	b	b*
	-1	.	-1	.	.	1	-a	-a*	-ia	ia*
	1	.	.	1	-1	.	-a*	-a	ia*	-ia
	.	1	1	.	-1	.	1	1	b*	b
	1	.	-1	.	.	1	a	a*	ia	-ia*
	-1	.	.	1	-1	.	-a*	-a	.	ia
	.	1	-1	.	1	.	1	1	b*	b
	-1	.	1	.	.	1	a	a*	ia	-ia*
	-1	.	.	1	1	.	a*	a	ia*	-ia
	.	1	1	.	-1	.	-1	-1	b	b*
Repetition	4	5	4	5	4	5	1	1	2	2

Anions (contd)

Λ Modes: Symmetry Coordinates

Symbol	Angle	Symbol	Angle
a	90°	g	45°
b	-81°	h	33°
c	45°	k	-27°
d	30°	ℓ	-15°
e	39°	m	-87°
f	-21°		

Octahedral Ions

Representation	Λ_1			Λ_2	Λ_3							
Partner	1			1	1				2			
	a	·	·	∘	d	∘	∘	·	-d*	∘	·	·
	a	·	·	·	-d*	·	·	∘	d	·	·	·
	a	·	∘	·	a*	·	·	·	a*	·	·	·
	∘	b	·	∘	·	e	∘	∘	∘	f	∘	∘
	·	·	b	b	∘	∘	g	g*	∘	·	k	ik
	·	·	b	-b	∘	∘	h	ih	·	·	ℓ	-iℓ
	∘	·	b	-b	·	·	k	ik	·	·	g	g*
	·	b	·	·	∘	f	∘	∘	∘	e	∘	·
	∘	·	b	b	∘	·	ℓ	-iℓ	·	·	h	ih
	∘	·	b	b	·	∘	iℓ*	ℓ*	·	·	m	im
	·	·	b	-b	∘	·	m	im	·	·	iℓ*	ℓ*
	∘	b	·	·	∘	-b	·	∘	·	-b	∘	·
Repetition	1	2	3	1	1	2	3	4	1	2	3	4

Tetrahedral Ions

Repetition	Λ_1		Δ_3			
Partner	1		1		2	
	c	ic	g	g*	ℓ	-iℓ
	c	ic	ℓ	-iℓ	g	g*
	c	ic	iℓ*	ℓ*	iℓ*	ℓ*
	-c*	ic*	-ℓ*	-iℓ*	-g*	-g
	-c*	ic*	-g*	-g	-ℓ*	-iℓ*
	-c*	ic*	iℓ	-ℓ	iℓ	-ℓ
Repetition	4	5	5	6	5	6

Λ Modes

Representation	Λ_1						Λ_2	
Partner	1						1	
	c	∘	•	ic	•	•	∘	∘
	c	•	∘	ic	•	•	•	•
	c	•	•	ic	•	•	•	•
	•	c	•	•	ic	•	•	•
	•	∘	c	•	•	ic	c	ic
	•	∘	c	•	•	ic	-c	-ic
	•	•	c	•	•	ic	c	ic
	•	∘	c	•	•	ic	-c	-ic
	∘	c	•	•	ic	∘	•	•
	∘	•	c	∘	•	ic	-c	-ic
	•	c	•	•	ic	•	•	•
	∘	∘	c	•	∘	ic	c	-ic
	-c*	∘	∘	ic*	•	•	•	•
	-c*	•	•	ic*	•	•	•	•
	-c*	•	•	ic*	•	•	•	∘
	∘	-c*	∘	•	ic*	•	•	•
	•	∘	-c*	•	∘	ie*	-c*	ic*
	∘	•	-c*	•	•	ic*	c*	-ic*
	•	•	-c*	•	•	ic*	c*	-ic*
	•	-c*	∘	•	ic*	•	•	∘
	∘	∘	-c*	•	∘	ic*	-c*	ic*
	∘	•	-c*	∘	•	ic*	-c*	ic*
	•	∘	-c*	•	•	ic*	c*	-ic*
	∘	-c*	•	∘	ic*	•	•	•
Repetition	6	7	8	9	10	11	2	3

Anions

Λ Modes

Representation	Λ_3															
Partner	1								2							
	g	g*	∘	•	•	•	∘	∘	ℓ	-iℓ*	•	•	•	∘	•	∘
	ℓ	iℓ*	•	∘	•	•	•	•	g	g*	∘	•	•	∘	•	•
	iℓ*	ℓ	•	•	•	•	•	∘	iℓ*	ℓ	•	•	•	•	•	∘
	•	•	g	•	•	•	•	-g*	∘	∘	ℓ	•	•	•	•	iℓ
	•	•	∘	g	•	-g*	•	•	•	•	•	•	ℓ	•	-iℓ*	•
	•	•	∘	•	g	∘	-g*	•	•	∘	•	ℓ	•	iℓ*	∘	•
	∘	∘	•	iℓ*	•	-ℓ	•	•	•	•	•	•	iℓ*	•	-ℓ	∘
	•	•	∘	•	iℓ*	∘	ℓ*	•	•	•	∘	iℓ*	•	-ℓ*	∘	•
	∘	∘	iℓ*	•	•	•	•	-ℓ*	•	∘	iℓ*	•	•	•	•	-ℓ*
	•	•	•	∘	ℓ	∘	iℓ	•	∘	•	∘	g	•	-g*	•	•
	∘	•	ℓ	•	•	•	•	iℓ	•	•	g	•	•	•	∘	-g*
	∘	∘	∘	ℓ	•	-iℓ*	•	•	•	•	•	•	g	•	-g*	∘
	-ℓ	-iℓ*	•	•	•	•	∘	•	ℓ	-iℓ	•	•	•	•	∘	•
	-g*	-g	•	•	•	•	•	•	g	g*	•	•	•	•	•	∘
	iℓ	-ℓ	•	•	•	•	•	•	iℓ*	ℓ*	•	•	•	•	•	•
	∘	∘	-ℓ*	•	•	•	•	iℓ*	•	∘	-g*	•	•	•	•	g
	•	•	•	•	-ℓ*	•	iℓ*	•	•	•	•	-g*	•	g	•	•
	∘	•	•	-ℓ*	•	iℓ*	•	•	•	•	•	•	-g*	∘	g	•
	∘	∘	∘	-g*	∘	g	•	∘	•	•	∘	•	-ℓ*	∘	iℓ*	∘
	∘	∘	-g*	•	•	•	∘	g	•	∘	-ℓ*	•	•	•	•	iℓ*
	•	•	∘	•	-g*	∘	g	•	•	•	∘	-ℓ*	•	iℓ*	•	•
	•	•	•	•	iℓ	•	ℓ	•	•	•	•	iℓ	•	ℓ	•	•
	∘	∘	•	iℓ	•	ℓ	•	•	∘	•	∘	•	iℓ	•	ℓ	•
	•	∘	iℓ	∘	•	•	•	•	•	∘	iℓ	•	•	•	∘	ℓ
Repetition	7	8	9	10	11	12	13	14	7	8	9	10	11	12	13	14

Anions (contd)

Δ Modes: Symmetry Coordinates

Symbol	Angle
a	90°
b	-85.5°
c	-83.25°
d	45°
e	-40.5°

Representation	Δ_1		Δ_1'	Δ_5							Δ_2	Δ_2'	
Partner	1		1	1			2				1	1	
	a	.	.	.	-d*	.	.	d	.		.	a	.
	.	a	a	d	.	d*	-d*	.	-d		a	.	a
	.	a	a*	-d	.	d*	d*	.	-d		a*	.	a
	a	.	.	.	d*	.	.	-d	.		.	a	.
	.	a*	a*	d	.	d*	-d*	.	-d		a*	.	a*
	.	a*	a	-d	.	d*	d*	.	-d		a	.	a*
	b	.	.	.	ie	.	.	-e	.		.	-b	.
	.	-b	b	e	.	ie	-ie	.	-e		-b	.	b
	.	b	b	e	.	-ie	-ie	.	e		-b	.	-b
	b	.	.	.	-ie	.	.	e	.		.	-b	.
	.	b	-b	e	.	ie	-ie	.	-e		b	.	-b
	.	-b	-b	e	.	-ie	-ie	.	e		b	.	b
Repetition	1	2	1	1	2	3	1	2	3		1	1	2

Octahedral Ions

Representation	Δ_1	Δ_5				Δ_2'
Partner	1	1		2		1
	c	.	.	.	.	-ic
	.	-ic	.	.	-ic	.
	.	.	c	-c	.	.
	-c*	.	.	.	.	-ic*
	.	.	-ic*	-ic*	.	.
	.	c*	.	.	-c*	.
Repetition	3	4	5	4	5	3

Tetrahedral Ions

Δ Modes

Representation	Δ_1				Δ_1'		Δ_2		Δ_2'			
Partner	1				1		1		1			
	d	.	-d*	∘	.	.	.	.	d	.	d*	∘
	.	d	.	-d*	d	d*	d	-d*	.	d	.	d*
	.	d	.	-d*	-d	-d*	-d	d*	.	d	.	d*
	d	∘	-d*	.	.	.	.	.	d	.	d*	∘
	.	-d	.	d*	-d	-d*	-d	d*	.	-d	.	-d*
	.	-d	.	d*	d	d	d	-d*	.	-d	.	-d*
	ie*	∘	e*	.	.	.	.	∘	-ie*	.	e*	.
	.	ie*	.	e*	-ie*	e*	ie*	e*	.	-ie*	.	e*
	.	-ie*	.	-e*	-ie*	e*	ie*	e*	.	ie*	.	-e*
	ie*	.	e*	.	.	.	.	.	-ie*	∘	e*	.
	.	-ie*	∘	-e*	ie*	-e*	-ie*	-e*	.	-ie*	∘	e*
	.	ie*	.	e*	ie*	-e*	-ie*	-e*	.	ie*	.	-e*
	-e*	.	d	.	.	∘	.	∘	-ie*	.	e*	∘
	.	-d*	.	d	-d*	-d	-d*	d	.	ie*	.	-e*
	.	-d*	.	d	d*	d	d*	-d	.	-ie*	.	e*
	-d*	.	d	∘	.	.	∘	.	-d*	.	-d	.
	.	d*	.	-d	d*	d	d*	-d	.	d*	.	d
	.	-d*	.	-d	-d*	-d	-d	d	.	d*	.	d
	ie	.	-e	.	.	.	.	∘	-ie	.	-e	.
	.	-ie	∘	e	ie	e	-ie	e	∘	-ie	.	e
	∘	ie	.	-e	ie	e	-ie	e	.	ie	.	e
	.	.	-e	.	∘	.	.	∘	-ie	.	-e	∘
	.	ie	.	-e	-ie	-e	ie	-e	∘	ie	∘	-e
	∘	-ie	.	e	-ie	-e	ie	-e	∘	-ie	.	e
Repetition	5	5	6	7	2	3	2	3	4	5	6	7

Anions

Δ Modes

Representation	Δ_5											
Partner	1						2					
	d	.	.	d*	.	.	d*	.	∘	-d	.	.
	∘	d	.	.	d*	.	∘	.	d*	.	.	-d
	.	.	d	.	.	-d*	.	d*	.	.	d	∘
	-d	.	.	-d*	.	.	-d*	∘	.	d*	.	.
	.	d	.	∘	d*	.	∘	.	d*	.	.	d
	.	.	d	.	.	-d*	.	d*	.	.	-d	∘
	-ie*	.	.	e*	.	.	e*	.	.	ie*	.	.
	.	-ie*	.	.	e*	.	.	.	e*	∘	.	-ie*
	.	.	ie*	.	.	e*	.	-e*	.	.	-ie*	.
	ie*	.	.	-e*	.	∘	-e*	.	.	-ie*	.	.
	∘	-ie*	.	.	e*	∘	.	.	e*	.	.	-ie*
	.	.	ie*	.	.	e*	∘	-e*	.	.	ie*	.
	.	.	∘	-d*	.	.	-d*	.	.	-d	.	.
	∘	.	-d	.	.	-d*	∘	-d*	.	.	-d	.
	.	-d	.	.	d*	.	.	.	d	∘	.	d
	d	.	.	-d*	∘	.	d*	.	.	d	.	.
	.	.	-d	∘	.	-d*	.	-d*	.	.	-d	∘
	.	-d	.	∘	d*	.	∘	.	-d*	.	.	d
	e	.	.	-ie	.	.	ie	.	.	e	.	.
	.	.	-e	.	.	-ie	.	-ie	.	.	-e	∘
	.	e	.	.	-ie	.	.	.	ie	.	.	-e
	-e	.	∘	ie	.	.	.	.	.	-e	.	∘
	.	∘	-e	.	.	.	∘	.	.	.	-e	.
	.	e	.	∘	∘	.	∘	∘	∘	.	.	-e
Repetition	6	7	8	9	10	11	6	7	8	9	10	11

Anions (contd)

Σ Modes: Symmetry Coordinates

Symbol	Angle
a	90°
b	-81°
c	-85.5°
d	-76.5°
e	45°
f	-54°

Octahedral Ions

Representation	Σ_1			Σ_2		Σ_4			Σ_3			
Partner	1			1		1			1			
	a	.	.	a	.	a	.	.	a	.	.	.
	a	.	.	a*	.	a*	.	.	a	.	.	.
	.	a	.	.	.	.	.	.	.	a	.	.
	.	.	c	.	c	.	c	.	.	.	c	.
	.	.	c	.	c	.	-c	.	.	.	-c	.
	.	.	.	.	.	.	.	c	.	.	.	c
	.	.	c	.	-c	.	c	.	.	.	-c	.
	.	.	c	.	-c	.	-c	.	.	.	c	.
	.	.	.	.	.	.	.	-c	.	.	.	c
	b	.	.	-b	.	b	.	.	-b	.	.	.
	b	.	.	b	.	-b	.	.	-b	.	.	.
	.	-b	.	.	.	.	.	.	.	b	.	.
Repetition	1	2	3	1	2	1	2	3	1	2	3	4

Tetrahedral Ions

Representation	Σ_1		Σ_2	Σ_4	Σ_3	
Partner	1		1	1	1	
	d	.	-id	d	id	.
	d	.	id	-d	id	.
	.	id*	.	.	.	d
	-d*	.	-id*	-d*	-id*	.
	-d*	.	id*	d*	-id*	.
	.	id	.	.	.	-d*
Repetition	4	5	3	4	5	6

Σ Modes

Representation	Σ_1							Σ_2				
Partner	1							2				
	e	.	.	.	.	-e*	.	e	.	.	.	e*
	e	.	.	.	.	-e*	.	-e	.	.	.	-e*
	.	e	.	.	.	.	e*	.	.	.	.	.
	.	.	e	-e*	.	.	.	.	e	-e*	.	.
	.	.	f	-if*	.	.	.	.	f	-if	.	.
	.	.	.	.	ic*	.	.	.	.	.	ic*	.
	f	.	.	.	.	-if	.	-f	.	.	.	if
	f	.	.	.	.	-if	.	-f	.	.	.	-if
	.	f	.	.	.	.	-if	.	.	.	.	.
	.	.	f	-if	.	.	.	.	-f	if	.	.
	.	.	e	-e*	.	.	.	.	-e	e*	.	.
	.	.	.	.	ic*	.	.	.	.	.	-ic*	.
	-e*	.	.	.	.	e	.	-e*	.	.	.	-e
	-e*	.	.	.	.	e	.	-e*	.	.	.	e
	.	-e*	.	.	.	.	-e	.	.	.	.	.
	.	.	-e*	e	.	.	.	.	-e*	e	.	.
	.	.	-f*	-if*	.	.	.	.	-f*	-if*	.	.
	.	.	.	.	ic	.	.	.	.	.	ic	.
	.	.	-f*	-if*	.	.	.	.	f*	if	.	.
	.	.	-e*	e	.	.	.	.	e*	e*	.	.
	.	.	.	.	ic	.	.	.	.	.	-ic	.
	-f*	.	.	.	.	-if*	.	-f*	.	.	.	-if*
	-f*	.	.	.	.	-if*	.	-f*	.	.	.	if*
	.	f*	.	.	.	.	-if*	.	.	.	.	.
Repetition	6	7	8	9	10	11	12	4	5	6	7	8

Anions

Σ Modes

Representation	Σ_4					Σ_3						
Partner	1					1						
	e	.	.	.	-e*	e	.	.	.	.	e*	.
	-e	.	.	.	e*	e	.	.	.	.	e*	.
	.	.	.	.	.	.	e	.	.	.	.	-e*
	.	e	e*	.	.	.	.	e	e*	.	.	.
	.	-f	if	.	.	.	.	-f	-if	.	.	.
	.	.	.	-c*	.	.	.	.	.	-c*	.	.
	f	.	.	.	-if	-f	.	.	.	.	-if	.
	-f	.	.	.	if	-f	.	.	.	.	-if	.
	.	.	.	.	.	.	f	.	.	.	.	f
	.	f	-if	.	.	.	.	-f	-if	.	.	.
	.	e	-e*	.	.	.	.	e	e*	.	.	.
	.	.	.	c*	.	.	.	.	.	-c*	.	.
	e	.	.	.	e	-e*	.	.	.	.	-e	.
	e*	.	.	.	-e	-e*	.	.	.	.	-e	.
	.	.	.	.	.	.	-e*	.	.	.	.	e
	.	-e*	-e	.	.	.	.	-e*	-e	.	.	.
	.	f*	-if*	.	.	.	.	f*	-if*	.	.	.
	.	.	.	c	.	.	.	.	.	c	.	.
	.	-f*	if	.	.	.	.	f*	-if*	.	.	.
	.	e*	e	.	.	.	.	-e*	-e	.	.	.
	.	.	.	-c	.	.	.	.	.	c	.	.
	-f*	.	.	.	-if*	f*	.	.	.	.	-if*	.
	f*	.	.	.	if*	f*	.	.	.	.	-if*	.
	.	.	.	.	.	.	f*	.	.	.	.	-if
Repetition	5	6	7	8	9	7	8	9	10	11	12	13

Anions (contd)

PUBLICATION

REFERENCES

Basu A.N. and Sengupta S. 1968 Phys.Stat.Solidi 29 367-375
Deformable Shell Models for Alkali Halides

Beals R.J. and Cook,R.L. 1957 J.Am.Ceram.Soc.40 279-284
Directional Dilation of Crystal Lattices at
Elevated Temperatures

van den Berg K.G, Lodder,J.C. and Mensinga,T.C. 1976
Thin Solid Films 34 243-247
Magnetic Anisotropy and Domain Structure of Manganese
Ferrite Grown Epitaxially on MgO

Bertaut,F, Forrat,F. and Dulac,J. 1959 Compt.Rend. 249 726-728
Rhodites Spinelles

Bilz H,Buchanan,M, Fischer,K,Haberkon,R, and Schroder,U.
1975 Solid State Comm. 16 1023-1026
Overlap Polarization and Lattice Dynamics of Ionic Crystals.

Biman,J.L. 1966 Phys.Rev.Lett.17 1216-1219
Simplified Theory of Symmetry Change in Second Order
Phase Transitions: Application to V_3Si

Boldish,S.I. and White,W.B, 1978a J.Sol.Stat.Chem.25 121-135
Vibrational Spectra and Force Constants of Rare Earth
and Scandium Thiospinels

Boldish,S.I. and White,W.B. 1978b Plenum Press, New York
editors: McCarthy,G.J. and Rhyne,J.J.
The Rare Earths in Modern Science and Technology

Bongers,P.F. and Zanmarchi,G. 1968 Solid State Comm.6 291-294
Infrared Absorption Spectrum and Faraday Rotation of
Ferromagnetic $CdCr_2Se_4$.

Born,M. and Huang,K 1954 Clarendon Press,Oxford
Dynamical Theory of Crystal Lattices.

Bouchkaert,L.P, Smoluchowski,R, and Wigner,E. 1936,Phys.Rev.50 58-67
Theory of Brillouin Zones and Symmetry Properties of
Wave Functions in Crystals.

Boyer,L.L. 1974 Phys.Rev. B9 2684-2691
Determination of Interionic Interactions in Complex Ionic
Crystals from Structural Conditions for a Rigid Ion Crystal

Boyer,L.L. and Fleury,P.A. 1974 Phys.Rev.B9 2693-2700
Determination of the Interionic Interations in $Ca_{10}(PO_4)_6F_2$ (Fluorapatite) from Structural and Lattice Dynamical Data

Boyer,L.L. and Hardy,J.R. 1973a Phys.Rev.B7 2886-2888
Static Equilibrium Conditions for a Rigid Ion Crystal.

Boyer,L.L. and Hardy,J.R. 1973b Phys.Rev. B8 2205-2213
Lattice Dynamics of a Rigid Ion Model for Gadolinium Molybdate

Bragg,W.H, 1915 Phil.Mag. 30 305-315
The Structure of the Spinel Group of Crystals

Brockhouse,B.N. 1961 in:-
Inelastic Scattering of Neutrons in Solids and Liquids vol.1 IAEA Vienna

Brockhouse,B.N, 1966 in:-
Phonons in Perfect Lattices and in Lattices with Point Defects
editor: Stevenson. Oliver and Boyd, Edinburgh.

Brockhouse,B.N, and Stewart,A.T, 1958 Rev.Mod.Phys.30 236-249
Normal Modes of Aluminium by Neutron Spectrometry

Bruesch,P, and D'Ambrogio 1972 Phys.Stat.Solidi (b) 50 513-526
Lattice Dynamics and Magnetic Ordering in the Chalcogenide Spinels $CdCr_2S_4$ and $CdCr_2Se_4$

Brun,E, and Hafner,S, 1962 cited in
Kirsch,R, Gerard,A, and Wautelet,M, 1974 J.Phys.C.7 2633-2644
Nuclear Quadruple Couplings and Polarizability of the Oxygen Ion in Spinel-Structure Compounds

Casella,R.C, 1975 Phys.Rev.B11 4795-4800
Algorithm for Computing the Number of Independent Real Parameters in the Phonon Dynamical Matrix

Catlow,C.R.A,Diller,K.M, and Norgett,M.J, 1977 J.Phys C 10 1395-1412
Interionic Potentials for Alkali Halides

Chang,Z.P, and Barsch,G.R, 1973 J.Geophys Res 78 2418-2433
Pressure Dependence of Single-Crystal Elastic Constants and Anharmonic Properties of Spinel.

Cochran,W, 1959 Proc.R.Soc. A253 260-276
Theory of the Lattice Vibrations of Germanium.

Cochran ,W, 1960 Advan.Phys.9 387-423
Crystal Stability and Theory of Ferroelectricity.

Cochran,W. 1971a CRC Critical Reviews in Solid State Sciences 2 1-44
Lattice Dynamics of Ionic and Covalent Crystals

Cochran,W, 1971b Acta Cryst. A27 556-559
The Relation between Phonon Frequencies and Interatomic Force Constants

Cochran,W, and Cowley,R.A, 1962 J.Phys.Chem.Solids 23 447-450
Dielectric Constants and Lattice Vibrations

Cochran ,W, and Zia,A, 1968 Phys.Stat.Solidi 25 273-283
Structure and Dynamics of Pervoskite - Type Crystals

Cooper,M.J, and Nathans,R, 1967 Acta Cryst. 23 357-367
The Resolution Function in Neutron Diffractometry

Cowley,E.R, and Pant,A,K, 1970 Acta Cryst. A26 439-442
Artificial Splitting of One Phonon Neutron Groups Due to Relaxed Vertical Collimation

Cowley,R.A, 1962a Acta Cryst. 15 687-690
Some Calcuations Using the Ewald Transformation.

Cowley,R.A, 1962b Proc.R.Soc, A268 109-120
The Lattice Dynamics of Ionic and Covalent Crystals

Cowley,R.A, 1962c Proc.R.Soc. A268 121-144
The Elastic and Dielectric Properties of Crystals with Polarizable Ions

Cowley,R.A, 1963 Advan.Phys.12 421-480
Lattice Dynamics of an Anharmonic Crystal

Cowley,R.A, 1964 Phys.Rev. 134 A980-A995
Lattice Dynamics and Phase Transitions in Strontium Titanate

Cowley,R.A, 1967 Proc.Phys.Soc. 90 1127-1147
Zero Sound,First Sound and Second Sound in Solids

Cowley,R.A, Cochran,W, Brockhouse,B.N, and Woods,A.D.B, 1963
Phys.Rev. 131 1030-1039
Lattice Dynamics of Alkali Halide Crystals III Theoretical

Cran,G.C, and Sangster,M.J.L, 1974 J.Phys.C 7 1937-1948
Lattice Dynamics of Manganese Fluoride

Dick,B.G, and Overhauser,A.W, 1958 Phys.Rev. 112 90-103
Theory of the Dielectric Constants of Alkali Halide Crystals

Dimmock,J.O, 1963 Phys.Rev. 130 1337-1344
Use of Symmetry in the Determination of Magnetic Structure

Dolling,G, 1974 in:-
Dynamical Properties of Solids vol 1
editors: Horton,G.K, and Maradudin,A.A North Holland

Dolling,G, 1976 Methods in Computational Physics 15 1-40
The Calculation of Phonon Frequencies

Dunitz,J.D, and Orgel,L.E, 1957a J.Phys.Chem.Solids 3 20-29
Electronic Properties of Transition Metal Oxides I

Dunitz,J.D, and Orgel,L.E. 1957b J.Phys.Chem.Solids 3 318-323
Electronic Properties of Transition Metal Oxides II
Cation Distribution Amongst Octahedral and Tetrahedral Sites

Finch,G.I, Sinha,A.P.B, and Sinha,K.P, 1957
Proc.R.Soc. A242 28-35
Crystal Distortion in Ferrite-Manganites

Fujii,Y, Laurie,N.A, Pynn,R, and Shirane,G, 1974 Phys.Rev.B10 3647-3659
Inelastic Neutron Scattering from Solid ^{36}Ar

Ganesan,S,Maradudin,A.A, and Oitmaa,J.J, 1970 Ann.Physics 56 556
A Lattice Theory of Morphic Effects in Crystals of Diamond Structure

Gashimzade,F.M, and Rustamov,K.A, 1975 Phys.Stat.Solidi (b) 71 125-134
Selection Rules for the Spinel Structure

Gehring,G.A, and Gehring,K.A, 1975 Rep.Prog.Phys.38 1-89
Co-operative Jahn-Teller Effects

Gibbons,D.F, 1957, J.Appl.Phys. 28 810-814
Acoustic Relaxations in Ferrite Single Crystals

Goldrich,F.E, and Birman,J.L, 1968 Phys.Rev. 167 528-532
Theory of Symmetry Change in Second-Order Phase Transitions in Perovskite Structure

Gorter,E.W, 1954 Philips Res.Rep. 9 295-320
Saturation Magnetisation and Crystal Chemistry of Ferrimagnetic Oxides

Grimes,N.W, 1971 J.Phys.C 4 L342-L344 Structural Distortions in $MgCr_2O_4$

Grimes,N.W, 1972a Phil.Mag. 25 1217-1226
'Off-Centre' Ions in Compounds with Spinel Structure

Grimes,N.W, 1972b Spectrochim. Acta A28 2217-2225
Interpretation of the Infrared Spectrum of Spinels

Grimes,N.W, 1973 J.Phys.C 6 L78-L79
Antiferroelectricity Among Compounds with Spinel Structure?

Grimes,N.W, 1974 Proc.R.Soc.London A338 209-221
On the Specific Heat of Compounds with Spinel Structure I: The Ferrites

Grimes,N.W, 1975 Physics in Technology 22-27
The Spinels: Versatile Materials

Grimes,N.W, 1979 Private Communication

Grimes,N.W, and Collett,A.J, 1971a Phys.Stat.Solidi(b) 43 591-599
Correlation of Infrared Spectra with Structural Distoritions in the Spinel Series $Mg(Cr_xAl_{2-x})O_4$

Grimes,N.W, and Collett,A.J, 1971b Nature 230 158
Infrared Absorption Spectra of Ferrites

Grimes,N.W, and Hilleard,R.J, 1970 J.Phys.C 3 866-871
X-Ray Diffraction Studies of the Spinel Series $Mg(Cr_xAl_{2-x})O_4$. I: Lattice Parameters and Structure

Grimes,N.W, O'Connor,P.J, and Thompson,P, 1978 J.Phys.C L505-L507
Comments on the Interpretation of the Infrared Spectraum from $MgAl_2O_4$ Spinel

Haas, C, 1965 J.Phys.Chem.Solids 26 1225-1232
Phase Transitions in Crystals with the Spinel Structure

Hafner,S, 1961 Z.Kristallog. 115 331-358
Ordnung/Unordnung und Ultrarotabsorption IV Die Absorption einiger Metalloxyde mit Spinellstruktur

Hafner,S, and Laves,S, 1961 Z.Kristallog. 115 321-330
Ordnung/Unordnung und Ultrarotabsorption III Die Systeme $MgAl_2O_4$-Al_2O_3 und $MgAl_2O_4$-$LiAl_5O_8$

Harada,J,Axe,J.D, and Shirane,G, 1970 Acta Cryst.A26 608-612
Determination of the Normal Vibrational Displacements in Several Perovokites by Inelastic Neutron Scattering

Hardy,J.R, 1962 Phil.Mag. 7 315-336
On Lattice Dynamics of Alkali Halide Crystals in Relation to Specific Heat Data

Harrison,W.A, 1966 Benjamin, New York
Pseudopotentials in the Theory of Metals

Herman,F, 1959 J.Phys.Chem.Solids 8 405-418
Lattice Vibrational Spectrum of Germanium

Huang,K, 1949 Phil.Mag. 40 733-747
Lattice Theory of Dielectric and Piezoelectric Constants of Crystals

Hwang,L, Heuer,A.H, and Mitchell,T.E, 1973 Phil.Mag 28 241-243
On the Space Group of $MgAl_2O_4$ Spinel

Iizumu,M, and Shirane, G, 1974 Solid State Comm. 17 433-436
Crystal Symmetry of the Low Temperature Phase of Magnetite

International Tables for X-Ray Crystallography 1972
editors: Henry,N.F.M and Lonsdale,K, Kynoch Press Birmingham

Iyengar,P.K, 1965 in:-
Thermal Neutron Scattering
editor: Egelstaff, P.A. Academic Press, London

Jasperse,J.R, Kahan,A, Plendl,J.N, and Mitra,S.S, 1966
Phys.Rev. 146 526-542
Temperature Dependence of Infrared Dispersion in Ionic Crystals LiF and MgO

Jones,G.O, Martin,D.H, Mawer,P.A, and Perry,C.H, 1961
Proc.R.Soc.London A261 10-27
Spectroscopy at Extreme Infrared Wavelengths II
The Lattice Resonances of Ionic Crystals

Kadanoff,L,P, Gotze,W, Hamblen,D, Hecht,R, Lewis,E.A,S, Palciauskas,V,V, Rayl,M, Swift,J, Aspnes,D and Kane,J, 1967 Rev.Mod.Phys. 39 395-431
Static Phenomena Near Critical Points: Theory and Experiment

Kellermann,E.W, 1940 Phil.Trans.Roy.Soc. A238 513-548
Vibrations of the Sodium Chloride Lattice

King,E.G, 1955 J.Phys.Chem. 59 218-219
Thermodynamic Properties of Crystalline Calcium and Magnesium Aluminates

Koester,L.L, 1977 Spinger Tracts in Modern Physics, Berlin 80
Neutron Physics

Kino,Y, and Luthi,B, 1971 Solid State Comm. 9 805-808
Magnetic and Elastic Properties of Zinc Chromite

Kino,Y, Luthi,B, and Muller,M.E, 1972 J.Phys.Soc. Japan 33 687-697
Co-operative Jahn-Teller Phase Transition in the
Nickel-Zinc Chromite System

Kurasawa,T, 1961 J.Phys.Soc.Japan 16 1298-1308
Polarization Waves in Solids

Landau,L.D, 1937 in English in:
Collect Papers of L.D.Landau Gordon and Bresch, London

Landau,L.D, and Lifshitz,E.M, 1960a Pergamon Press
Statistical Physics

Landau,L.D, and Lifshitz,E.M, 1960b Pergamon Press
Electrodynamics of Continuous Media

Lax,M, 1965 Phys.Rev. 138 A793-A802
Subgroup Techniques in Crystal and Molecular Physics

Lee,T.H, 1971 J.Appl.Phys. 42 1441-1442
Infrared Reflectance Spectrum of $CdCr_2S_4$ and $CdCr_2Se_4$

Leibfried,G, 1963 in:-
Proc.Int.Conf.Lattice Dynamics, Copenhagen 1963
editor: Wallis,R.F

Leibfried,G, and Ludwing,W, 1961 Solid State Physics 12 271-444
Theory of Anharmonics in Crystals

Leigh ,R.S, Szigeti,B, and Tewary,V.K, 1971
Proc.R.Soc. London A320 505-526
Force Constants and Lattice Vibrations

Littlewood,P.B, and Heine,V, 1979 J.Phys.C 12 4431-4439
The Infrared Effective Charge in IV-VI Compounds

Liubarskii,G.Y, 1960 Pergamon Press London
The Application of Group Theory in Physics

Lomer,W.M, and Low,G.G, 1965 in:-
Thermal Neutron Scattering
Editor: Egelstaff, P.A Academic Press,London

Lou,F.H, and Ballentyne,D.W.G, 1968 J.Phys.C. 1 608-613
Visible and Ultra Violet Emission and Absorption
Spectra of $MgAl_2O_4$:Cr

Loudon,R, 1967 Advan.Phys. 13 432-482 The Raman Effect in Crystals

Lutz ,H.D. 1969 Z.Naturforsch. 24A 1417-1419
Gitterschwingungsspektren III. Mitteilung

Lyddane,R.H, and Herzfeld,K.F, 1938 Phys.Rev. 54 846-861
Lattice Vibrations in Polar Crystals

Lyddane,R.H, Sachs,R.G, and Teller,E, 1941 Phys.Rev. 59 673-676
On the Polar Vibrations of Alakli Halides

Maradudin,A.A, Montroll,E.W, Weiss,G.H, and Ipatova,I.P, 1971
Solid State Physics Supplement 3
Theory of Lattice Dynamics in the Harmonic Approximation

Maradudin,A.A, and Vosko,S.H, 1968 Rev.Mod.Phys. 40 1-37
Symmetry Properties of the Normal Vibrations of a Crystal

Marumo,F, Isobe,M, Saito,Y, Yagi,T, and Akimoto,S, 1974
Acta Cryst. B30 1904-1906
Electron Density Distribution in Crystals of γ-Ni_2SiO_4

Mashkevich,V.S, 1961 Sov.Phys.Solid State 2 2345-2351
Fiz.Tverd.Tela 2 2629 (1960)
The Dipole Approximation in the Microscopic Theory of
Crystals I.Lattice Vibrations as Affected by
Electronic Dispersion

McClure,D.S, 1957 J.Phys.Chem.Solids 3 311-317
The Distribution of Transition Metal Cations in Spinels

Miller,A, 1959 J.Appl.Phys. 30 24S-25S
Distribution of Cations in Spinels

Mishra,R,K and Thomas,G, 1977 Acta Cryst. A33 678
Structural Phase Transition in Spinel $MgAl_2O_4$

Mitra,S.S, and Marshall,R, 1964 J.Chem.Phys. 41 3158-3164
Trends in the Characteristic Phonon Frequencies in the
NaCl, Diamond, Zinc Blende and Wurtzite Type Crystals

Montgomery,H, 1969 Proc.R.Soc. A309 521-549
The Symmetry of Lattice Vibrations in the Zinc Blende
and Diamond Structures

Moran,T.J, and Luthi,B, 1969 Phys.Rev. 187 710-714
Elastic and Magnetoelastic Effects in Magnetite

Muller,O, and Roy,R, 1974 Springer Verlag, New York
The Major Ternary Structural Families

Navrotsky,A, and Kleppa,O.J, 1967 J.Inorg.Nucl. Chem. 29 2701-2714
The Thermodynamics of Cation Distributions in Simple Spinels.

Nielsen,M, and Bjerrum Moller H, 1969 Acta Cryst.A25 547-550
Resolution of a Tiple Axis Spectrometer

Nowick,A.S, 1969 Comments on Solid State Physics 1 49-51
Paraelastic Effects of "Off-Centre" Ions

Nowick,A.S, and Heller,W.R, 1965 Advan.Phys. 14 101-166
Dielectric and Anelastic Relaxation of Crystals Containing Point Defects

O'Horo,M.P, Frisillo,A.L, and White,W.B, 1973
J.Phys.Chem.Solids 34 23-28
Lattice Vibrations of $MgAl_2O_4$ Spinel

Pantelides,S.T, 1975 Phys.Rev.Lett. 35 250-254
Mechanisms that Determine the Dielectric Constants of Ionic Crystals

Peckham,G.E, Saunderson,D.H, and Sharp,R.I, 1967 Brit.J.Appl.Phys.
Focussing Conditions for a Triple Axis Neutron Spectrometer

Peierls,R.E, 1955 Clarendon Press, Oxford
Quantum Theory of Solids

Perel,J, Batterman,B.W, and Blount,E.I, 1968
Phys Rev. 166 616-621
Search for Sublattice Distortion in V_3Si

Peters,J, and Standley,K.J, 1958 Proc.Phys.Soc. 71 131-133
The Dielectric Behaviour of Magnesium Manganese Ferrite

Polder,D, 1950 Proc.IEEE 97 pt(II)246-256 Ferrite Materials

Preudhomme,J, and Tarte,P, 1970a Spectrochim.Acta 27A 961-968
Infrared Studies of Spinels I. A Critical Discussion of Actual Interpretations

Preudhomme,J, and Tarte,P, 1970b Spectrochim. Acta 27A 845-851
Infrared Studies of Spinels II. The Experimental Bases for Solving the Assignment Problem

Preudhomme,J, and Tarte,P, 1970c Spectrochin. Acta 27A 1817-1835
Infrared Studies of Spinels III. The Normal II-III Spinels

Preudhomme,J, and Tarte,P, 1971 Spectrochim. Acta 28A 69-79
Infrared Studies of Spinels IV. Normal Spinels with High Valency Tetrahedral Cation.

Prince,E, 1957 Acta Cryst 10 554-556
Crystal and Magnetic Structure of Copper Chromite

Sammis,C.G, 1971 Ph.D. Thesis, Cal.Inst.Tech.
Seismological Applications of Lattice Theory

Samuelsen,E.J, 1974 J.Phys.C 7 L115-L117
Note on the Space Group of Spinel

Samuelsen,E.J, and Steinsvoll,O, 1974 Phys.Stat.Solidi(b)
61 615-620 Low Energy Phonons in Magnetite

Samuelsen,E.J, and Steinsvoll,O, 1975 J.Phys.C 8 L427-L429
On the Space Group of Spinel

Schlegel,A, Alvarado,S.F, and Wachter,P, 1979 J.Phys.C 12 1157-1164
Optical Properties of Magnetite

Schmocker,U, Boesch,H.R, and Waldner,F, 1972
Physics Letters 40A 237-238
A Direct Determination of Cation Disorder in
$MgAl_2O_4$ Spinel by ESR

Schmocher,U, and Waldner,F, 176 J.Phys.C 9 L235-L237
The Inversion Parameter with Respect to the Space
Group of $MgAl_2O_4$ Spinels

Schroder,U, 1966 Solid State Comm. 4 347-349
A New Model for Lattice Dynamics ("Breathing Shell Model")

Scott,J.F, 1974 Rev.Mod.Phys.46 83-128 Soft Mode Spectroscopy

Shannon,R.D, and Prewitt,C.T, 1968 Acta Cryst.B25 929-945
Effective Ionic Radii in Oxides and Fluorides

Shimanouchi,T, Tsuboi,M, and Miyazawa,T, 1961
J.Chem.Phys.Solids 35 1597-1612
Optically Active Lattice Vibrations as Treated by
the GF Matrix Method

Shimuzu,H, Ohbayashi,Y, Yamamoto,K, and Abe,K, 1975
J.Phys.Soc.Japan 38 750-754

Shirane,G, and Axe,J.D, 1971 Phys.Rev. B4 2957-2963
Neutron Scattering Study of the Lattice Dynamical
Phase Transition of Nb_3Sn.

Shirane,G, Chikazumi,S, Akimitsu,J, Chika,K, Matsui, M and Fujii,Y,
1975 J.Phys.Soc.Japan, 39 949-957
Neutron Scattering from the Low Temperature Phase of
Magnetite

Sinclair,R.N, and Brockhouse,B.N, 1960 Phys.Rev. 120 1638-1640
Dispersion Relation for Spin Waves in a f.c.c. Cobalt Alloy

Siratori,K, 1967 J.Phys.Soc. Japan 23 948-954
Effect of the Crystal Deformation on the Lattice Vibration of Oxide Spinels

Siratori,K, Tsuchida, A, and Tomono,Y, 1965 J.Appl.Phys.36 1050-1051
Lattice Vibration and Cubic-to-Tetragonal Transformation in Spinel-Type Chromite

Smit,J, 1958 Solid State Comm. 6 745-746
Ion Configuration in Spinels

Smit,J, and Wijn, H.P.J, 1959 Philips Technical Library Ferrites

Smith,P.P.K, 1978 Phil.Mag. B38 99-102
Note on the Space Group of Spinel Mineral

Squires,G.L, 1978 Cambridge University Press
Introduction to the Theory of Thermal Neutron Scattering

Stahl-Brada, R. and Low,W, 1959 Phys.Rev. 116 561-564
Paramagnetic Resonance Spectra of Chromium and Manganese in the Spinel Structure

Stirling,W, 1972a Phd.Thesis Edinburgh University Excitations in Strontium Titanate and Palladium-Iron

Stirling,W, 1972b J.Phys.C 5 2711-2730
Neutron Inelastic Scattering Study of the Lattice Dynamics of Strontium Titanate: harmonic models

Striefler,M.E, and Barsch,G.R, 1972 J.Phys.Chem.Solids 33 2229-2250
Lattice Dynamics at Zero Wave Vector and Elastic Constants of Spinel in the Rigid Ion Approximation

Szigeti,B, 1949 Trans.Faraday Soc. 45 155-166
Polarizability and Dielectric Constant of Ionic Crystals

Szigeti,B, 1950 Proc.R.Soc. A204 51-62
Compressibility and Absorption Frequency of Ionic Crystals

Tarte,P, and Preudhomme,J, 1963 Acta Cryst. 16 227
Infrared Spectrum and Cation Distribution in Spinels

Thompson,P, and Grimes,N.W, 1977a Phil.Mag. 36 501-505
Madelung Calculations for the Spinel Structure

Thompson,P, and Grimes,N.W, 1977b J.Appl.Cryst.10 369-371
Multiple Diffraction in Spinel and the Space-Group Ambiguity

Thompson,P, and Grimes,N.W, 1977c Solid State Comm. 25 609-611
Observations of Low Energy Phonons in Spinels

Vedam,K, Kirk,J.L, and Archar,B.N,N, 1975 J.Solid State Chem 12 213-218
Peizo- and Thermo- Optic Behaviour of Spinel ($MgAl_2O_4$)

Venkateraman,G, Feldkamp,L.A, and Sahni,V.C (1975) M.I.T.Press
Dynamics of Perfect Crystals

Venkateraman,G, and Sahni,V.C, 1970 Ev.Mod.Phys. 42 409-470
External Vibrations in Complex Crystals

Verble,J.L, 1974 Phys.Rev. B9 5236-5248
Temperature-Dependent Light-Scattering Studies of the Verwey Transition and Electronic Disorder in Magnetite

Wakamura,K, Arai,T, and Kudo,K, 1976 J.Phys.Soc.Japan 40 1118-1121,
Lattice Vibrations in Spinel Type Crystals $Cd_xZn_{1-x}Cr_2Se_4$

Wakamura,K, Arai,T, Onari,S, Kudo,K, and Takahashi,T, 1973
J.Phys.Soc.Japan 35 1430-1436
The Lattice Vibrations of Magnetic Semiconductor Chalcogenide Spinels $Hg_xZn_{1-x}Cr_2Se_4$

Waldron,R.D, 1955 Phys.Rev. 99 1727-1735
Infrared Spectra of Ferrites

Wang,C.C, and Zanzucchi,P.J, 1971 J.Electrochem.Soc. 118 586-596
Dielectric and Optical Properties of Stoichiometric Magnesium Aluminate Spinel Single Crystals

Warren,J.L, 1968 Rev.Mod.Phys.40 38-76
Further Considerations on the Symmetry Properties of the Normal Vibrations of a Crystal

Warren,J.L, 1974 Phys.Rev. B9 3603-3608
Time Reversal Invariant Projection Operators for Lattice Dynamics

Warren,J.L, and Worlton,T.G, 1973 Argone National Laboratory,Illinois
Symmetry Properties of the Lattice Dynamics of Twenty Three Crystals

Warren,J.L, and Worlton,T.G, 1974 Computer Physics Comm. 8 71-84
Improved Version of Group Theoretical Analysis of Lattice Dynamics

Warren,J.L, and Worlton,T.G, 1976 Methods in Computational Physics 15 77-118
Group Theory of Lattice Dynamics by Computer

Watanabe,K, and Brockhouse,B.N, 1962 Phys.Lett. 1 180-190
Observation of Optical and Acoustical Magnons in Magnetite

White,W.B, and DeAngelis,B.A, 1967 Spectrochim. Acta 23A 935
Interpretation of the Vibrational Spectra of Spinels

Woods,A.D.B, Brockhouse,B.N, and Cowley,R.A, 1963 Phys.Rev.131 1025-1059
Lattice Dynamics of Alkali Halide Crystals II Experimental Studies of KBr and NaI

Woods,A.D.B, Cochran,W, and Cowley,R.A, 1960 Phys.Rev.119 980-999
Lattice Dynamics of Alkali Halide Crystals

Worlton,T.G, and Warren,1972 Computer Physics Comm. 3 88-117
Group Theoretical Analysis of Lattice Vibrations

Wyckoff,R.W.G, 1965 Wiley, New York, Crystal Structures vol 3

Yamada,Y, 1974, Proc.Conf.Magnetism and Magnetic Materials, San Francisco Dec 3-6 1974

Yamamoto,K, Murakaura,T, Ohbayashi,Y, Shimuzu,H, and Abe,K, 1973
J.Phys.Soc.Japan 35 1258
Lattice Vibrations in $CdIn_2S_4$

Zallen,R, 1968 Phys.Rev. 173 824-832
Symmetry and Restrahlen in Elemental Crystals

Ziman J.M, 1960 Clarendon Press,Oxford
Electrons and Phonons

ACKNOWLEDGEMENTS

I would like to thank Dr.V.Wagner of the I.L.L. for his assistance during the neutron scattering experiments and the staff of the Computer Centre at Aston for their help, particularly with problems associated with the link to the Manchester computers.

I would like to express my gratitude to my supervisor Dr.N.W.Grimes for his advice and encouragement throughout this project.

I would also like to thank Professor S.E.Hunt in whose department the work was performed and the Science Research Council for providing financial support.